

Remote Work and City Structure*

Ferdinando Monte Charly Porcher Esteban Rossi-Hansberg
Georgetown University *Georgetown University* *University of Chicago*

February 21, 2025

Abstract

Relative to remote work, working downtown facilitates valuable interactions with other in-office workers, but entails commuting costs. The resulting coordination mechanism can lead to multiple stationary equilibria with different levels of remote work. Temporary reductions in commuter shares, such as the COVID-19 pandemic, can then lead to persistently large fractions of remote workers. Consistently, using cell-phone-based mobility data for the U.S., we document that trips in the largest cities have stabilized at levels that are only about 60% of pre-pandemic levels, while smaller cities have returned to pre-pandemic levels. U.S. cities that exhibit multiplicity experience average welfare losses of 2.3%.

*Monte: ferdinando.monte@georgetown.edu, Porcher: charly.porcher@georgetown.edu, Rossi-Hansberg: rossi-hansberg@uchicago.edu. We thank Shijian Yang and Reigner Kane for excellent research assistance and Treb Allen, Arnaud Costinot, Jonathan Dingel, Cecile Gaubert, Maria Hansen, Maurice Kugler, Maisy Wong, three anonymous referees and numerous seminar participants for excellent comments.

1 Introduction

Many of us work at least partially from home these days. A phenomenon that was only marginal a few years ago has become widespread and has challenged, in potentially profound ways, the basic organization of work in firms and cities. Information technology has improved to a point where workers can talk, chat, and send information in documents, databases, audio, and video without delays and at extremely low costs. However, although information technology clearly complements remote work, significant advances in information and communication technologies (ICT) increased remote work only marginally between 1980 and 2019. In contrast, since the COVID-19 pandemic, remote work has boomed. Suddenly, commuting has declined by half in many of our largest cities and seems to have stabilized at those low levels.¹ What generated this abrupt and seemingly permanent increase in work from home since the pandemic? What are its consequences for the structure of cities? Will the change be uniform across them? Importantly, what are the welfare consequences of permanent shifts in commuting and agglomeration patterns? In this paper, we aim to address these questions by proposing, and estimating for most U.S. cities, a dynamic theory of city structure with a labor delivery choice. We also contrast and verify its implications with data on individual cell phone mobility and zip code-level house prices.

At the core of our theory is the idea that the value of working at the CBD, in short “office work”, depends on proximity to other workers. Workers’ productivity is enhanced by interactions with others in their office, across businesses, and more generally with other workers at city centers. This is an old idea from Marshall, of course. Remote work offers workers and employers the possibility to work in the same city but without interacting in person. Since workers do not internalize many of the benefits they convey to others, this alternative possibility leads to a novel coordination problem: Workers prefer to work in the CBD only if others do too, but prefer to work from home otherwise. In a dynamic economy, where workers face idiosyncratic preferences for remote work (e.g., having a baby or remodeling) and fixed costs from switching between labor delivery modes (e.g., setting up a home office or buying a car), this mechanism can lead to multiple stationary equilibria with different permanent shares of commuters. In these cases, abrupt changes to the number of commuters can make a city converge to a stationary equilibrium that is very different from the initial one. For many places, we postulate, this abrupt change was the COVID-19 pandemic and the lockdowns and self-isolation it generated. This one-time temporary change has led, for several U.S. cities, to a permanent change in one of the most enduring characteristics of human organization: work at city centers.

Of course, not all cities are equal. Some cities specialize in industries where interactions between workers lead to large spillovers and correspondingly large populations. Other cities specialize in industries with low spillovers and are small. Commuting costs can vary dramatically depending on transport infrastructure and geographic characteristics. Furthermore, the ability to work from

¹These trends have been reported from survey data (Barrero et al., 2023; Brynjolfsson et al., 2020; Aksoy et al., 2022; Brynjolfsson et al., 2023), administrative data (Dalton et al., 2022), changes in job advertisements for remote positions (Hansen et al., 2023), or changes in internet usage of firms (Matthies and Kwan, 2022).

home varies sharply with the worker’s occupation, and occupations are, clearly, not uniformly distributed in space. We all know about the concentration of bankers in New York or programmers in Palo Alto. All these characteristics of cities determine the extent to which the coordination problem we identify leads to multiplicity in stationary equilibria. We characterize these conditions and prove that, naturally, the intensity of the coordination problems, and therefore the likelihood of multiple stationary equilibria, increases with the strength of agglomeration forces minus that of congestion forces and in the relative productivity of remote work to office work. We show that, in the U.S., the particular configuration of urban characteristics that leads to multiplicity in stationary equilibria was prevalent, before the pandemic, in many of the larger cities. That is, we estimate parameter configurations for large cities that, in general, although not always, put them in the “multiplicity cone”: the parameter set where cities exhibit multiplicity in stationary equilibria.

Our finding that large cities tend to be in the multiplicity cone implies that the abrupt reduction in commuters caused by the COVID-19 pandemic made many of them switch to a path that seems to be converging to the low commuting stationary equilibrium. Of course, even in the stationary equilibrium with little commuting, some people commute; their idiosyncratic preference for office work and the fixed cost of switching make it the better choice for them. Our interpretation is that the pandemic reduced the share of commuters below the share of commuters in the low commuting stationary equilibrium. Hence, commuting has increased in some of these cities, but only slightly, and has stabilized way below pre-pandemic levels. In contrast, small cities tend to have parameter configurations outside the multiplicity cone, so their stationary equilibrium is unique. These cities experienced the same abrupt reduction in commuters as large cities did during the pandemic, but their dynamic evolution simply brings them back to the pre-pandemic stationary equilibrium. Hence, they exhibit no permanent change in the number of commuters. In sum, we argue that the pandemic acted as an equilibrium selection device for cities where multiple stationary equilibria existed ex-ante. In a rare – in our view – empirical occurrence, the spatially uniform temporary push of most workers into a remote state during the pandemic has revealed the set of cities featuring multiple stationary equilibria and has served as a selection mechanism to determine the stationary equilibrium to which these cities are converging.

We contrast these predictions of our model with cell-phone-based data on worker mobility from SafeGraph, available from before the pandemic until mid-2022. We first identify CBDs in all cities by finding the group of census tracks that receive the largest numbers of commuters pre-pandemic.² We then track the number of trips to these CBDs over time. The results are revealing. In New York, NY, for example, relative to pre-pandemic levels, the pandemic reduced the number of trips to the CBD by more than 80%. After the pandemic, the number of trips increased slightly, but it has now stabilized at about 40% of the pre-pandemic level. San Francisco, CA, shows a similar pattern. In contrast, Madison, WI, experienced a drop in the pandemic as large as New York

²In some cases, we identify multiple CBDs when several areas have more than 80% of the commuters to the main CBD. One example is Midtown and Downtown in Manhattan.

but has recovered fully to pre-pandemic levels. The implications of the apparent multiplicity of stationary equilibria are present more broadly in the data. The largest U.S. cities, with employment above 1.5 million workers, experienced a drop of 80% in trips to the CBD during the pandemic but now have stabilized at only 60% of pre-pandemic levels. In contrast, the smallest CBSAs, with employment below 150 thousand workers, experienced a comparable drop in CBD trips during the pandemic, but have now gone, on average, fully back to pre-pandemic levels.

The available housing data is also consistent with the mechanism in our theory. As others have documented, the pandemic generated a flattening of house price distance gradients in cities ([Gupta et al., 2021](#)). Namely, prices at the CBD declined relative to prices further away from the city. This is a natural consequence of the expansion of work from home since the advantage of living close to work is diminished if workers do not commute to the office or do so only a couple of days a week. What has not been documented, but we document here using Zillow zip code-level data, is that the flattening in the rent gradient has continued in the largest cities but has reversed and disappeared in the smaller ones. The cities where trips to the CBD have gone back to pre-pandemic levels, like Madison, or Durham, NC, exhibit housing price gradients that are not statistically different from pre-pandemic ones. In contrast, the larger cities where CBD trips have stabilized at much lower levels, like New York and San Francisco, exhibit a large and significant flattening of this gradient, which has been exacerbated since the pandemic.

What are the welfare implications of our findings? For small cities outside the multiplicity cone, the long-run welfare effect is zero. These cities have simply reverted to the pre-pandemic equilibrium. The transition lasted a couple of years, but the transition costs are probably only marginal. In contrast, for cities that have permanently switched to the work-from-home intensive stationary equilibrium, the welfare implications depend on the welfare ranking of both stable stationary equilibria. A direct comparison of these stationary equilibria in the 199 cities that we estimate are inside the multiplicity cone reveals that the welfare costs are positive but relatively modest. The costs are about around 3.7% for Los Angeles and San Jose, 3.2% for New York, 2.8% for San Francisco, and 2% for Phoenix. A stationary equilibrium with office work is indeed better than the remote work intensive stationary equilibrium, but the benefits from the lack of commuting compensate for most of the losses. Of course, these numbers depend on the details of the estimation strategy of our model and the many sources of data, including the ACS and the NLSY, that we use to implement it. We discuss the details of the estimation of our dynamic discrete choice model in the body of the paper.

Our paper is related to several strands of the literature. First, we contribute to the emerging literature studying the effects of remote work on urban environments. [Liu and Su \(2023\)](#) document a decrease in the urban wage premium of occupations with higher levels of remote work since the COVID-19 pandemic, consistent with a decline in the agglomeration externality for these occupations. [Davis et al. \(2024\)](#) develop a model where remote work productivity increases via adoption externalities and study the response of remote work employment to improvements in its technology. [Parkhomenko and Delventhal \(2024\)](#) develop a quantitative spatial equilibrium model

with work from home and commuting that predicts the optimal frequency of remote work. They study the spatial redistribution of economic activity induced by an increase in the amenity value of remote work. We propose an alternative interpretation to the large and persistent increase in remote work that does not rely on exogenous productivity or amenity shocks. Duranton and Handbury (2023) show that exogenous changes in which workers are allowed to work remotely in a monocentric city model can replicate observed changes in commuting and demand for housing. Instead, we show how the coordination of agents in a city can lead to multiple stationary equilibria, and how temporary shocks to the number of commuters can permanently affect the structure of cities by selecting a different stationary equilibrium.

Remote work has been linked to changes in residential and commercial housing prices within and across cities (Mondragon and Wieland, 2022; Gupta et al., 2022; Brueckner et al., 2021; Liu and Su, 2021; Ramani and Bloom, 2021; Althoff et al., 2021). Our finding that residential housing rent gradients with respect to distance to the CBD are diverging between larger and smaller cities is, to our knowledge, a new fact. We also provide an interpretation for this fact, since these housing rent gradients map directly into structural parameters of our model.³ We show how the divergence between larger and smaller cities is predicted by our model, given that larger cities are more likely than smaller cities to converge to the remote-work-intensive stationary equilibrium.

Understanding the productivity of remote work relative to in-person work remains an active area of research. Building on earlier studies (Oettinger, 2011; Cappelli and Keller, 2013), recent work indicates that remote workers may perform better than in-person workers in some contexts (Choudhury et al., 2022; Bloom et al., 2022; Barrero et al., 2021; Etheridge et al., 2020; Bloom et al., 2015). However, workers employed in occupations involving a significant amount of problem-solving tend to experience lower performance when working remotely (Emanuel et al., 2022; Künn et al., 2020). Gibbs et al. (2023) study employee productivity before and during the COVID-19 pandemic among skilled professionals at an Indian information technology services company. They find that employee productivity fell by 8% to 19%, and point to higher communication costs and longer time spent on coordination activities and meetings as sources for this decline. They also find that employees networked with fewer individuals and business units, both inside and outside the firm.⁴ Other studies emphasize that the higher earnings of remote workers can be partly explained by their selection into remote work based on unobservable characteristics (Harrington and Emanuel, 2022; Atkin et al., 2022). Our model recognizes workers' heterogeneous preferences for remote work (Mas and Pallais, 2017; Lipowska et al., 2022). Our analysis of the NLSY79 provides new estimates of the remote work premium from non-experimental data that account for unobserved persistent heterogeneity in worker performance. Our findings indicate that the technology of remote work has been improving steadily over the past decades while remaining less productive than in-person work on average across occupations.

³Duranton and Puga (2019) also link housing rent gradients to the elasticity of urban costs with respect to city size.

⁴See also Yang et al. (2022). They find that firm-wide remote work resulted in a less collaborative network among workers, with fewer connections between different parts.

Agglomeration economies are a central tenet of urban economics (Henderson, 2003; Combes et al., 2012). When cities successfully bring people together, positive spillovers abound. People interact, learn from each other, and foster entrepreneurship, leading to greater productivity within the city (Moretti, 2004; Gennaioli et al., 2012; Glaeser and Maré, 2001; Baum-Snow and Pavan, 2011; De La Roca and Puga, 2016).⁵ We contribute to the literature examining urban agglomeration economies by studying how remote work alters their workings. Canonical theories of cities predict that more central locations command higher house prices because of better accessibility to the locus of production (Alonso, 1964; Muth, 1969). By removing the need to travel across locations to reach the workplace, remote work deprives cities of one of their most fundamental organizational principles. The main insight from our analysis is that cities with strong agglomeration externalities, typically viewed as successful, are also the most at risk of dramatic shifts in their structure when people choose to stay home. Similar to us, Owens et al. (2020) uses coordination problems generated by residential externalities to rationalize the existence of depopulated and successful neighborhoods with similar underlying characteristics in Detroit.

The remainder of the paper is organized as follows. Section 2 presents stylized facts on remote work that emphasize the sudden increase in remote work since 2020, despite no large increase in the earnings premium for remote work. Section 3 documents the widely heterogeneous post-pandemic experience across cities in trips to the CBD (Subsection 3.1) and housing value gradients (Subsection 3.2), before considering alternative explanations and presenting an intuitive case for multiple stationary equilibria (Subsection 3.3). Section 4 presents our dynamic monocentric model with a choice of labor delivery mode. Section 5 quantifies the model, including our estimation of the relative productivity of remote work and externality parameters. We evaluate the ability of our estimated model to rationalize the evolution of commuting across cities in Section 6 and compute the resulting welfare implications in Section 7. We relegate many of the model’s and quantification’s details, additional robustness exercises, and counterfactuals to the Appendix.

2 The Evolution of Remote Work

We begin by documenting changes in the shares of workers delivering work remotely and changes in the hourly earnings’ remote work premium between 1980 and 2023. We rely on two data sources. First, we use the decennial census waves of 1980, 1990, and 2000, and the annual American Community Survey waves between 2005 and 2023. From this source, we obtain large repeated cross-sectional information on the individual earnings per hour of workers who work in person or remotely. Second, we use the National Longitudinal Survey of Youth 1979 (NLSY79), a panel of 4,147 individuals from which we collect information on the number of hours of remote work, hourly pay, and occupation every two years from 1998 to 2022. The repeated observations of the same workers allow us to control for permanent unobserved heterogeneity among workers and

⁵The productivity premium in larger cities has also been linked to the combination of more efficient firms and workers selecting these areas (Combes et al., 2008; D’Costa and Overman, 2014; Gaubert, 2018).

obtain estimates of the remote work premium that are not biased by selection on unobservable characteristics (Harrington and Emanuel, 2022; Atkin et al., 2022). We provide details about the construction of our samples in Appendix A.2.

Remote work has become an increasingly common form of labor delivery over the past few decades.⁶ While part of this increase is likely due to improvements in communication technologies or remote work preferences, another part may arise via gradual changes in the composition of the labor force, both in terms of educational attainment and employment by occupation and industry. Our first exercise aims at removing the effect of compositional changes.

In Figure 1a, we report time-varying estimates of a logit model for the probability of being a remote worker. We use Census/ACS and NLSY data separately. In both datasets, we control for workers' education, gender, age, marital status, race, experience on the job, and broad industry and occupation fixed effects. In the Census/ACS data, we define as "remote workers" those who report working from home when asked about their means of transportation to work. In the NLSY data, we define as "remote workers" those who work for more than 24 hours (i.e., three days) at home in a week. We then predict the shares of remote workers, varying the year and setting the values of all covariates to their mean value over the sample: these shares can be interpreted as the probability of being a remote worker for someone with typical and time-invariant characteristics.⁷ Both datasets reveal a small and gradual rise in the share of remote work over time and a sudden post-pandemic jump. In the ACS, this share increases from less than 1 percent in 1980 to 2.6 percent in 2019, jumping to 12 percent in 2020 and peaking at 15 percent in 2021, before returning to 11 percent in 2023. The NLSY features a similar pattern, increasing from 1.4 percent in 1998 to 3.7 percent in 2018, then rising to 9.2 percent in 2020, before dropping back to 7.8 percent in 2022. Importantly, since these patterns control for individual characteristics and compositional changes, the gradual increase is likely due to changes in technology or remote work preferences, but the large change in 2020 is probably related to the pandemic.

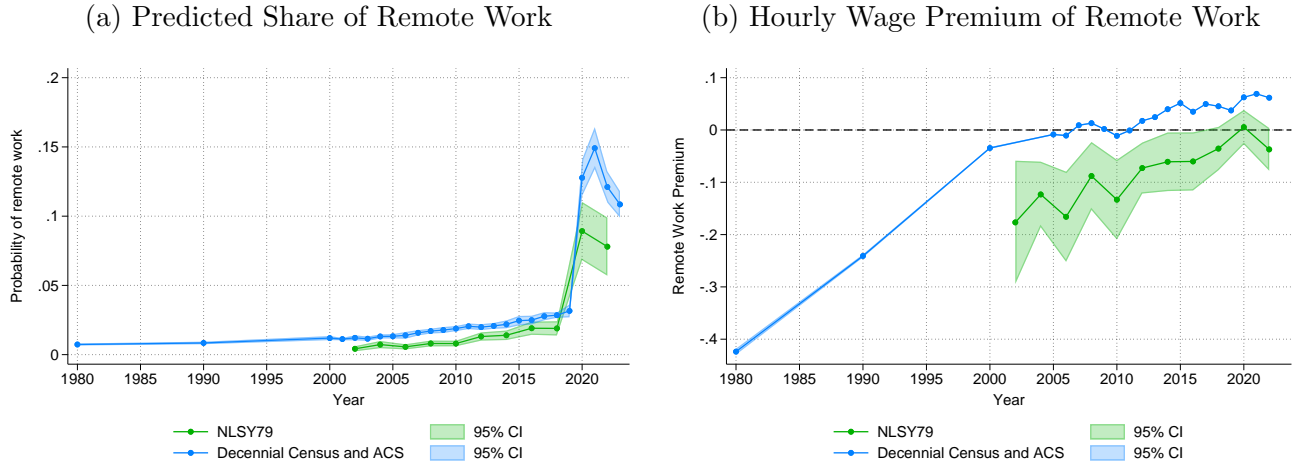
In Figure 1b, we estimate the hourly wage premium of remote work relative to in-person work over time. In the Census/ACS data, we regress log hourly wages on year-specific indicators of remote work, the same controls as those used in the logit model described above, and allowing in addition for year-specific effects for occupation, industry, education, region, and demographics. In the NLSY data, we complement the specification by adding individual fixed effects. Both exercises indicate a steady increase in the premium for remote work. Estimates from the ACS data indicate that, in 1980, remote work implied a discount of 44.5 percent in hourly rates compared to in-person work; in 2022, remote workers with similar observable characteristics earned 6.5 percent higher earnings relative to observationally equivalent office workers.⁸ In the NLSY sample, the discount for remote work went from 18.5 percent in 2000 to 3.1 percent in 2022. The stronger wage discount in the NLSY is consistent with remote workers having unobserved characteristics that make them

⁶Statistics typically report the share of all working hours performed at home over time Oettinger (2011); Cappelli and Keller (2013); Liu and Su (2023)

⁷In Table A1 of Appendix A.2, we report the actual share of remote workers over time as measured in the ACS.

⁸The ACS series stops in 2022 since the 2023 ACS did not report industry codes at the time of analysis.

Figure 1: Prevalence and Earnings Premium of Remote Work



Panel (a) reports the predicted share of remote workers from a logit model with year fixed effects and controlling for workers' education, gender, age, marital status, race, experience on the job, and broad industry and occupation fixed effects. The estimates report the predicted probability that an individual with sample-average characteristics is a remote worker in any given year. Panel (b) reports the coefficients on yearly remote work indicators from a regression of log hourly wages on all the Panel (a) controls plus year-specific effects for occupation, industry, education, region, and demographics. In the Census/ACS data, “remote workers” are defined as those reporting working from home when asked about their means of transportation to work. In the NLSY data, “remote workers” are defined as those who work for more than 24 hours at home per week. Each point represents an estimate for a year. The shaded areas represent the 95 confidence interval around the estimates.

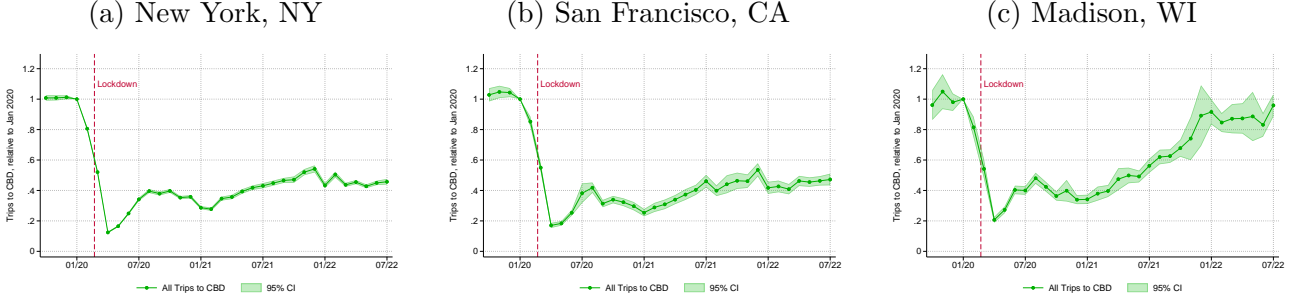
higher earners, everything else equal. Remarkably, the remote work premium did not increase substantially between 2018 and 2022.⁹ This is consistent with the large increase in remote work being driven by other mechanisms rather than by a large productivity increase of remote work. The sudden increase in the probability of remote work, coupled with a stable wage discount, is consistent with the rapid shift to remote work being driven by mechanisms other than large remote work productivity or preference shocks. In the next section, we present evidence and articulate the case of multiple equilibria as such a mechanism.

3 Heterogeneous Responses Across Cities

Individual decisions to reduce social contact during the pandemic and the related stay-at-home policies had dramatic consequences on the level and evolution of commuting and the value of proximity to the CBD across cities. We provide evidence of this impact using individual cell phone mobility data and estimates of the gradient of housing prices relative to distance to the CBD. We

⁹In Figure A1 of Appendix A.5.2, we show that this stability is also present separately for occupations with high and low teleworkable indices, as defined by Dingel and Neiman (2020).

Figure 2: Change in Visits to the CBD for Selected Cities



Estimates of monthly indicators in a separate regression for each CBSA of visits to the CBD at the block group-month level. The outcome variable is the number of visits to the CBD from the specified block group, divided by the number of residing devices in that block group, as defined in (37), scaled by the value of this ratio in January 2020. The shaded areas represent the contour delimited by the consecutive 95 percent confidence intervals of each monthly indicator. Standard errors are clustered at the census tract of origin.

argue that, taken together, the evidence we provide can be rationalized only with mechanisms that allow cities to respond in drastically different ways to a common lockdown shock. Multiplicity of stationary equilibria provides such a mechanism.

3.1 The Evolution of Commuting Patterns Across Cities

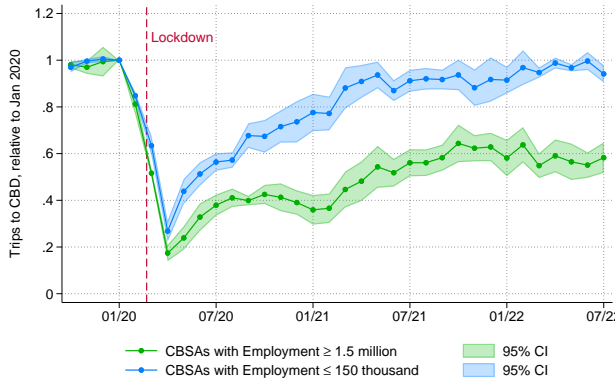
To analyze individual mobility, we use anonymized data from SafeGraph, a data provider that tracks foot traffic to businesses relying on mobile phone GPS locations from third-party applications. We use the Neighborhood Patterns dataset, which aggregates the amount of foot traffic at the census block group level, to study the monthly evolution of trips to the CBD.¹⁰ We first make use of the SafeGraph data to define the location of CBDs in each CBSA. The Neighborhood Patterns dataset provides information on the number of monthly visits recorded in each census block group. In particular, these visits are broken down by their most likely purpose, based on their observed characteristics.¹¹ We identify the center point of the CBDs as the center of a disc with a radius of 2 kilometers that receives the largest amount of work-related foot traffic. We then include all the block groups within this 2-kilometer disk into the CBD. We also allow cities to have several CBDs. We provide the details of our procedure in Appendix A.6.

The Neighborhood Patterns dataset also records the number of visits to each destination block

¹⁰Chapple et al. (2023) also use SafeGraph data to document patterns of downtown foot traffic in 62 North-American Cities. They combine SafeGraph data with another private data source to obtain estimates until 2023. Their results confirm that, while downtown visits have recovered to pre-pandemic levels in some smaller cities, they have stabilized between 40 and 60 percent of their pre-pandemic levels in most larger cities, with little change between July 2022 and April 2023.

¹¹Workplace visits are defined as those recorded Monday through Friday between 7:30 am and 5:30 pm and that dwelled for at least six hours. While the workplace visit count is missing for many CBSAs and census block groups in each CBSA, the coverage is sufficient to compute the version of Figures 2 and A4 for office trips only in Appendix A.8. We find similar patterns.

Figure 3: Visits to the CBD Relative to January 2020



The figure reports the estimates of the average volume of visits to the CBD from block groups located in i) CBSAs with total employment above 1.5 million (25 largest CBSAs), ii) CBSAs with total employment below 150,000 (663 smallest CBSAs) expressed as a share of their values in January 2020. The shaded areas represent the contour delimited by the consecutive 95 percent confidence intervals of each monthly indicator. Standard errors are clustered by month and census region.

group by block group of origin, allowing to compute bilateral flows of foot traffic at the monthly level.¹² On average, SafeGraph tracks around 30 million devices each month between January 2020 and July 2022.¹³ However, the number of mobile phones recorded in a city and the set of block groups of origin in which they are located vary across months. Some of the variation in the raw counts of foot traffic is therefore due to changes in the size of the sample and in the set of origin block groups included in the dataset. We control for these variations by analyzing the change in foot traffic flows at the origin block group level. In particular, we compute the share of monthly foot traffic originating from each block group that is directed to the CBD, we normalize the share of visits to the CBD from each origin block group by its value in January 2020, and then regress the normalized origin block group-level shares of visits to the CBD on month indicators.¹⁴

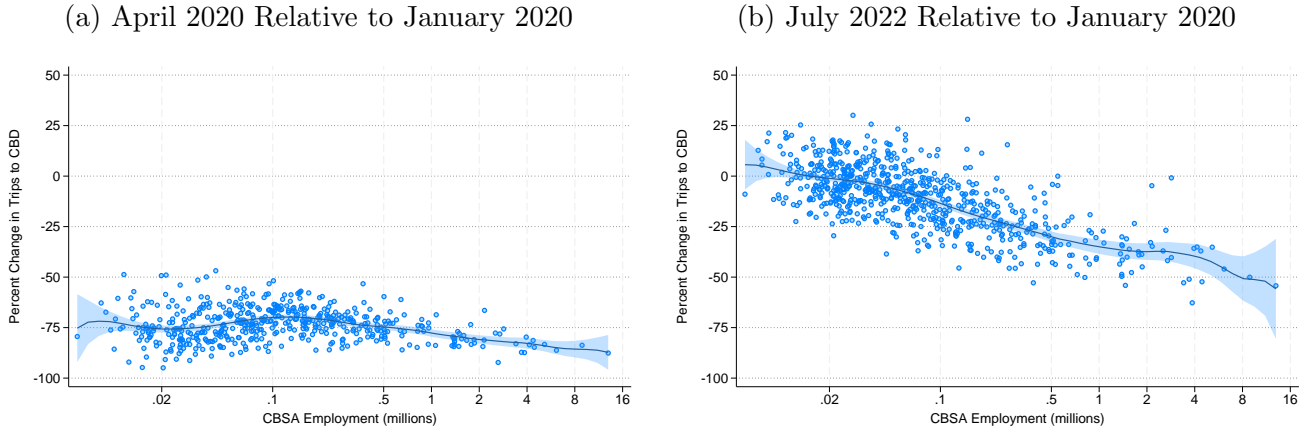
Figure 2 shows the volume of monthly trips to the CBD over the course of the pandemic, relative to its value in January 2020, for New York, NY, San Francisco, CA, and Madison, WI. For all three cities, the first months of the pandemic saw a drastic drop in trips to around 20 percent of their initial value. The recovery, however, has been quite different. While Madison, a relatively smaller city, essentially went back to its pre-pandemic levels by the end of our sample period, CBD trips for larger cities like New York and San Francisco have stabilized at around 40 percent of their

¹²The block group of origin is imputed by assigning to each mobile phone the block group in which the phone is recorded at night as the block group of residence.

¹³In the largest cities (New York, Los Angeles, Chicago), between 400,000 and 800,000 devices are recorded each month.

¹⁴Chapple et al. (2023) measure foot traffic by counting visits to downtown businesses, scaled by the sampling rate of the state. Instead, we count visits from any block group to downtown block groups, scaled by the sampling rate of each origin block group. That is, we control for changes in sampling rates across neighborhoods of each city, which we view as more robust than using the state-level sampling rate.

Figure 4: Response of Trips to the CBD



Panel (a) reports the change in the average level of visits to each CBSA's CBD between January 2020 and April 2020, against employment (BEA). Panel (b) reports the change in visits to the CBD in July 2022 relative to January 2020. Each marker represents a CBSA. The solid line represents a fitted kernel-weighted local polynomial smoothing, with the shaded area corresponding to the 95 percent confidence interval around the fitted value.

pre-pandemic levels, a dramatic drop.

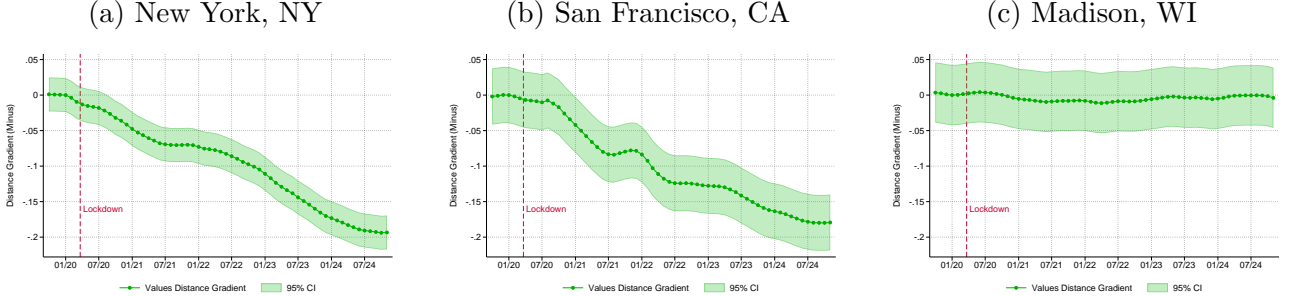
This behavior is, in fact, systematic. Figure 3 shows the monthly trips to the CBD relative to January 2020 for cities grouped by size. Our measure of size is total non-farm employment in the CBSA in 2019, published by the Bureau of Economic Analysis.¹⁵ The green line reports the estimates of the trips to the CBD for the largest CBSAs with employment of more than 1.5 million, while the blue line collects the smallest CBSAs in our sample, with employment below 150,000.¹⁶ We normalize to 1 the number of trips in January 2020. Both groups experienced a sharp decline to less than 30 percent of pre-pandemic trips up to April 2020, but their paths are remarkably different afterward: while the group of small CBSAs returned to their pre-pandemic levels of visits to the CBD around early 2021, large CBSAs stabilized at around only 60 percent of their initial level.

Figure 4 considers the relation of trips with city size in more detail. In the left panel, we show the extent to which these trips declined in April 2020 compared to January 2020, plotted against the city's total employment. Trips to the CBD declined by about 75 percent of the pre-pandemic level on average, with only little variation in the experiences of different cities. Importantly, this initial drop does not appear related to city size. In contrast, city size is systematically related to the return-to-office for the latest available data. The right panel of Figure 4 shows that in July 2022,

¹⁵This measure has the advantage of being available for all CBSAs, allowing us to describe patterns of recovery for the largest set of CBSAs—847 in total. In Appendix A.18, we reproduce the key graphs from Section 3 using as size the measure of employment used in the quantification, computed from Census microdata, and consistent with our measure of commuting. We confirm that the patterns described below hold for the subset of CBSAs for which we can measure employment in the Census.

¹⁶The smallest CBSA with employment above 1.5 million is Austin, TX, while the largest CBSA with employment below 150,000 is Rochester, MN.

Figure 5: Change in Housing Values Gradients for Selected Cities



Estimates of monthly coefficients for log distance between zip codes and the CBD, relative to their value in January 2020. In a separate regression for each CBSA, we regress log housing values at the zip code level, on log distance by month, and geographic controls. The shaded areas represent the 95 percent confidence intervals of each monthly indicator, computed from robust standard errors. Data on housing values from Zillow's ZHVI index.

the largest cities are substantially more likely to have trip levels way below their pre-pandemic levels.

3.2 Descriptive Evidence: Distance Gradients in House Prices

The previous section showed that the evolution of flows to the CBD has been heterogeneous across cities. Of course, changes in remote work patterns imply changes in demand for housing within cities. As workers spend less time on-site, a short commute becomes less important, leading to lower demand for housing next to centers of economic activity, and, everything else equal, a lower premium for proximity to the CBD.

Changes in urban land gradients may be driven by a large number of factors varying at the CBSA level. Some of these include constraints on local housing development (Gyourko et al., 2008; Saiz, 2010; Lutz and Sand, 2022) or the connectivity between urban and suburban parts of the CBSA.¹⁷ For this reason, we estimate the CBSA-specific price and rent gradients in our bid-rent regression. We use monthly housing price zip code level data from Zillow.¹⁸ This high-frequency data allows us to follow the monthly changes in housing prices for many cities since 2019.

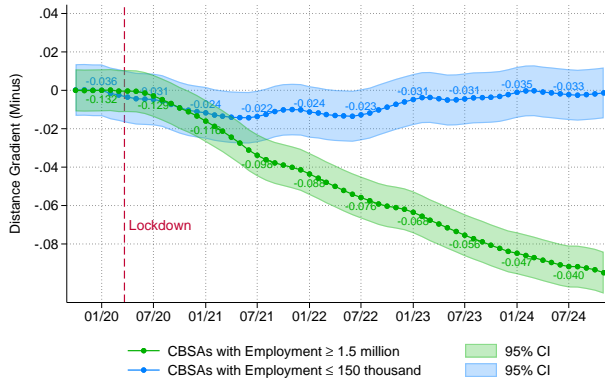
Indexing CBSAs by j , zip codes by i , and months by t , we estimate the monthly slope of the bid-rent function, using the following empirical specification,

$$\ln p_{ijt} = \delta_{jt} \ln(dist_{ij}) + \beta X_{ij} + \alpha_{jt} + e_{ijt}, \quad (1)$$

¹⁷See Bailey et al. (2018) for measures of social connections using Facebook data.

¹⁸The monthly housing price dataset is the Zillow Home Value Index (ZHVI). Zillow also publishes the Zillow Observed Rent Index (ZORI), a monthly housing rent data that would be a closer analog to the ACS rent data. However, the ZORI is reported for fewer zip codes, making the estimation of the gradient imprecise for many CBSAs.

Figure 6: Distance Gradient of Housing Prices Relative to January 2020



This figure reports the difference between the average housing price gradients in January 2020 and each following month, using the same employment thresholds as in Figure 3. In this figure, 25 cities have employment above 1.5 million and 225 have employment below 150,000. A negative value for the difference in housing price gradients implies a lower premium for housing located close to the CBD. The value of the average housing price gradient in each group is reported next to the marker of the associated group every six months. The shaded areas represent the contour delimited by the consecutive 95 percent confidence intervals of each monthly indicator.

where units of observation are zip code-months. We refer to p_{ijt} as the price in zip code i of CBSA j in month t , and $dist_{ij}$ is the distance in kilometers between the centroid z_{ij} of zip code i and the CBD of CBSA j . We include CBSA-month fixed effects, α_{jt} , and zip code level control variables, X_{ij} . The zip code controls contain the log of median household income, the share of households in the top national income quintile, the median age, and the share of Black residents, all measured in 2019, and geographic controls.¹⁹

Figure 5 plots the time evolution of $-(\delta_{jt} - \delta_{jt_0})$, the drop in the distance coefficient at time t relative to the baseline of January 2020: a decrease in the reported coefficients constitutes a flattening of the price gradient. Consistent with the evidence presented in Figure 2, we find that the willingness to pay for proximity to the CBD is permanently lower in New York and San Francisco, while it barely starts decreasing before returning to its initial values in Madison.

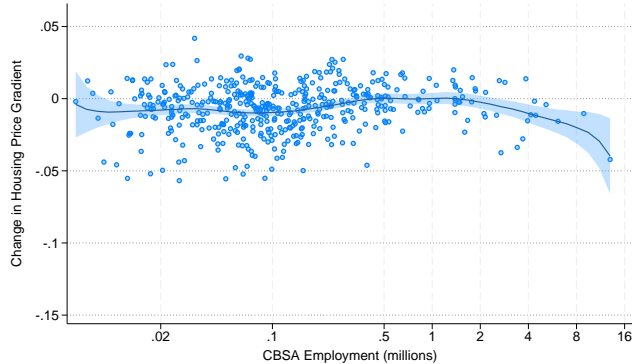
Figure 6 shows the average distance elasticity of house prices relative to January 2020 for the same group of city sizes as in Figure 3. In particular, the vertical axis reports again $-(\delta_{jt} - \delta_{jt_0})$, the drop in the distance coefficient at time t relative to the baseline of January 2020, so that a decrease in the reported coefficients implies a flattening of the price gradient. Quite naturally, prices move more slowly than trips over time. All cities experience a flattening of the housing price gradients of around 0.01 by January 2021. This decline stops and reverses for small cities, which return to around their pre-pandemic level; the drop in the gradient of larger cities, instead, persists and appears to stabilize around 0.095 by the end of 2024.

Figure 7 illustrates the cross-sectional variation as a function of city size in the drop of housing

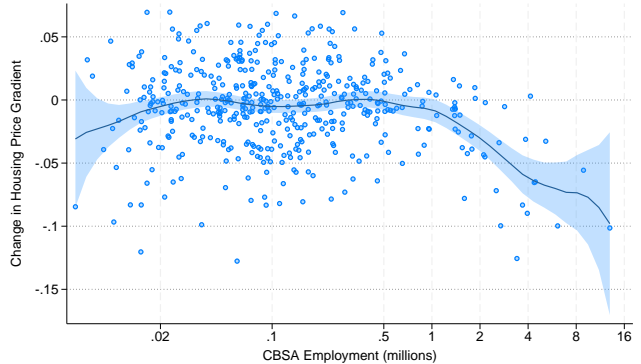
¹⁹The geographic controls are the tract-level controls in footnote 41, averaged by zip code, using tract population as weights.

Figure 7: Response of House Price Gradients

(a) January 2021 Relative to January 2020



(b) November 2024 Relative to January 2020



This figure reports the difference between the housing price gradients in January 2020 and November 2024, against employment (BEA). Each marker represents a CBSA. The gradients are estimated using zip code level data from Zillow for 278 CBSAs. A negative value for the difference implies a lower premium for housing located close to the CBD. The solid line represents a fitted kernel-weighted local polynomial smoothing, with the shaded area corresponding to the 95 percent confidence interval around the fitted value.

price gradients at two different points during and after the pandemic. As above, the vertical axis represents the drop in the distance coefficient at time t relative to the baseline of January 2020. During the first year of the pandemic (January 2020 to January 2021, left panel), the distance elasticity of housing prices flattened by about 0.01 on average. This drop is sizeable relative to the average price gradient in January, equal to -0.044. The heterogeneity is moderate and again unrelated to city size. Consistently with evidence on CBD trips, however, the flattening in the price gradient becomes negatively associated with city size as the pandemic progresses and then recedes (right panel).

3.3 Potential Explanations

The dramatic changes in large cities documented in the last two subsections have received the most attention from researchers. However, our results stress that not all cities have followed the same path after the COVID-19 pandemic commuting shock. In particular, the return of smaller cities to their pre-pandemic structure is a salient feature of the post-pandemic experience as well.

Existing explanations for the sharp increase in remote work rely on large and sudden increases in either aggregate remote work productivity or worker preferences (or a combination thereof).²⁰ These rapid and large technology and preference changes, however, should have produced some noticeable changes across *all* cities, including those that, as we document, have reverted to pre-

²⁰Davis et al. (2024) calibrate a short-term increase in remote work productivity of 83% among high-skilled workers. Parkhomenko and Delventhal (2024) opt for a calibration combining a rise in remote work productivity of about 10% with a decline in the aversion to remote work of 46 to 70%.

pandemic conditions. Of course, cities differ in their share of employment amenable to remote work, so even a large nationwide improvement in remote work productivity or attractiveness might affect remote work adoption only moderately in cities with low shares of teleworkable employment. However, [Dingel and Neiman \(2020\)](#) estimate that this share varies from 25 to 55 percent across CBSAs. Hence, at least one-fourth of jobs remain teleworkable even in the cities least amenable to remote work, while in the city most apt to remote work, almost one in two workers are employed in non-teleworkable occupations. In our data, cities that fully returned to pre-pandemic CBD trips by July 2022, and for which there is little to no change in the willingness to pay for proximity to downtown by the end of 2024 still have 34 percent of workers employed in teleworkable occupations. While large country-level changes in preferences or productivity should then imply permanent change in trips to the CBD or distance-rent gradients even in small cities, our evidence does not detect such a change. Importantly, the share of teleworkable occupations in cities with a permanent decline of at least 40 percent in trips to CBD is 43 percent, a higher - but not sufficiently higher - value to explain the large differences in the evolution of commuting across cities. Although plausible, explanations based on large preference or technology shocks appear, at best, incomplete in reproducing the full range of heterogeneous behavior that we uncover.

A related series of candidate explanations suggest that cities differ in other characteristics, unrelated to occupational composition, which produce differential evolution of commuting patterns. One possibility, for example, is that large cities can be congested, making commuting to the city center costly and workers more willing to transition to remote work. If congestion was the main driver of these patterns, however, we would expect a lower propensity to travel to the CBD even before the pandemic. Yet, the data reveal the opposite pattern. In particular, over the last three months of 2019, 30.6 percent of all trips in CBSAs with employment above 1.5 million were directed toward the CBD, compared with only 15.6 percent in CBSAs with fewer than 150 thousand workers. This higher rate of CBD trips in larger CBSAs is consistent with the idea that those cities' central areas are congested precisely because workers want to have access to the wages and benefits they provide.

A second possibility is that the differential behavior of large and small cities is driven by differential employment concentration across establishments. In particular, if smaller CBSAs are more likely to host large establishments, they may be more likely to return to high levels of commuting if those establishments participate in bringing workers back to the office. We examine this possibility in Appendix A.11 by estimating, for each CDSA the share of employment accounted for by the largest 5% and 10% of establishments. We find that employment is in fact *less* concentrated in smaller cities than in larger ones. We interpret this finding as indicative that the differential rates of return to the office between large and small CBSAs are unlikely to be facilitated by the idiosyncratic decisions of the largest establishments.

Another possibility is that, during the pandemic, workers shifted towards occupations that are more amenable to remote work. This shift might be driven, for example, by national changes in preferences or technology. However, we see no footprint of these changes in the wage premium by

occupations. In Appendix A.5.2, we re-estimate the wage premium dividing occupations according to how amenable they are to remote work, using the Dingel and Neiman (2020) index. Figure A1 shows no differential evolution of this premium over the pandemic years. Regardless of the evolution of the wage premium, we could still observe the patterns described in the sections above if employment shifted towards teleworkable occupations at a higher rate in larger than in smaller cities. In Appendix A.12 we examine this possibility in detail. We find that, in the wake of the pandemic, the share of teleworkable employment increased by about 5%, a value much smaller than the large drops in foot traffic; crucially, by the end of 2023 the share of teleworkable employment increased *more* in smaller CBSAs (7.9%) than in larger ones (5.8%). This finding makes it unlikely that differential changes in the occupational composition can explain the patterns we have described.

While all plausible, these arguments appear limited in their ability to jointly reconcile all the pieces of evidence we have uncovered. This evidence highlights the need for a theory that rationalizes heterogeneous responses across cities to a common shock to the number of commuters. The theory we propose rationalizes heterogeneous responses depending on whether a city exhibits multiplicity of stationary equilibria, which in turn depends on the balance between agglomeration externalities, occupational composition, and commuting costs. In particular, when externalities are the main reason for downtown's attractiveness and so a city features multiplicity, high levels of pre-pandemic commuting were only one possible stationary equilibrium. In those cases, the pandemic shock can move the city to a dynamic path that converges to a stationary equilibrium with much higher levels of remote work.

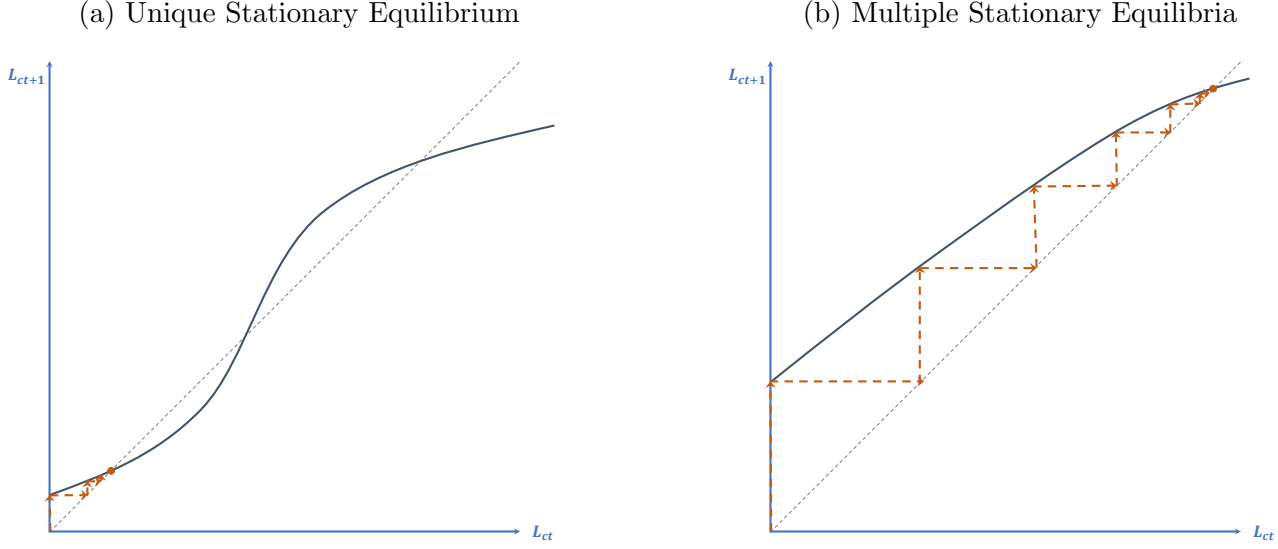
To illustrate this intuition, Figure 8 presents a phase diagram for the dynamics of the number of commuters in our model. The axes represent the number of computers in two adjacent periods. All stationary equilibria are represented as crossing with the 45-degree line, where the number of commuters (the state variable) is constant over time. We compare how a city with a single stationary equilibrium (left panel) and a city with multiple stationary equilibria, initially in the high-commuting stationary equilibrium (right panel), respond to the same commuting shock.²¹

From the stationary equilibrium with high levels of commuting, this shock initially reduces the measure of commuters $L_{c,t}$ to almost zero. Subsequently, as the restrictions are lifted and public confidence returns, individuals re-optimize their labor delivery mode. The set of incentives workers face, however, is now different between the two city structures.

In cities with a unique equilibrium, the aggregate number of commuters $L_{c,t}$ has limited influence on the net individual benefit of working in the office. In this environment, technology is the primary determinant of wage differentials, and the amenity value of being downtown is largely independent of the CBD's overall vibrancy. Because externalities have little impact on individual choices, the city's fundamentals ultimately restore the initial equilibrium, as depicted by the path of the orange line in Panel (a).

²¹Here, and in all of the phase diagrams below, we implicitly assume a unique dynamic equilibrium. Although we cannot exclude the presence of multiple dynamic equilibria, Appendix B.6 provides extensive testing suggesting that this possibility is limited in practice.

Figure 8: Heterogeneous Responses to Lockdown Shocks



This figure shows the adjustment towards the stationary equilibrium in the case of unique vs. multiple stationary equilibria. In both panels, the orange line depicts the adjustment towards a stationary equilibrium following an initial shock that brings the number of commuters $L_{c,t}$ to zero. The dashed gray line in the right panel shows the 45-degree line. When the stationary equilibrium is unique (left panel), the city returns to the initial stationary equilibrium. With multiple stationary equilibria, the city converges to the low-commuting one.

In contrast, the economy's fundamentals are not the sole determinant of the final aggregate state of cities with multiple stationary equilibria. In this case, the current number of commuters powerfully shapes the incentives to return to the office. A lockdown pushing the city into low commuting levels significantly alters the individual productivity differential in favor of remote work. While travel congestion may decrease, the allure of the downtown area also diminishes, and the amenity value of working in the central business district vanishes. As illustrated by the orange line in Panel (b) of Figure 8, the city finally settles into a low commuting stationary equilibrium. Since the number of commuters is permanently lower, the rent gradient is also flatter and closer to zero. This logic explains how the same temporary shock can have large permanent effects in some cities and no effect in others. It also explains why pre-pandemic changes in preferences and technology that did not change the stationary equilibrium only led to marginal effects on the number of commuters.

Equipped with this intuition, we set up the formal model in Section 4 and derive testable predictions on the existence of multiple equilibria for multiple cities. We then investigate in Section 5 whether cities like Madison are predicted to respond like Panel (a) of Figure 8, whether cities like New York and San Francisco are predicted to respond like Panel (b), and the welfare and cross-city implications of these different responses.

4 Model

4.1 Overview

We model a disk-shaped city with an exogenous population of size L .²² Each city location houses one resident. Time is discrete. A worker starts period t in a labor delivery mode $\ell \in \{c, m\}$ (commuting or remote) that has been determined the previous period, and is thus fixed within the period. The worker chooses a residence location, housing quality, and consumption, supplying labor according to mode ℓ . Workers then see their idiosyncratic shocks $\varepsilon_t = \{\varepsilon_{ct}, \varepsilon_{mt}\}$ for each choice, make a labor delivery mode decision for next period, and enjoy the associated idiosyncratic benefit. These benefits are drawn from a Gumbel distribution with location parameter $\tilde{\gamma}$ (the Euler constant) and scale parameter s , $G(\varepsilon) = \exp\{-e^{\varepsilon/s-\tilde{\gamma}}\}$. The current period ends, and in the next one the new composition of labor delivery modes is again pre-determined.

The city's layout is radially symmetric with respect to the central business district (CBD). Locations are indexed by $d \in [0, +\infty)$, where d represents distance from the CBD. Production occurs in the CBD, at $d = 0$. Land is owned by absentee landlords. A worker living in location d pays a rent $r(d)$ per unit of housing. Land has an alternative use that yields an exogenous return equal to r_a and landowners can enhance it to supply the units of housing demanded by the household.

In what follows, we describe a simple production environment and then formalize the problem of a worker. The within-period part determines indirect flow utilities and the city rent function. The dynamic part determines the transition shares across labor delivery modes, and hence the aggregate evolution of the city. We conclude with a characterization of the equilibrium of a city.

4.2 Production

There are two goods in the economy: final consumption and housing. Final consumption is a homogeneous good produced in the CBD by profit-maximizing firms under constant returns to scale: one efficiency unit of labor produces one unit of good, at a constant marginal cost of \bar{w} .²³ The number of efficiency units of a worker, and hence her total wage w_ℓ , both depend on the chosen labor delivery mode ℓ . In particular, define

$$\tilde{L}_c \equiv L_c^\mu L^{1-\mu} \tag{2}$$

as the aggregate measure of labor units delivered in the city center, a function of the current number of commuters L_c , the total city size L , and the fraction of days per week a remote worker

²²In Appendix A.9 we explore in detail possible systematic relations between changes in population changes and trips to the CBD. We find that population changes have been too limited, and too uncorrelated with the post-Covid behavior to threaten the plausibility of this assumption.

²³Our model abstracts from heterogeneous occupations. This choice is motivated by the empirical findings, in Appendix A.12, that transitions between occupations differentially amenable to remote work are too rare to be an empirically relevant margin of adjustment at our time horizon.

spends at home, μ . Then, the wage of commuters and remote workers (really *mixed* workers since they spend only a fraction of their work time at home) is given by²⁴

$$w_\ell \equiv \begin{cases} w_c \equiv \bar{w} \cdot A \tilde{L}_c^\delta & \text{if } \ell = c, \\ w_m \equiv \bar{w} \cdot z^\mu (A \tilde{L}_c^\delta)^{1-\mu} & \text{if } \ell = m. \end{cases} \quad (3)$$

In particular, the efficiency units offered by a commuting worker depend on the in-office productivity, $A > 0$, and on how many workers are on average in the CBD, \tilde{L}_c , with an elasticity $\delta > 0$. The efficiency units of a remote worker are a combination of the efficiency of remote work $z > 0$, and the efficiency of commuting work, weighted by the fraction of time remote workers spend on each mode. Free entry in production implies $\bar{p} = \bar{w} = 1$, after a normalization.

Absentee landlords invest their effort to produce housing on their unit-size plot and receive $r(d)$ per unit of housing. Land has an alternative use that yields r_a .

4.3 Problem of the Worker

A worker starts period t in state $\ell \in \{c, m\}$, solves a within-period problem delivering a flow utility u_ℓ , observes idiosyncratic shocks associated with the next period's labor delivery mode options, and makes a new choice ℓ' .

4.3.1 Within-Period Problem

We write the within-period problem of a worker in state ℓ , in a city with L_c commuters, as

$$u_\ell(L_c) = \max_{Q_\ell, H_\ell, d} \log T^{\mu_\ell} \left(\frac{B(\tilde{L}_c)}{\tau(\tilde{L}_c)d^\gamma} \right)^{1-\mu_\ell} Q_\ell^\alpha H_\ell^{1-\alpha}, \quad (4)$$

$$\text{s.t.} \quad \mu_\ell \equiv \begin{cases} 0 & \text{if } \ell = c \\ \mu \in (0, 1] & \text{if } \ell = m \end{cases}, \quad (5)$$

$$w_\ell = Q_\ell + r(d)H_\ell. \quad (6)$$

where we have omitted the time index. The worker chooses consumption of a homogeneous good, Q_ℓ , housing H_ℓ , and housing location d . μ_ℓ is the fraction of days per week spent at home in mode ℓ . Amenity and disutility terms include $T > 0$, a benefit of working from home; $B(\tilde{L}_c)$, a benefit of visiting the CBD, increasing in \tilde{L}_c ; $\tau(\tilde{L}_c)$, the general level of congestion in commuting, also increasing in \tilde{L}_c , and commuting costs d^γ , where $\gamma > 0$ captures the elasticity of commuting costs to distance. The exponent $\alpha \in (0, 1)$ is the weight of consumption in utility. Workers obtain

²⁴In Appendix A.13, we show that this wage structure is the outcome of a linear production function in remote and in-person workers. More generally, if we use a CES production function and estimate the elasticity of substitution between these two types of labor, we find very large values. This finding motivates our linear production function.

a wage w_ℓ described in (3), and spend it on consumption, with a price normalized to one, and housing with unit price $r(d)$.

Our formulation captures the key trade-offs between commuting and remote work. On the amenity side, remote work allows an individual to enjoy the flexibility of working from home and paying lower commuting and congestion costs, at the price of lower enjoyment of the social and consumption opportunities in the CBD, all for a fraction μ of the time. On the wage side, remote work trades off the positive externalities arising from in-office interactions with the efficiency of communication technology z , again for a fraction μ of the time. The scale of economic activity in the CBD, as measured by \tilde{L}_c , shapes the balance of these tradeoffs: when more agents visit the city center, individual productive efficiency is higher, the CBD is more lively, but congestion is heavier.

4.3.2 Dynamic Problem

The solution to the within-period problem described above delivers the within-period utility flow. The worker then observes two new idiosyncratic shocks for the next period's labor delivery mode, $\varepsilon_{\ell't}$, and chooses ℓ' accounting for the evolution of the state of the economy. In particular, the dynamic decision of a worker who starts the period in state ℓ is

$$U_\ell(\{\varepsilon_{ct}, \varepsilon_{mt}\}; L_{ct}, \omega^t) = u_\ell(L_{ct}) + \max_{\ell' \in \{c, m\}} \{\beta V_{\ell'}(L_{ct+1}; \omega^{t+1}) - F_{\ell\ell't} + \varepsilon_{\ell't}\}, \quad (7)$$

where $\omega^t \equiv \{\omega_k\}_{k=t}^{+\infty}$ and $\omega_t \equiv \{A_t, z_t, F_{\ell\ell't}, T_t, B_t(\cdot), \tau_t(\cdot)\}$ is a known exogenous sequence of (possibly) time-varying technology, fixed costs, and amenities, and

$$V_\ell(L_{ct}; \omega^t) = \int_{\varepsilon_m} \int_{\varepsilon_c} U_\ell(\{\varepsilon_c, \varepsilon_m\}; L_{ct}, \omega^t) dG(\varepsilon_c) dG(\varepsilon_m), \quad (8)$$

is the expected utility of a worker starting in state ℓ if L_{ct} workers are commuting. In these expressions, $F_{\ell\ell't}$ is the cost of transitioning from mode ℓ to mode ℓ' at time t .²⁵ Although the theory can accommodate any non-negative values, we will set $F_{\ell\ell} = 0$ for $\ell \in \{c, m\}$. The term ε_ℓ is the idiosyncratic shock received by the worker in mode ℓ .

²⁵Note that, in the flow utility, the willingness to pay to live close to the CBD is a function of the labor delivery mode choice: agents will enjoy the remote work utility only if they pay the associated switching cost. As in standard urban models, the average utility of agents is equalized *across* locations where commuters live, and *across* locations where remote workers live, as a consequence of the first-order condition for residence location choice, d ; the average flow utility, however, is not equalized between commuters and remote workers. Hence, the fixed cost F should be interpreted as jointly capturing the cost of changing labor delivery mode and of switching the residence location between any location where commuters live and any location where remote workers live. Ultimately, it represents the cost of accessing the average flow utility of a different state.

4.4 Equilibrium

We start by defining a within-period equilibrium condition that has to hold at each time, given the current distribution of commuters and remote workers. We then define a dynamic equilibrium, which describes the evolution of the economy when the within-period equilibrium holds at each time, and forward-looking workers make commuting and remote work choices based on—and consistent with—the aggregate evolution of the economy. Finally, we define a stationary equilibrium as a dynamic equilibrium where all endogenous variables are constant.

4.4.1 Within-Period Equilibrium

We now define a within-period equilibrium. In the section, we eliminate the time index to simplify notation.

Definition 4.1 Given L_c and ω , a within-period equilibrium is a rent function $r(d)$, $d \in [0, L]$ and an allocation $\{Q_c, Q_m, H_c, H_m\}$ such that i) individuals solve (4)-(6), ii) firms maximize profits and free entry drives profits to zero and iii) the housing market clears.

We construct a within-period equilibrium by first solving for consumption and housing demand conditional on a distance, and then letting the agent pick the distance that delivers the highest (indirect) utility. From the Cobb-Douglas structure, we have

$$Q_\ell = \alpha w_\ell, \tag{9}$$

$$H_\ell(d) = \frac{(1-\alpha)w_\ell}{r(d)}, \tag{10}$$

which implies an indirect utility of

$$u_\ell = \log \bar{\alpha} T^{\mu_\ell} \left(\frac{B(\tilde{L}_c)}{\tau(\tilde{L}_c)d^\gamma} \right)^{1-\mu_\ell} \frac{w_\ell}{r(d)^{1-\alpha}}, \tag{11}$$

with $\bar{\alpha} \equiv \alpha^\alpha (1-\alpha)^{1-\alpha}$, for $\ell \in \{c, m\}$. Taking the first-order conditions for the optimal distance to the CBD yields

$$\frac{r'_\ell(d)d}{r_\ell(d)} = -\frac{\gamma(1-\mu_\ell)}{(1-\alpha)} \implies r_\ell(d) = k_\ell d^{-\frac{\gamma(1-\mu_\ell)}{(1-\alpha)}}, \tag{12}$$

where $r'_\ell(d)$ is the slope of the rent function in the segment relevant to workers with delivery mode ℓ , and k_ℓ is a constant of integration. At the optimal residence location, the savings on rents of a marginally farther location exactly compensate for the increased disutility in travel time. Since remote workers suffer less for a given travel time increase (by eq. (5), $\mu_m \equiv \mu \in (0, 1] > \mu_c = 0$), their willingness to pay for proximity to the CBD is lower. Hence, commuters live in $[0, \bar{d}]$, remote workers live in $[\bar{d}, \bar{D}]$, where \bar{D} is the outer boundary of the city, and the equilibrium rent function has a steeper (constant) elasticity for commuters than for remote workers.

In our formulation, these conditions translate into a constant elasticity rent, with constants of integration k_c and k_m . These constants of integration k_c and k_m are characterized by two no-arbitrage conditions. First, the rent per unit of housing in the last residence location has to coincide with the alternative land use r_a , so that $r_m(\bar{D}) = r_a$. Second, land owners must be indifferent between renting to commuters and remote workers at $d = \bar{d}$, so that $r_c(\bar{d}) = r_m(\bar{d})$. Using these two conditions, the equilibrium rent function is

$$r(d) = \begin{cases} (\bar{D}/d)^{\gamma/(1-\alpha)} (\bar{d}/\bar{D})^{\mu\gamma/(1-\alpha)} r_a & \text{if } d < \bar{d} \\ (\bar{D}/d)^{(1-\mu)\gamma/(1-\alpha)} r_a & \text{if } d \geq \bar{d} \end{cases}. \quad (13)$$

An implication of this result is that the average elasticity of rent to distance κ is given by

$$\kappa \equiv \frac{1}{\bar{D}} \int_{x=0}^{\bar{D}} \frac{\partial r(x)}{\partial x} \frac{x}{r(x)} dx = -\frac{\gamma}{1-\alpha} \left[(1-\mu) + \mu \frac{\bar{d}}{\bar{D}} \right]. \quad (14)$$

In this circular city, the total number of units in the disk of radius \bar{d} is $\pi\bar{d}^2$ and must equal the number of residents L_c in that disk. Similarly, $\pi\bar{D}^2 = L$. These conditions imply that $\bar{d} = (L_c/\pi)^{1/2}$ and $\bar{D} = (L/\pi)^{1/2}$. Hence, the rent gradient reflects the strength of distance frictions, as measured by γ , and the average value of being close to the CBD, as proxied by the commuting population L_c .

A within-period equilibrium is then described by this rent function, and the allocation implied by equations (9)-(10). The indirect utility function (11) then becomes,

$$u_\ell = \begin{cases} \log \left[r_a^{\alpha-1} \bar{\alpha} \left(\frac{B(\tilde{L}_c)}{\tau(\tilde{L}_c)} \right) w_c / (\bar{d}^\mu \bar{D}^{1-\mu})^\gamma \right] & \text{if } \ell = c \\ \log \left[r_a^{\alpha-1} \bar{\alpha} T^\mu \left(\frac{B(\tilde{L}_c)}{\tau(\tilde{L}_c)} \right)^{1-\mu} w_m / \bar{D}^{\gamma(1-\mu)} \right] & \text{if } \ell = m \end{cases}. \quad (15)$$

These indirect utilities of each labor delivery mode are an element of the dynamic problem of a worker, to which we now turn.

4.4.2 Dynamic Equilibrium

A worker starts the period in state ℓ and enjoys the utility flow u_ℓ . The worker then observes two new idiosyncratic shocks $\varepsilon_{\ell't}$ and decides the new state for next period ℓ' , accounting for the exogenous evolution ω^t and the aggregate measure of commuting workers, L_{ct+1} .

The evolution of the measure of commuting workers is governed by the law of motion²⁶

$$L_{ct+1} = L_{ct} \lambda_{cct} + (L - L_{ct}) (1 - \lambda_{mmt}), \quad (16)$$

²⁶All calculations are reported in Appendix B.1.

where the share of workers in state ℓ transitioning to ℓ' is given by

$$\lambda_{\ell\ell't} = \frac{\exp(\bar{\varepsilon}_{\ell\ell't}(L_{ct+1})/s)}{\exp(\bar{\varepsilon}_{\ell ct}(L_{ct+1})/s) + \exp(\bar{\varepsilon}_{\ell mt}(L_{ct+1})/s)}. \quad (17)$$

Naturally, the term $\bar{\varepsilon}_{\ell\ell',t}(L_{ct+1})$ denotes the average value of switching from ℓ to ℓ' and is given by

$$\bar{\varepsilon}_{\ell\ell't}(L_{ct+1}) \equiv \beta [V_{\ell'}(L_{ct+1}; \omega^{t+1}) - V_\ell(L_{ct+1}; \omega^{t+1})] - (F_{\ell\ell't} - F_{\ell t}). \quad (18)$$

We are ready to define a dynamic equilibrium, as well as a stationary equilibrium.

Definition 4.2 *Given a known exogenous sequence of parameters $\{\omega^t\}_{t=0}^{+\infty}$ and an initial condition $0 \leq \bar{L}_{c0} \leq L$, a dynamic equilibrium is a pair of value functions V_ℓ , $\ell \in \{c, m\}$ and a matrix of transition probabilities $\lambda_{\ell\ell't}$, $\ell, \ell' \in \{c, m\}$ such that equations (8) and (17) hold, and the state of the economy evolves according to (16), with $L_{c0} = \bar{L}_{c0}$.*

Definition 4.3 *Given a time-invariant sequence of exogenous parameters $\omega \equiv \{\bar{\omega}\}_{t=0}^{+\infty}$, a stationary equilibrium is a dynamic equilibrium where all endogenous variables are constant over time.*

Throughout the text, we focus on multiplicity of stationary equilibria. In principle, the model might feature multiple equilibria, something we have not fully explored theoretically. In our numerical exercises, we have not found indications of the presence of such multiplicity.

4.4.3 Characterization of Stationary Equilibria

To discuss the existence and other properties of stationary equilibria, we specify the shape of $B(\cdot)$ and $\tau(\cdot)$, and ensure that the model does not deliver corner solutions. In the rest of the paper, we maintain the following two assumptions.

Assumption 1 *$B(\cdot)$ and $\tau(\cdot)$ are isoelastic functions:*

$$B(\tilde{L}_c) \equiv \bar{B}\tilde{L}_c^\xi \text{ and } \tau(\tilde{L}_c) = \bar{\tau}\tilde{L}_c^\theta, \text{ with } \bar{B}, \bar{\tau}, \xi, \theta > 0.$$

Assumption 2 *The dispersion in the idiosyncratic shocks is large enough:*

$$s > \mu^2 \left(\xi + \delta - \theta - \frac{\gamma}{2\mu} \right).$$

Assumption 1 allows a characterization of stationary equilibria in terms of comparisons among (constant) elasticity values. Assumption 2 guarantees that as an economy approaches a purely remote equilibrium, the average value of switching from commuting to remote goes to $-\infty$.

Proposition 4.1 *There always exists at least one stationary equilibrium.*

Proof. See Appendix B.2. ■

The proof makes a formal case that, under Assumptions (1) and (2), any stationary equilibrium is always interior regardless of the switching costs. On one hand, the average benefit of switching to commuting approaches $+\infty$ when almost everybody is working remotely, which causes the number of commuters to stay above zero. On the other, when almost all employees commute, the number of remote workers tends to stay above zero. Since the law of motion for L_c is continuous, there must be at least one level of current commuters for which the number of commuters in the following period remains constant.

Having established existence, we now investigate the properties of the set of stationary equilibria in this economy. Proposition 4.2 establishes that if agglomeration forces are weak enough, there is a unique stationary equilibrium.

Proposition 4.2 *Assume $\delta + \xi < \theta + \gamma/(2\mu)$. Then there is a unique stationary equilibrium. The stationary equilibrium value of the commuting population L_{css} monotonically increases with A and \bar{B} , and monotonically falls with Z , T and $\bar{\tau}$.*

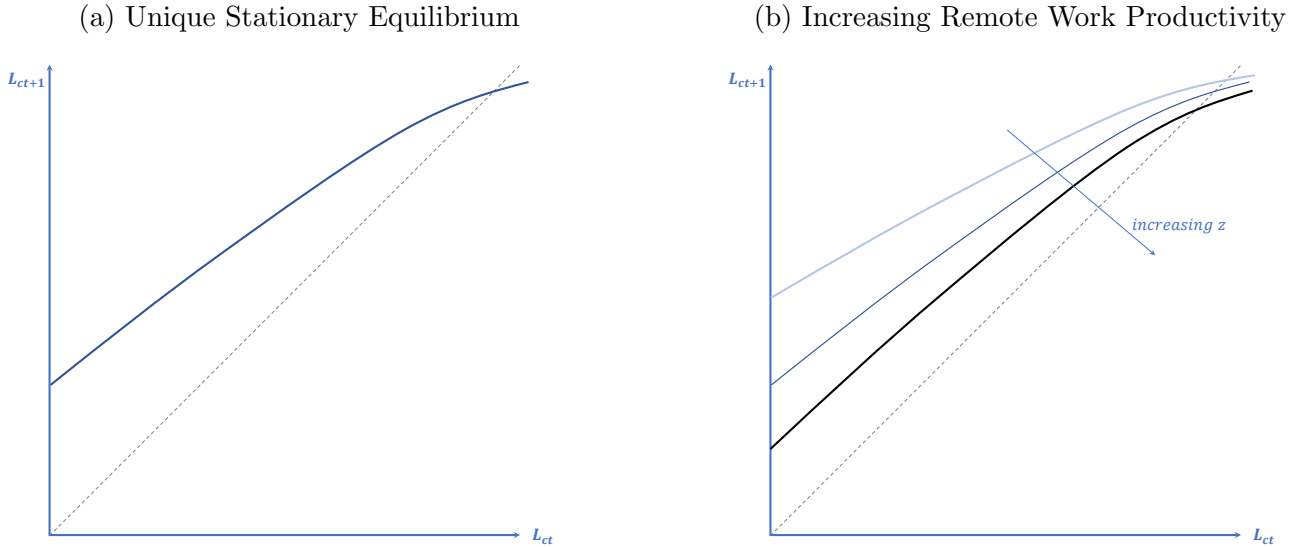
Proof. See Appendix B.3. ■

A unique stationary equilibrium requires that having more commuters increases the individual incentive to become a remote worker. We can break down this individual incentive into two parts: the current benefit of working remotely instead of commuting, and the option value of becoming a remote worker. If the measure of commuters increases, the option value of becoming a remote worker always grows - a dynamic congestion force. Under the assumptions of Proposition 4.2, static congestion forces dominate agglomeration forces and so the current net benefit, $u_m - u_c$, from being a remote worker also increases with the number of commuters. This is sufficient for uniqueness. The left panel of Figure 9 depicts a typical phase diagram for this case. The blue line indicates how the measure of commuters changes from one period t (horizontal axis) to the next $t + 1$ (vertical axis). The city's unique stationary equilibrium occurs at the crossing with the dashed 45° line. A city below the stationary equilibrium value will experience an increase in the number of commuters over time. However, congestion forces will eventually slow this growth as the number of commuters rises.

Increases in office productivity A and amenity benefits \bar{B} reduce the static gains of remote work, lowering the share of commuters that switch to remote work. These changes would move the blue line up and to the left, increasing the number of steady-state commuters. Conversely, improvements in the efficiency of remote work Z or its amenity benefit, T , or higher commuting frictions $\bar{\tau}$ increase the motivation to move to remote work, pushing the line down and to the right, and reducing the equilibrium number of commuters. Panel (b) of Figure 9 shows the consequences of a progressive improvement in remote work productivity. This is reminiscent of the gradual and modest adjustment in the number of commuters before the pandemic, likely in response to advances in information and communication technology.

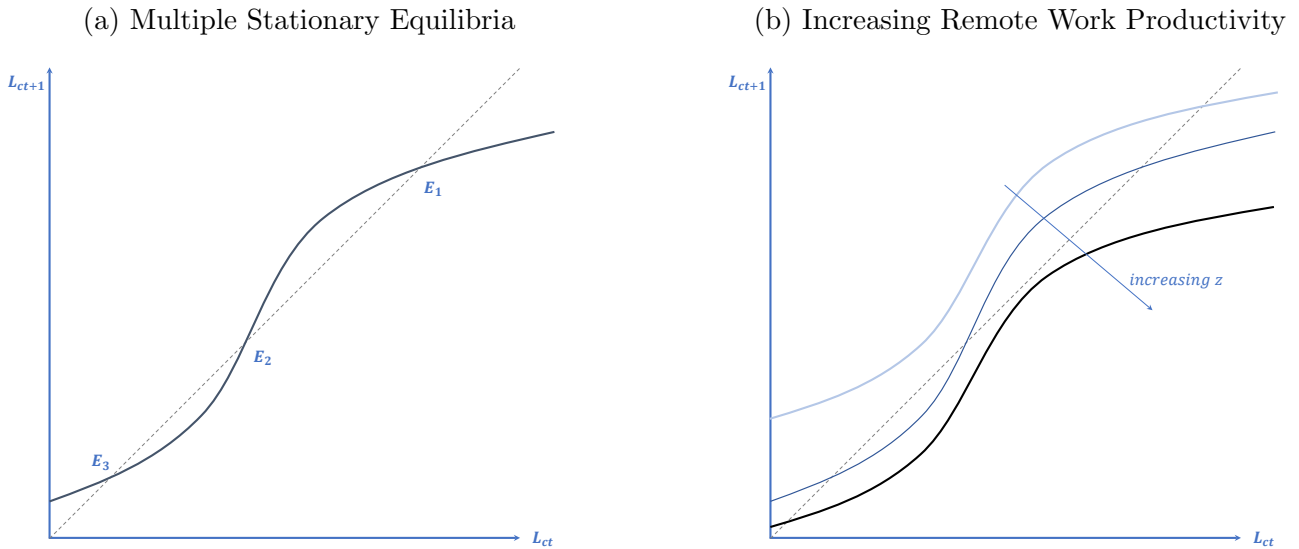
The discussion above suggests that multiplicity can arise when an increase in the number of commuters strengthens the incentive to become a commuter. These conditions occur when static

Figure 9: Phase Diagram for a Unique Stationary Equilibrium



The left panel of this figure shows a typical phase diagram for a city with a unique stationary equilibrium. The right panel shows how the phase diagram shifts in response to increases in remote work productivity, from the light blue line to the black line. In both panels, the dashed gray line is the 45-degree line.

Figure 10: Phase Diagram for Multiple Stationary Equilibria



The left panel of this figure shows a typical phase diagram for a city with multiple stationary equilibria. The right panel shows how the phase diagram shifts in response to increases in remote work productivity, from the light blue line to the black line. In both panels, the dashed gray line is the 45-degree line.

agglomeration forces overcome dynamic congestion forces. The left panel of Figure 10 illustrates a typical phase diagram for this scenario with three stationary equilibria, E_1 , E_2 , and E_3 . If a city is located between E_1 and E_2 , the number of commuters increases towards E_1 . However, if a city is situated between E_2 and E_3 , the number of commuters decreases until it reaches the stationary equilibrium E_3 . Thus, E_2 is an unstable stationary equilibrium, and any perturbation away from it will cause the city to depart from that equilibrium.

Perhaps surprisingly, strong agglomeration forces alone are not sufficient for multiplicity. The right panel of Figure 10 shows that the phase diagram shifts down and to the right, from lighter to darker colors, as remote work efficiency improves. If remote work is not efficient, having fewer commuters does not increase the relative incentive to work from home enough to induce more workers to work remotely. Conversely, if remote work is highly efficient, the “high commuting” equilibrium vanishes as the incentive to switch to remote work is consistently strong. Proposition 4.3 makes this intuition formal and characterizes the “cone of multiplicity,” namely, the set of parameters for which we obtain multiplicity of stationary equilibria.

Proposition 4.3 *Suppose $F_{cc} = F_{mm} = 0$. Then, there exist a finite threshold $\eta_{min} > \theta + \gamma/(2\mu)$, and a set $\mathcal{Z} \subset \mathbb{R}_{++}$, such that:*

- i) *for $\delta + \xi > \eta_{min}$, \mathcal{Z} is a non-empty interval (Z_{min}, Z_{max}) and there are multiple stationary equilibria if $z/A \in \mathcal{Z}$; further, Z_{min} and Z_{max} are functions of all the parameters of the model, they grow with L and \bar{B} , and fall with T and $\bar{\tau}$;*
- ii) *there is a unique stationary equilibrium in all other cases.*

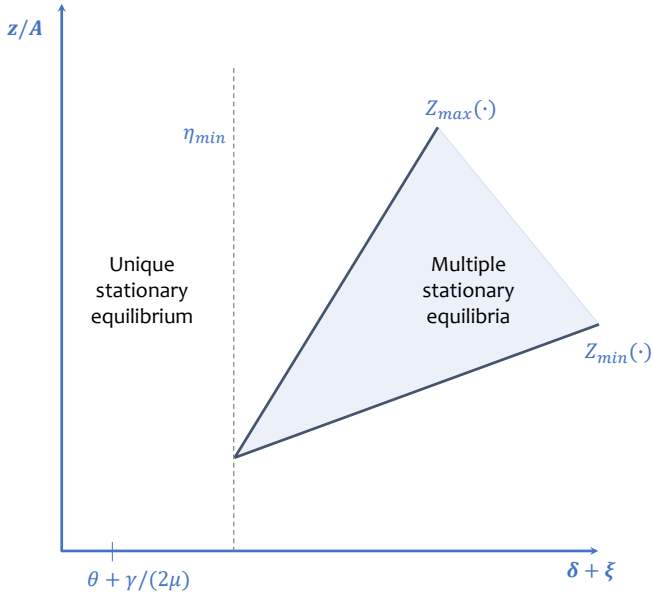
Proof. See Appendix B.4. ■

Figure 11 provides a visual representation of this Proposition. The figure displays the combinations of $(\delta + \xi, z/A)$ for which a city exhibits multiple stationary equilibria, holding the remaining parameters constant. When $\delta + \xi < \theta + \gamma/(2\mu)$, no values of z/A can generate multiple stationary equilibria. This is essentially a re-statement of Proposition 4.2.²⁷ If agglomeration forces are high enough ($\delta + \xi > \eta_{min} > \theta + \gamma/(2\mu)$), there is a range of z/A where the city exhibits multiplicity. Intuitively, η_{min} summarizes the minimum level of static and dynamic congestion forces that agglomeration forces need to overcome for multiple stationary equilibria to be possible, although not guaranteed: as in the right panel of Figure 10, the efficiency of remote work can neither be too low nor too high.

An implication of Proposition 4.3 is that for some values of z/A , increasing agglomeration forces will change the structure of the city from a single to multiple stationary equilibria. This fact is easily seen in Figure 12. In the left panel, we consider a movement from point P_1 , outside

²⁷Proposition 4.3 imposes $F_{cc} = F_{mm} = 0$, a slightly more restrictive assumption. Without it, \mathcal{Z} need not be an interval for low values of $\delta + \xi$. Instead, there are two thresholds, η_{min} and $\eta_{max} \geq \eta_{min}$; \mathcal{Z} is generally the union of disjoint intervals, and it is exactly one interval only when $\delta + \xi > \eta_{max}$. We believe it is reasonable to assume no fixed costs to remain in the same labor delivery mode. Therefore, we focus on this case in the main text.

Figure 11: Cone of Multiplicity

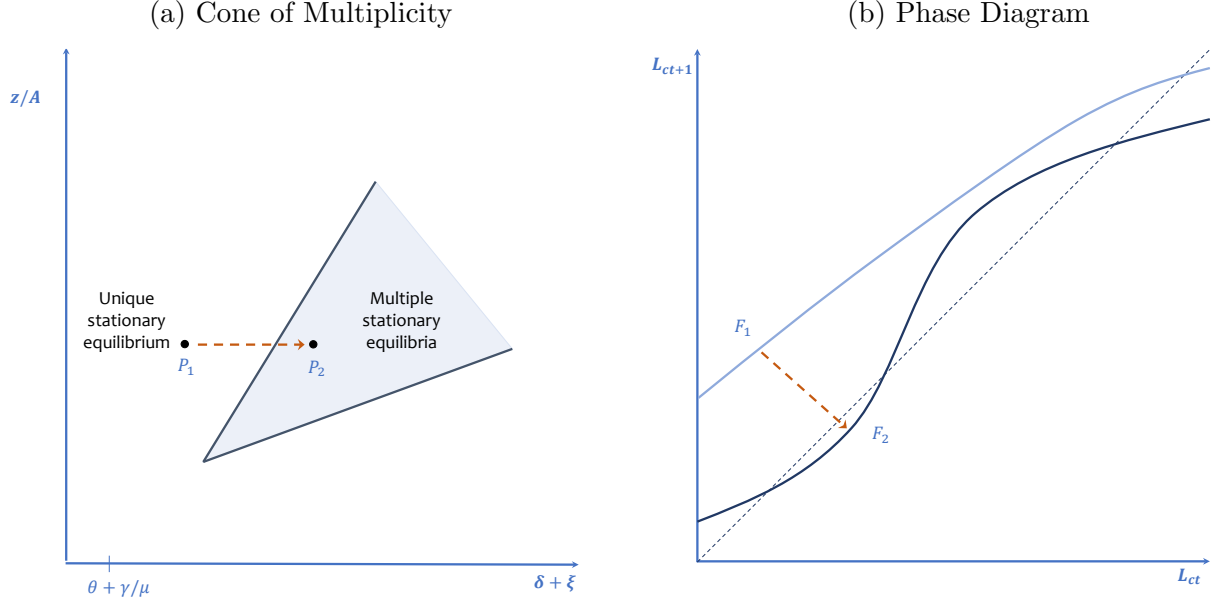


This figure represents the combinations of z/A and $\delta+\xi$ for which, given the remaining parameters, the city displays multiple stationary equilibria. Changes in the remaining parameters move the cone. The dashed gray line indicates the minimum value of agglomeration externalities that generate multiple stationary equilibria.

the cone of multiplicity, towards P_2 , inside the cone. We know this movement can be generically constructed because \mathcal{Z} is non-empty for at least some values of $\delta+\xi$. This comparison corresponds to the movement from the phase diagram F_1 to F_2 in the right panel. An increase in the strength of agglomeration forces exacerbates the role of coordination mechanisms and can create multiple stationary equilibria.

These results can speak to the organization of production in cities both in the long and short run. In the long run, secular trends alter the position of a city with respect to its cone. For example, the trends in remote work discussed in Section 2 suggest that a city with a high enough $\delta+\xi$ may traverse its cone from a single equilibrium to a region of multiplicity, and suddenly lose the high-commuting equilibrium in favor of the low-commuting one. From a shorter-run perspective, lockdown policies during the recent COVID-19 pandemic can be seen as a negative exogenous shock to the number of commuters. Our theory envisions heterogeneous adjustments across cities, depending on whether they find themselves inside or outside their cone when the shock occurs. We now turn to the estimation of the parameters of our model. After quantifying our model for most U.S. cities in Section 5, we relate the predictions of our model to the evidence in Section 6.

Figure 12: Implication of Higher Agglomeration Forces



This figure describes a comparison between low and high values of δ . The left panel shows that for some values of z/A , it is possible to move from a unique (P_1) to multiple (P_2) stationary equilibria. The right panel displays how the phase diagram changes from F_1 to F_2 in association with this move. The dashed gray line in the right panel shows the 45-degree line.

5 Quantification

When cities can potentially feature multiple equilibria, quantifying the model requires either taking a stand on which equilibrium the data is a realization of, or relying on relationships that hold in any equilibrium. For this reason, we rely entirely on data that was produced before 2019, a period during which every city was arguably in the high commuting equilibrium. More importantly, we only use predictions of the model that do not depend on which equilibrium—stationary or not—is being realized.

We quantify our model by estimating parameters that are specific to each Core-based Statistical Area in the United States when possible. We proceed in four steps. First, we estimate the dispersion of idiosyncratic preferences, which is inversely related to the elasticity of transitions into remote work with respect to earnings and the fixed cost of transitioning between delivery modes. Second, we construct estimates of the agglomeration externality in production. Third, we estimate the parameters of the remote work technology. Fourth, we estimate the transportation cost elasticity from city-specific measures of housing rent distance gradients.

5.1 Estimation of the Transition Elasticity and Transition Costs

We start with the identification of the variance of idiosyncratic preference shocks for labor delivery modes, the fixed costs, and a time trend for the amenity value of remote work. As in Proposition 4.3, we assume $F_{cc} = F_{mm} = 0$. We further assume that $F_{cm} = F_{mc} = F$, reducing the quantification of fixed transition costs to the identification of F . Following the work of Artuç et al. (2010) on the estimation of discrete choice models, and of Arcidiacono and Miller (2011) in the structural labor literature on conditional choice probabilities (CCPs), we exploit the log-linear relationship between observed transition probabilities across labor delivery modes and workers' payoffs, including transition costs, income, and continuation values. Through a linear regression, the elasticity of transitions between labor delivery modes is identified from the responsiveness of transitions to income changes, while fixed transition costs are additionally identified from the overall level of transitions.²⁸ We use the following result, which provides an expression of forward-looking relative transition probabilities as a function of the within-period flows of utility, transition costs F , and transition elasticity s only.

Lemma 5.1 Suppose $F_{cc} = F_{mm} = 0$ and $F_{cm} = F_{mc} = F$. Then

$$y_{\ell\ell't} \equiv \ln \frac{\lambda_{\ell\ell't} \lambda_{\ell'\ell't+1}^\beta}{\lambda_{\ell\ell't} \lambda_{\ell\ell't+1}^\beta} = \frac{\beta}{s} (u_{\ell't+1} - u_{\ell t+1}) - \frac{(1-\beta)F}{s}. \quad (19)$$

Proof. See Appendix B.5. ■

Intuitively, a sluggish response of transitions to differences in utility flows suggest that a large variance in idiosyncratic shocks (high s) is overshadowing the significance of those differences; conditional on a variance, high average gross flows are then indicative of small switching costs (low F) between states. Technically, this approach considers one-period deviations from an otherwise common sequence of labor delivery modes to difference out continuation values. We can write the difference in the utility flows from (15) as

$$u_{mt+1} - u_{ct+1} = \ln \frac{w_{mt+1}}{w_{ct+1}} + \mu \ln T_{t+1} - \mu \ln B(\tilde{L}_{ct+1}) + \mu \ln \tau(\tilde{L}_{ct+1}) + \frac{\gamma\mu}{2} \ln L_{ct+1} - \frac{\gamma\mu}{2} \ln \pi. \quad (20)$$

In order to obtain a specification that can be estimated in a linear regression, we maintain Assumption 1 about the parametric specification of the city-center amenity $B(\tilde{L}_c)$ and congestion $\tau(\tilde{L}_c)$, and assume that the remote work amenity takes the form of a log-linear function of time. That is, we let $T_t = \exp\{\alpha_0 + \alpha_1 t\}$. Our estimating equation can then be written as:

$$y_{\ell\ell't} = \eta_0 \cdot \ln \frac{w_{\ell\ell't+1}}{w_{\ell t+1}} + \eta_1 + d_{\ell\ell'} \cdot (\eta_2 + \eta_3 \cdot (t+1) + \eta_4 \cdot \ln L_{ct+1} + \eta_5 \cdot \ln L_{t+1}) + \hat{\varepsilon}_{\ell\ell't}, \quad (21)$$

where $d_{\ell\ell'} = 1$ is a discrete variable taking the value 1 if the transition is from commuting to

²⁸See Traiberman (2019) for an application to occupational and sectoral transitions.

remote, i.e. if $\ell\ell' = cm$ and takes the value -1 if the transition is from remote to commuting, i.e. $d_{\ell\ell'} = -1$ if $\ell\ell' = mc$, and $\hat{\varepsilon}_{\ell\ell't}$ is an expectation error.

With this specification, the estimated coefficients can be recovered according to

$$s = \frac{\beta}{\eta_0}, \quad F = -\frac{\beta}{1-\beta} \frac{\eta_1}{\eta_0}, \quad \alpha_0 - \ln \frac{\bar{B}}{\bar{\tau}} = \frac{1}{\eta_0} \left(\frac{\eta_2}{\mu} + \left(\frac{\eta_4}{\mu} - \frac{\eta_5}{1-\mu} \right) \ln \pi \right), \quad (22)$$

$$\alpha_1 = \frac{\eta_3}{\eta_0 \mu}, \quad \xi - \theta = -\frac{1}{\mu(1-\mu)} \frac{\eta_5}{\eta_0}, \quad \gamma = \frac{2}{\eta_0} \left(\frac{\eta_4}{\mu} - \frac{\eta_5}{1-\mu} \right). \quad (23)$$

In principle, we should compute $y_{\ell\ell't}$ for each city. However, the NLSY sample does not contain enough observations of these transitions to obtain them accurately for each city. This is especially true if we define remote work as spending three days per week or more at home, a choice that was rare before the COVID-19 pandemic.²⁹ For this reason, we impose additional assumptions to implement the estimation of (21). In our main specification, we partition cities based on four U.S. regions, the most precise geographic units recorded in the NLSY public-use data.³⁰ We define transition shares for each of these four regions and for two groups of educational attainment (with or without a college degree). That is, for each year we construct the empirical equivalent of $y_{\ell\ell't}^r$ in (21) for eight region-education groups, indexed by r . We define a remote worker as someone who spends at least 1 day per week at home to maximize the number of observed transitions.³¹

The construction of $y_{\ell\ell't}^r$ for each group r is based on the fraction of individuals $\lambda_{\ell\ell't}^r$ who make a transition to or from remote work between two consecutive periods of time. To compute these shares for each group r , we first control for the role of covariates other than education and region in driving the transition shares of each group that are not directly captured by our model. These include differences in the industrial and occupational composition across groups that could drive differences in transition shares. Specifically, we estimate a probit model for the share of remote workers, controlling for year-group r, t indicators, the role of age and experience, and occupation and industry fixed effects. We use as measures of $\lambda_{\ell\ell't}^r$ the predicted transition shares from our probit model for each group r , setting all other covariates to their mean value. We then assemble the yearly transition shares into the relative shares $y_{\ell\ell't}^r$, setting β to 0.96 on an annual basis, corresponding to a discount rate of about 4 percent.

To construct wages w_{ct}^r and w_{mt}^r , we follow a similar approach by removing the contribution of industrial and occupational determinants of the wage levels. We regress individual log hourly wages on age, tenure and their square, year-group r, t indicators, and person, industry, and occupation fixed-effects. We use the residuals from these regressions to obtain a measure of wages for each

²⁹Out of the 4,847 individuals observed between 2000 and 2018 in our sample, only 386 ever reported working remotely for 3 days per week, while 650 and 1,074 worked remotely two days or more per week, and one day or more per week, in at least one of the survey years, respectively.

³⁰The four regions are Northeast, North-Central, South, and West.

³¹In Appendix A.3.2, we conduct an alternative exercise assuming that cities can be partitioned into subsets that offer similar remote work conditions and define remote work as spending at least two days per week at home. We then combine the decisions of individuals in cities in a given subset and form transition shares at that level. We obtain similar parameter estimates.

year-group r, t after controlling for individual variation. The wage for a region is then the average residual wage for all the observations in a region-time. Finally, we construct measures of total employment L_t^r and of the number of commuters L_{ct}^r in each year-group r, t from the ACS.

Our model assumes workers are forward-looking and make decisions in period t based on wages in period $t + 1$. However, if the relative wages of remote workers and commuters are imperfectly observed by workers or measured with error, OLS estimates will likely yield downward-biased estimates of η_0 . We address this concern by using past values of the wage ratio as an instrument for the future ratio.

Table 1 reports the results of the estimation of (21) and the implied structural parameters.³² In the first two columns, we report the OLS and IV estimates from the specification in (21), respectively. Consistent with the intuition that workers only respond to the part of the wage ratio that they observe, better captured by using the past wage ratio as an instrument, the IV estimates of the coefficient on the log hourly wage difference are higher than the OLS estimates. They provide estimates of the elasticity of transitions to wages s , and of the fixed transition cost that are statistically significant at the 1 percent level. Note that, in practice, the number of commuters, L_{ct+1}^r , and total employment, L_{t+1}^r , are highly correlated, and so the coefficients on these two covariates are noisy.

We obtain an estimate of s equal to 0.30. We are not aware of existing estimates of this parameter. As indicated by the coefficient in the first row of Table 1, this value of s corresponds to an elasticity of transitions into remote work of 3.09. This elasticity can be interpreted in two slightly different ways. First, if we return to (19) and (20), it means that an increase of 1 percent in the wage of remote workers relative to the wage of commuters can induce an “acceleration” of transitions to remote work by 3.09 percent. That is, transitions into remote work would increase in period t to benefit from these higher wages—the numerator in the definition of $y_{\ell\ell't}$ —relative to transitions that would have occurred in period $t + 1$ —the denominator. Alternatively, one can easily show from (17) that the elasticity of the probability of transition to remote work λ_{cmt} (relative to the probability of not transitioning λ_{cct}) with respect to the relative *value* of remote work, $V_{mt+1} - V_{ct+1}$, is also β/s . That is, if the wage of remote workers relative to the wage of commuters were to increase permanently by 1 percent, then transitions into remote work would increase by 3.09 percent in period t .

Our estimate for the transition cost F is 1.78. Given the specification of the utility of consumption in log terms, we can interpret the cost F as being equivalent to giving up $100(1 - \exp(-F)) = 83$ percent of earnings in year t in order to transition into remote work. This large number is reminiscent of the very large transition costs estimated in structural labor models.³³ These large

³²The total number of possible observations is the product of the number of groups r (8) with the number of distinct years (9 for every two years between 2000 and 2016), times two for each direction of transition (to remote, or to commute), i.e. 144 observations. In practice, however, there are only 48 observations with non-missing values of $y_{\ell\ell't}^r$.

³³[Artuç et al. \(2010\)](#) estimate switching costs between occupations that are equal to at least four times annual wages. In their study of location decisions, [Kennan and Walker \(2011\)](#) estimate moving costs amounting to \$312 thousand 2010 dollars on average.

Table 1: Estimates of the Gravity Equation for Mode Transitions and Structural Parameters

Covariate	OLS $y_{\ell\ell't}^r$	IV $y_{\ell\ell',t}^r$	Parameter	OLS Estimates	IV Estimates
$\ln \frac{w_{\ell\ell't+1}^r}{w_{\ell\ell't+1}^r}$	1.955 (0.411)	3.092 (0.997)	s	0.471 (0.099)	0.298 (0.096)
$d_{\ell\ell'}$	4.559 (6.165)	3.924 (6.077)	F	2.816 (0.842)	1.783 (0.695)
$d_{\ell\ell'}(t+1)$	-0.078 (0.055)	-0.082 (0.067)	$\alpha_0 - \ln \frac{\bar{B}}{\bar{\tau}}$	3.887 (5.369)	2.115 (3.540)
$d_{\ell\ell'} L_{ct+1}^r$	-2.906 (14.589)	-1.465 (14.959)	α_1	-0.067 (0.050)	-0.044 (0.041)
$d_{\ell\ell'} L_{t+1}^r$	2.665 (14.368)	1.271 (14.730)	$\xi - \theta$	5.681 (30.650)	1.713 (19.991)
$cons$	-0.468 (0.103)	-0.469 (0.097)	γ	0.931 (5.949)	0.238 (3.870)
N	48	48			
R^2	0.26	0.19			

Robust standard errors in parentheses. Structural parameters estimated with the Delta method.

estimates for the cost F reflect the fact that despite the existence of wage differentials between labor delivery modes, the mobility of workers remains quite low.³⁴ Of course, if transitioning between modes also implies changing homes in order to live at the appropriate distance to the CBD, these large fixed costs are natural.

All other coefficients are imprecisely estimated, and we have no further guidance on the values for ξ , θ , α_1 and the combination $\alpha_0 - \ln(\bar{B}/\bar{\tau})$. Hence, we set them all to zero for the rest of our analysis, except for $\bar{\tau}$. The parameter $\bar{\tau}$ will be calibrated for each city to match the initial value of L_c/L , as described in Section 5.5.

5.2 Agglomeration Externalities

We estimate the agglomeration externality δ_j for each CBSA j . The interpretation of δ_j is the percentage increase in labor value added for a one-percent increase in the number of commuters to the CBD in city j .

Our estimation strategy relies on the expression of wages in equation (3), which we augment to allow for time varying in-office productivity A_{jt} . The wage of a commuter in CBSA j is therefore given by

$$w_{cjt} = A_{jt} \tilde{L}_{cjt}^{\delta_j}. \quad (24)$$

³⁴In Appendix A.3.2, we estimate s and F with the restricted-use version of the NLSY data that is geocoded at the county level. We obtain similar estimates.

Denoting with $S_{cjt} \equiv L_{cjt}/L_{jt}$ the share of commuters, and defining $\Delta x_t = x_t - x_{t-\Delta t}$ as the τ -period change in variable x , the change in commuters' wages in CBSA j is given by

$$\Delta \log w_{cjt} = \Delta \log A_{jt} + \mu \delta_j \Delta \log S_{cjt} + \delta_j \Delta \log L_{jt}. \quad (25)$$

where we have used the definition of \tilde{L}_c above. Equation (25) indicates that the wages of commuters should vary more with the share of commuters in cities with strong agglomeration externalities, and it is the basis for our estimation strategy of the agglomeration externality.

Our empirical strategy relies on the following steps. First, we define the empirical equivalent of the commuters' wage in CBSA j as the average wage \bar{w}_{cjt} of commuters in that CBSA after controlling for individual characteristics. See Appendix A.14.1 for details.

Second, we decompose the in-person log-productivity, $\log A_{jt}$, into a nationwide term, plus a city-specific linear trend, and a residual, $\log A_{jt} = \tilde{a}_t + \tilde{b}_j t + \tilde{c}_j + \tilde{u}_{jt}$, so

$$\Delta \log A_{jt} = a_t + b_j + u_{jt}, \quad (26)$$

where $a_t \equiv \Delta \tilde{a}_t$, $b_j \equiv \tilde{b}_j \Delta t$, and $u_{jt} = \Delta \tilde{u}_{jt}$.

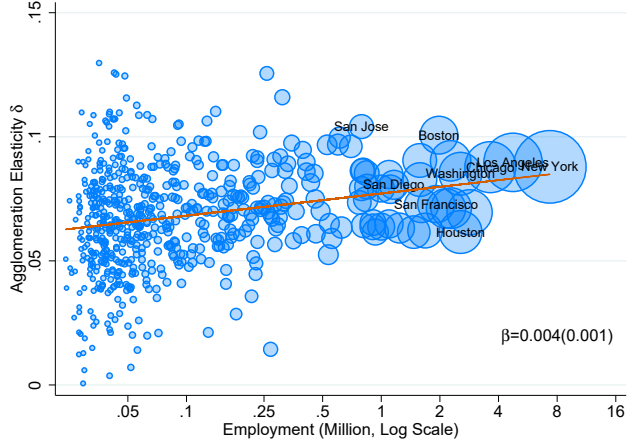
Third, we adopt an instrumental variables approach to isolate the variation in a CBSA's share of commuters that is orthogonal to the CBSA's changes in residual productivity u_{jt} . Variations in residual in-person productivity directly affect the commuters' wages, but they can also drive changes in the CBSA's total employment, L_{jt} , through migration, and in its commuting share S_{cjt} through changes in labor delivery modes. We identify the causal effect of changes in the share of commuters on wages by building a shift-share instrument.³⁵ For every year t and CBSA j , we predict the change in CBSA j 's share of commuters between $t - \Delta t$ and t , labeled IV_{jt} , as a function of its share of employment in each occupation s in $t_0 = 1980$, L_{sjt_0}/L_{jt_0} , and the economy-wide changes in occupation-specific commuter shares between $t - \Delta t$ and t , $\Delta \log S_{c,st}$. Namely, we define,

$$IV_{jt} = \sum_{s=1}^S \frac{L_{sjt_0}}{L_{jt_0}} \Delta \log S_{c,st}. \quad (27)$$

Fourth, we assume that agglomeration forces are specific to an industry and that CBSAs' effective agglomeration strengths differ due to their different employment shares in those industries. We follow Rossi-Hansberg et al. (2021) and consider five groups $g = 0, \dots, 4$, of industries along which agglomeration forces may vary: those industries are NAICS 1997-classifications of Retail, Utilities, and Construction (RUC), Health and education (HE), Professional and other services (PS), Manufacturing (M), Accommodation, trade, and transportation (ATT). We denote CBSA j 's labor-value-added weighted employment share in industry group g in 1980 by s_{gj0} , and postulate that CBSA j 's agglomeration externality takes the form $\delta_j = \beta_0 + \sum_{g=1}^4 \beta_g s_{g,j0}$. In conclusion, we

³⁵We treat the role of total employment L_{jt} as a city-specific slope without linking it to δ_j because of this potential endogeneity.

Figure 13: Agglomeration Externalities and CBSA size



This figure reports the city-specific δ_j against the CBSA's BEA employment. Each δ_j is estimated from eq. (28). The size of the circles represents CBSA's employment.

estimate

$$\Delta \log \bar{w}_{cjt} = a_t + b_j + \left(\beta_0 + \sum_{g=1}^4 \beta_g s_{gj0} \right) \Delta \log S_{cjt} + \gamma_j \Delta \log L_{jt} + u_{jt}, \quad (28)$$

using $s_{gj0}IV_{jt}$, $g = 1, \dots, 4$ as instruments for each interaction $s_{gj0}\Delta \log S_{c,jt}$. Table A8 in Appendix A.14.1 reports the estimates of individual coefficients. Combining the industry-specific IV coefficients with each CBSA j 's labor-value-added adjusted employment shares by group, we can form city-specific estimates of the agglomeration externalities δ_j . The summary statistics for these δ_j 's are reported in Table 2. Figure 13 shows these estimates, with mean value of 0.067 and standard deviation of 0.022, against employment for the 622 CBSAs in the sample. We estimate that a doubling in city size is associated to an elasticity 0.004 points higher on average.

5.3 Remote Work and In-Office Technology

We also estimate in-office and remote productivities A_{jt} and z_{jt} for each CBSA j . We develop further the exercise presented in Section 2 by estimating the remote work premium by occupation. Using data from the NLSY, we estimate the remote work premium for every incremental hour spent working from home. Specifically, we denote by $h_{remote,it}$ the number of hours worked at home, and predict $\hat{h} = 24$ hours per week, equivalent to three days per week of remote work.³⁶

We estimate a national trend and an intercept for each of the 22 occupation groups, denoted by o .³⁷ Specifically, we estimate

³⁶In Appendix A.5, we estimate the remote work premium from the ACS. Table A5 compares the two approaches.

³⁷We describe these occupation groups in Appendix A.4.

$$\ln w_{it} = (\psi_{o(i)}^0 + \psi^1 t) h_{remote_{it}} + X_{it} \beta_{o(i)} + \epsilon_{it}, \quad (29)$$

where $\ln w_{it}$ represents the log of the hourly wage for individual i at time t , $\psi_{o(i)}^0$ and ψ^1 represent the intercept for occupation group o and the national trend, respectively, and X_{it} is a vector of individual-level control variables, including age, age squared, tenure at the job, tenure squared, industry, marital status, race, education-year, number of children, metro area-year, and individual fixed effects. We focus on full-time US-born workers in metropolitan areas, observed between 2000 and 2018.

Finally, we estimate the remote work premium in city j using

$$\psi_{jt} = \sum_o sh_{oj}^{2018} (\psi_o^0 + \psi^1 t) \hat{h}, \quad (30)$$

where sh_{oj}^{2018} is the share of workers in city j working in occupation o in 2018. Figure 14 displays the estimates $(\hat{\psi}_{o(i)}^0 + \hat{\psi}^1 t) \hat{h}$ for $t = 2018$ for each of the 22 occupation groups obtained from (29), and the estimates ψ_{j2018} of the remote work premium by CBSA obtained from (30). Both are plotted against the share of teleworkable employment estimated by Dingel and Neiman (2020).³⁸

From equations (29) and (30), we can interpret $(\psi_{o(i)}^0 + \psi^1 t) \hat{h}$ as an estimate of $\ln(w_{mt}/w_{ct})$ for each occupation, and ψ_{jt} as an estimate of $\ln(w_{mt}/w_{ct})$ for each CBSA. We use the specification of wages in (3), to map our estimates of the remote work premium into the remote work technology parameter, z :

$$z_{jt} = \exp(\hat{\psi}_{jt}/\mu) w_{cjt}, \quad (31)$$

where w_{cjt} is the average hourly wage of commuters in each CBSA j . We then recover the in-office productivity using

$$A_{jt} = \tilde{L}_{cjt}^{-\delta_j} w_{cjt}, \quad (32)$$

given the city-level estimates of δ_j obtained in 5.2. Table 2 reports summary statistics for these estimates.

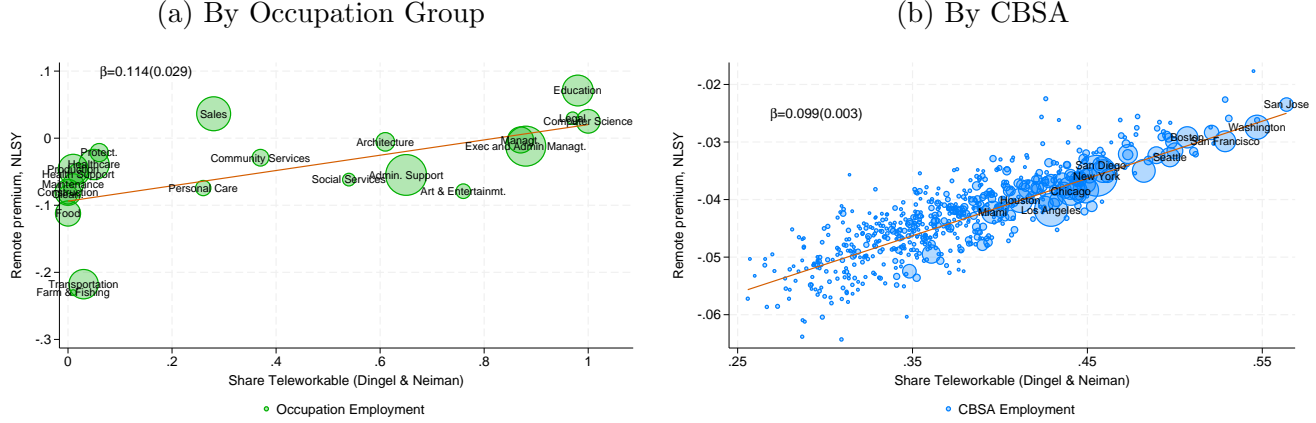
5.4 Transportation Costs Elasticity

We estimate the transportation costs elasticity γ_j for each CBSA j . We use the relationship that relates γ_j to the slope κ_{jt} of the housing rent schedule with respect to distance to the CBD.³⁹ From (14), the average elasticity of rent to distance in period t is exactly related to

³⁸In Appendix A.5, we report the estimates for each occupation group and CBSA.

³⁹Our model assumes that there is a fixed housing supply of one house per plot. In Appendix A.17, we show that a model where the number of housing units endogenously responds to the rents would deliver, for practical purposes, a very similar gradient. This result is a consequence of the number of commuters being a very high share of the overall employment before 2020.

Figure 14: Estimates of the Remote Work Premium



Panel (a) reports estimates for each of the 22 occupation groups obtained from (29), against the share of teleworkable employment from Table 1 in Dingel and Neiman (2020). Panel (b) reports the estimates of the remote work premium by CBSA obtained from (30) plotted against the share of teleworkable employment at the CBSA level. We compute the CBSA-level shares of teleworkable employment as the weighted average of the occupation-specific measures from Table 1 in Dingel and Neiman (2020). The weights are given by the CBSA share of employment of each occupation from the Census sample. The coefficient β and the associated robust standard error from the regression of the remote premium on the share of teleworkable employment are reported at the top right of each figure.

the slope of the housing rent schedule according to

$$\kappa_{jt} = -\frac{\gamma_j}{1-\alpha} \left(1 - \mu + \mu \frac{L_{cjt}}{L_{jt}} \right). \quad (33)$$

In order to estimate κ_{jt} , we use data on housing rents at the block group level from the ACS corresponding to average values between 2015 and 2019. For each CBSA, we estimate a regression at the block group level of the log of the median housing rental price p_{ij} in each block group i on the log of the distance, $dist_{ij}$, between the centroid of block group i and the centroid of the closest CBD of CBSA j .⁴⁰ We then estimate

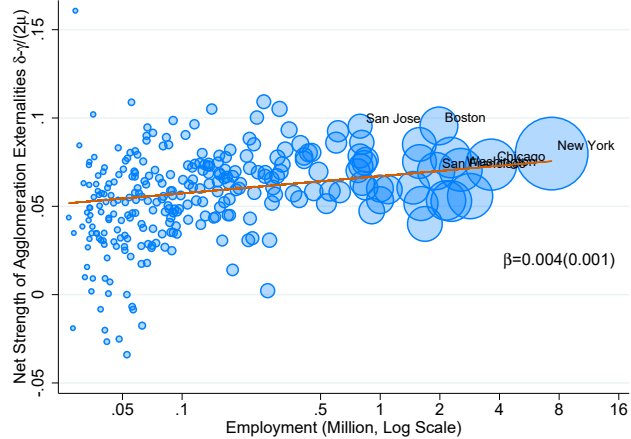
$$\ln p_{ij} = \kappa_j \ln(dist_{ij}) + \beta_j X_{ij} + \alpha_j + e_{ij}, \quad (34)$$

where the controls X_{ij} contain block-level measures of the percentages of Hispanic, Black, and Asian population, dwelling characteristics such as the percentage of dwellings by type of structure, by the number of bedrooms, and by construction decade, as well as other geographic controls defined at the tract level and obtained from Lee and Lin (2017).⁴¹ The summary statistics of the estimates of γ_j across CBSAs are reported in Table 2 and Appendix A.15 shows their relation with

⁴⁰We provide details on how we identify each CBSA's CBDs in Appendix A.6.

⁴¹Geographic controls include the log of land area in square kilometers, number of housing units, the average age of housing units, average terrain slope, the maximum average temperature in July, the minimum average temperature in January, annual precipitations, log of distance to the closest river, to the closest lake, and to the closest shore.

Figure 15: Net Strength of Agglomeration Externalities and CBSA size



This figure reports the city-specific $\delta_j + \gamma_j/(2\mu)$ against the CBSA's BEA employment. δ_j and γ_j are estimated as described in the text and $\mu = 3/5$. The size of the circles represents CBSA's employment.

city size.⁴²

Proposition 4.3 indicates that the resulting net strength of the agglomeration externalities, $\delta_j - \gamma_j/(2\mu)$ is a crucial statistic for the potential of a city to exhibit multiple stationary equilibria. In Figure 15 we plot such net strength against the CBSA's employment size. We find that this net strength is positively related to city size; a doubling in city size is associated to an increase of 0.004 of this net strength, out of a mean value of 0.049.

5.5 Quantification of Remaining Parameters

We calibrate $\bar{\tau}_j$ for each city to match its observed value of L_{jc}/L_j . As shown in Appendix B.2, a stationary equilibrium value for L_{jc}/L_j can be expressed in terms of λ_{cc} . Hence, we assume that the city is in the high-commuting stationary equilibrium in 2019, infer the value of λ_{jcc} that is consistent with L_{jc}/L_j , and then solve for the value of $\bar{\tau}_j$ that makes such λ_{jcc} a stationary equilibrium.

We set the share of consumption expenditures on tradable goods to $\alpha = 0.76$, following Davis and Ortalo-Magné (2011). The share of days per week spent at home for remote workers is set to $\mu = 3/5$. As discussed in Section 5.1, our estimation does not separately identify the amenity externality ξ from the congestion externality θ . In addition, our estimates of the difference are not statistically different from zero at the 95 percent level. Therefore, without more guidance on their value, we set them each to zero.

⁴²For small CBSAs, the number of block groups with non-missing observations on rents and other control variables is sometimes small, leading to estimates of γ_j that are not statistically different from zero at the 10 percent level. We drop those cities due to the lack of data.

Table 2: Estimates of City-Specific Parameters

	Agglomeration Externality δ_j	Remote Work Productivity z_j	Rel. Remote Work Productivity z_j/A_j	Transport Cost Elasticity γ_j
Mean	0.067	16.6	2.05	0.026
10 th perc.	0.040	13.5	1.43	0.002
50 th perc.	0.067	15.9	1.97	0.014
90 th perc.	0.092	20.3	2.82	0.044
Nb of CBSAs	622	622	622	278
Mean if emp. \geq 1 million	0.078	23.0	2.95	0.013
Mean if emp. \leq 100,000	0.065	15.6	1.91	0.038

The last two rows report the mean values of the parameters for i) the group of CBSAs with employment above 1 million (consisting of 19 CBSAs), ii) the group of CBSAs with employment below 100 thousand (consisting of 468 CBSAs). Employment is measured as the number of employed workers between 25 and 64 years old, not self-employed, listed as residents of the CBSA in the 2019 ACS. We are able to estimate the transport cost elasticity for a smaller number of CBSAs, given the data limitations on housing rents at the block group level in smaller CBSAs.

6 Permanent Responses to Transitory Shocks

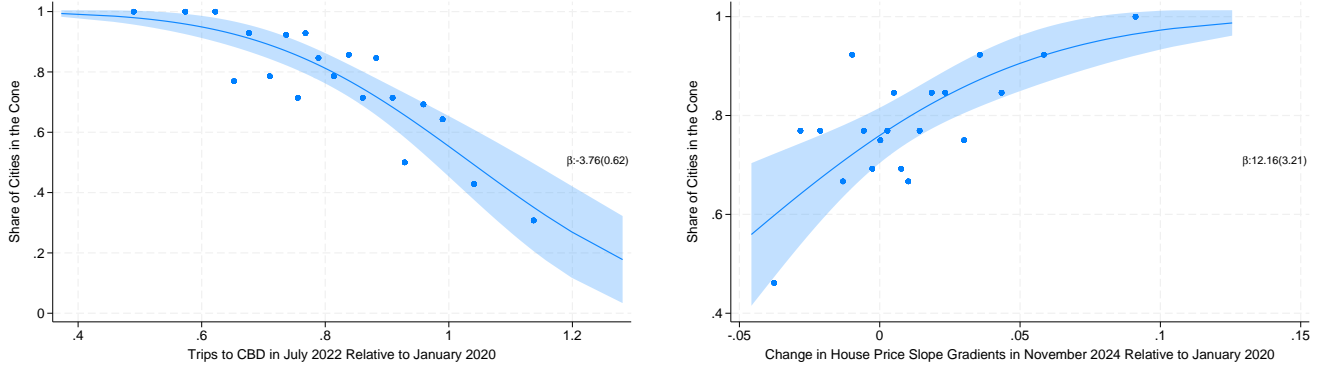
The analysis in Subsection 4.4 indicates that a city in the cone of multiplicity could permanently switch to a path that converges towards the low-commuting stationary equilibrium when subject to a large enough shock to the number of commuters. In this new stationary equilibrium, trips to the CBD are permanently lower, and the rent and value gradients are permanently flatter. In our data, the response heterogeneity as a function of city size of Figures 4 and 7 appears to have stabilized by 2022 (see Figures 3 and 6). To interpret this evidence, we turn to a quantified version of our model. We use city-specific parameters retrieved in Section 5 to calculate the values of z_j/A_j , $\delta_j - \gamma_j/(2\mu)$, and the corresponding set \mathcal{Z}_j defined in Proposition 4.3. We construct these values for 278 CBSAs with valid information on remote work premiums and elasticities.⁴³ For each city, we create an indicator variable $\mathbf{1}_j^{\text{cone}} = 1$ if $z_j/A_j \in \mathcal{Z}_j$, and zero otherwise, meaning the city is inside its cone of multiplicity. We find that 199 cities were in their respective cone before the pandemic. These cities could be pushed into a low commuting equilibrium by a large enough, albeit temporary, shock to the number of commuters.

Our theory appears to have explanatory power. We estimate a city-level probit of $\mathbf{1}_j^{\text{cone}}$ on the July 2022 measure of CBD trips, relative to January 2020. This regression returns a negative and significant coefficient: cities with a lower level of trips post-pandemic were indeed much more likely to be in their cone before the pandemic. Figure 16a reports this estimated share of cities that are inside the cone as a function of the trip shortfall, while the blue dots report the fraction of cities in the cone in each of 20 bins of the independent variable.

⁴³The model assumes positive δ and γ , and requires a remote work wage discount for a valid calibration.

Figure 16: Share of Cities in the Cone of Multiplicity

- (a) Cities in the Cone of Multiplicity vs. CBD Trips Shortfall (b) Cities in the Cone of Multiplicity vs. Change in House Price Distance Gradient



The blue line in this figure plots the predicted share of cities in their cone of multiplicity from a probit regression of the indicator variable 1_j^{cone} on the volume of trips in July 2022, relative to their value in January 2020 (Panel a), and on the log total employment of a city (Panel b), with the shaded area representing the 95 percent confidence interval. The figure also reports the coefficient and robust standard error of the independent variable in the probit regression. One blue dot is the average value of 1_j^{cone} in each of 20 quantiles of the trip shares.

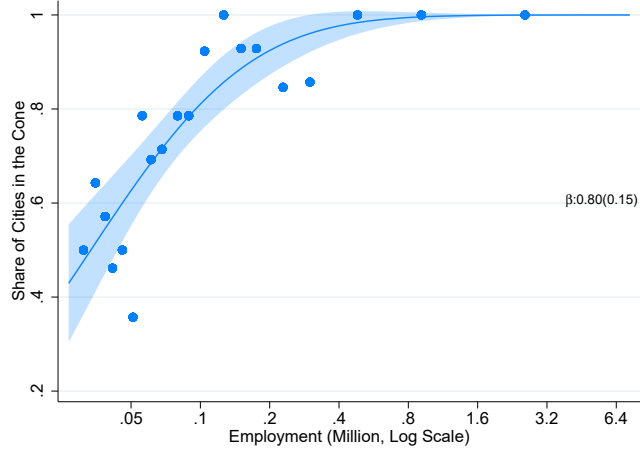
The propensity of being inside the cone is also associated with the observed flattening of the housing price gradient. As Figure 16b shows, a probit regression of 1_j^{cone} on the change in the bid-rent housing gradient between January 2020 and December 2022 yields a positive and significant coefficient. The blue dots report the fraction of cities in the cone in each of the 20 bins of gradient change. Hence, cities that display a large persistent flattening of the house price gradient are much more likely to be in their cone of multiplicity.⁴⁴

Overall, we find that larger cities exhibit a higher propensity to being inside their cone. A probit regression of 1_j^{cone} on the log employment of a city shows a positive and significant coefficient. Figure 17 shows this estimated share as a function of log employment, with a 95% robust confidence interval. The blue dots report the fraction of cities in the cone in each of the 20 bins of employment size. Larger cities, which in the data are more likely to display a permanent shift, are also more likely to be in the cone of multiplicity that our theory proposes. In Appendix A.10, we show that the probability of being in the cone also grows with δ_j and z_j/A_j , while falling with γ_j , as implied by the theory.

Our explanation of the post-pandemic empirical patterns rests on an indicator (1_j^{cone}) that summarizes all the relevant aspects of a city's propensity to exhibit multiple equilibria. Still,

⁴⁴Note that some small cities are missing from the analysis in Figures 16a and 16b since there is not enough data to estimate the full set of parameters required to determine if they were in the cone of multiplicity before the pandemic. However, in general, small cities are much more likely to be outside of the cone of multiplicity, and they mostly have gone back to pre-pandemic commuting levels, as shown in Figures 3 and 6. Hence, Figures 16a and 16b, would probably show an even starker relationship if we could include more small cities.

Figure 17: Share of Cities in the Cone of Multiplicity vs. CBSA size



The blue line in this figure plots the predicted share of cities in their cone of multiplicity from a probit regression of the indicator variable 1_j^{cone} on the log total employment of a city, with the shaded area representing the 95 percent confidence interval. The figure also reports the coefficient and robust standard error of the independent variable in the probit regression. One blue dot is the average value of 1_j^{cone} in each of 20 quantiles of the trip shares.

one might ask whether, as a purely empirical exercise, this specific summary measure retains power in explaining the post-pandemic behavior of cities once we control for alternative plausible explanations of the return to office –even though those controls contribute to determining the city parameters and, therefore, 1_j^{cone} . In Appendix A.19 we discuss the results of this exercise and show that, indeed, 1_j^{cone} continues to have strong predictive power beyond controls for alternative explanations.

Taken together, this evidence suggests that the observed, and by now stable, heterogeneous responses to the pandemic and related stay-at-home policies are well accounted for by the coordination mechanism we propose in our theory. Since this coordination happens, at least partly, outside firm boundaries, individual firms' return-to-work policies might be insufficient to revert a city's equilibrium shift. Of course, city governments could implement policies that put the city back on its path to the commuting equilibrium (like taxing remote work), but we do not know what would be the value of such policies and how effective they would be in actually achieving their goal. These considerations motivate an investigation of the welfare consequences of these shifts.

7 Welfare

The model gives us an expression to compute the average stationary equilibrium welfare in a city as a function of the measure of commuters. Evaluating equation (8) in a stationary equilibrium

Table 3: Percentage Welfare Difference Between the High and Low-Commuting Equilibrium

	Min	p10	p25	p50	p75	p90	Max	Mean	N
Welfare Loss ($-\hat{\mathcal{W}}_j$)	1.2	1.5	1.9	2.3	2.7	3.1	4.5	2.3	199

and rearranging terms, the average welfare \mathcal{W}_j can be computed as

$$\mathcal{W}(L_{cj}^{ss}) = \left(\frac{L_{cj}^{ss}}{L_j} \right) V_c(L_{cj}^{ss}) + \left(1 - \frac{L_{cj}^{ss}}{L_j} \right) V_m(L_{cj}^{ss}). \quad (35)$$

This is a utilitarian welfare function where all workers in the same delivery mode receive the same utility, despite living at different distances from the CBD.⁴⁵ In a city with multiple stationary equilibria, this welfare varies across stationary equilibrium. For the 199 cities inside the cone, we can then compute $\hat{\mathcal{W}}_j \equiv 100 \times (\mathcal{W}(L_{cj \text{ low}}^{ss})/\mathcal{W}(L_{cj \text{ high}}^{ss}) - 1)$ as the percentage change between the welfare in the low-commuting versus the high-commuting stationary equilibrium. All cities in the cone would lose from being permanently pushed to the low-commuting stationary equilibrium.⁴⁶ Table 3 shows some moments of the distribution of welfare losses.⁴⁷

The median potential loss from such a switch to the low-commuting stationary equilibrium is 2.2%, with a range from 1.2% to 4.5%. The loss stems from a drop in average wages, which is only partially compensated by a reduction in commuting costs and changes in the option values. A city switching equilibrium has lower wages both for commuters and remote workers since each individual interacts with a smaller average number of agents, \tilde{L}_{cj} . Fewer interactions lead to diminished production externalities. Specifically, the change in average wages is given by

$$\hat{w}_j \equiv 100 \times \left(\frac{\left(\frac{L_{cj \text{ low}}^{ss}}{L_j} \right) w_{cj \text{ low}} + \left(1 - \frac{L_{cj \text{ low}}^{ss}}{L_j} \right) w_{mj \text{ low}}}{\left(\frac{L_{cj \text{ high}}^{ss}}{L_j} \right) w_{cj \text{ high}} + \left(1 - \frac{L_{cj \text{ high}}^{ss}}{L_j} \right) w_{mj \text{ high}}} - 1 \right). \quad (36)$$

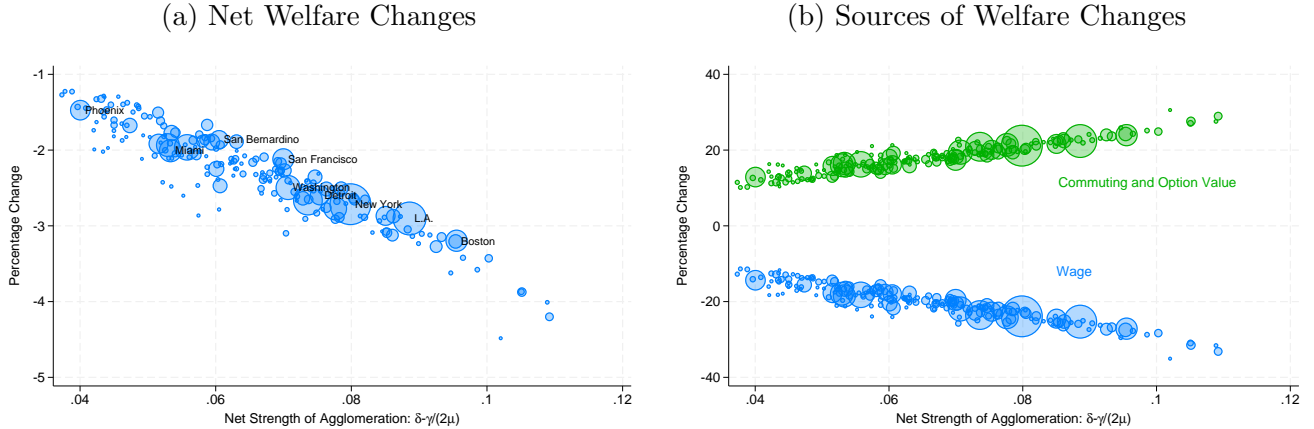
The residual component of the welfare impact, that accounts for changes in commuting costs and option values can be constructed as $\chi_j \equiv \hat{\mathcal{W}}_j - \hat{w}_j$. Figure 18, right panel, plots \hat{w}_j and χ_j against the net strength of agglomeration externalities, $\delta_j - \gamma_j/(2\mu)$, for all cities estimated to be in the cone. The fall in average wages is quite severe, between 15% and 35%. This large magnitude is to be expected, however, because agglomeration externalities tend to be significant precisely for cities more likely to be in the multiplicity region. Net welfare losses are then muted by the combined effect of changes in the average commuting disutility and option values. Overall, the net strength

⁴⁵This occurs because, within each group, individuals choose distance to trade off rents and commuting costs.

⁴⁶Although we do not have a proof, the intuitive reason why all cities in the multiplicity cone would rather be in the commuting-intensive stationary equilibrium is that the only active externality in our quantification is a positive agglomeration externality. This implies that, in all equilibria, there is too little commuting compared to the efficient benchmark.

⁴⁷Table A10 in the Appendix shows actual welfare changes for the largest U.S. cities in our calibration sample.

Figure 18: Welfare Ratio \hat{W} and its Decomposition



The left panel shows a scatterplot between \hat{W} and the net strength of agglomeration externalities, $\delta - \gamma/(2\mu)$. The right panel shows the percentage difference in wages across equilibria, \hat{w} , and the residual commuting and option value gains χ , plotted against the net strength of agglomeration externalities, $\delta - \gamma/(2\mu)$. The marker size is proportional to total city employment. These scatterplots can only be computed for the set of cities in the cone of multiplicity.

of the agglomeration externality (Figure 18, left panel) is a strong predictor of the final welfare loss: a regression of the estimated loss on $\delta_j - \gamma_j/(2\mu)$ delivers an R^2 of 0.85.

In Figure A15 in the Appendix, we also compare welfare losses to the observed drop in trips to the CBD. The largest drops in CBD trips are concentrated around welfare losses of 2.5 to 3%. In particular, we find that the welfare loss of the average resident in cities with trips to the CBD of 60% or less of the pre-pandemic level is 2.7%.⁴⁸

8 Conclusion

We have proposed a theory of remote work and city structure. At its core, our theory features a coordination problem: workers prefer to commute if others do as well, and prefer to work from home otherwise. This mechanism can lead to multiplicity in stationary equilibria if agglomeration forces are sufficiently larger than congestion forces and remote-work technology is decent relative to in-office technology. In the resulting dynamic discrete choice model, large exogenous changes in the number of commuters, a state variable of the model, can put the city on an equilibrium path that makes it converge to an alternative stationary equilibrium. We have argued that the COVID-19 pandemic constituted such an exogenous shock and that, as a result, many large cities

⁴⁸As welfare falls, one might also expect a population response. In Appendix A.9 we find that large cities are indeed experiencing a small differential drop in residents, although the changes are rather small and not very correlated with the change in trips to the CBD (see Figure A7b). This pattern is probably due to a low migration elasticity across cities, large migration costs, and the myriad of idiosyncratic shocks affecting individual cities. This is the reason we do not consider between-city employment flows in our analysis.

have switched from a stationary equilibrium where most workers commuted to one in which there is a large share of agents working from home. Small cities, in contrast, tend not to exhibit this multiplicity and therefore have converged back to the pre-pandemic stationary equilibrium. We find consistent evidence from our estimated model for 278 U.S. cities, from cell-phone-based individual mobility data, and from house price distance gradients. An arguably uniform shock to the labor delivery mode across cities has revealed which cities were exposed to this coordination problem – and thus, presented multiple stationary equilibria – before the pandemic, a rather unique empirical event.

The model can be used to estimate the welfare losses associated with the switch to remote work for all cities that exhibit this type of multiplicity in stationary equilibria. We find that welfare in the commuting-intensive equilibrium is between 1.2% and 4.5% larger than in the remote-work-intensive equilibrium. A significant, but not overwhelming, cost. This modest cost is, however, the result of a large drop in wages compensated by substantial utility gains from option values and commuting costs.

Although our analysis can fit the available data quite well, it inevitably abstracts from a number of important forces and issues. First, our model studies cities in isolation but not as a system of cities with migration, trade, and investment links. This is potentially relevant since the spatial equilibrium condition across cities will determine local welfare effects and population flows. The welfare implications we estimate for some of the large U.S. cities appear to be partially translating into smaller populations. Similarly, some of the small cities with unique stationary equilibria might grow and gain industries that transform them in ways that could put them in the multiplicity cone. Of course, remote workers could also commute across cities, another issue we abstract from but has received some recent attention in the media. Second, although we model remote work as “partial remote work,” where agents work from home only a fraction μ of days, we have kept this fraction constant rather than the agent’s choice. Of course, agents in different cities, or in different parts of a city, or with different occupations or skills, might choose different shares. Understanding the importance of these choices and the resulting heterogeneity across individuals could be important but complicates the analysis significantly. Third, some of the spillovers between workers could be internalized by firms and cities, which might then proactively affect workers’ delivery mode choice. Understanding the extent to which active policy can determine the dynamic path and stationary equilibrium that a city converges to, is an interesting topic for future research.

The repercussions of remote work are intriguing and potentially transforming for the organization of work in cities, firms, and labor markets. Our paper hopes to contribute to what will surely be an active area of research in the future, as the organization of work changes to accommodate the booming phenomenon of remote work.

References

- AKSOY, C. G., J. M. BARRERO, N. BLOOM, S. J. DAVIS, M. DOLLS, AND P. ZARATE (2022): “Working from Home Around the World,” Working Paper 30446, National Bureau of Economic Research.
- ALONSO, W. (1964): *Location and Land Use*, Cambridge, MA and London, England: Harvard University Press.
- ALTHOFF, L., F. ECKERT, S. GANAPATI, AND C. WALSH (2021): “The Geography of Remote Work,” Working Paper 29181, National Bureau of Economic Research.
- ARCIDIACONO, P. AND R. A. MILLER (2011): “Conditional Choice Probability Estimation of Dynamic Discrete Choice Models With Unobserved Heterogeneity,” *Econometrica*, 79, 1823–1867.
- ARTUÇ, E., S. CHAUDHURI, AND J. MCLAREN (2010): “Trade Shocks and Labor Adjustment: A Structural Empirical Approach,” *American Economic Review*, 100, 1008–45.
- ATKIN, D., A. SCHOAR, AND S. SHINDE (2022): “Worker Sorting, Worker Discipline and Development,” *Working Paper*.
- BAILEY, M., R. CAO, T. KUCHLER, J. STROEBEL, AND A. WONG (2018): “Social Connectedness: Measurement, Determinants, and Effects,” *Journal of Economic Perspectives*, 32, 259–80.
- BARRERO, J. M., N. BLOOM, AND S. J. DAVIS (2021): “Why Working from Home Will Stick,” Working Paper 28731, National Bureau of Economic Research.
- (2023): “The Evolution of Work from Home,” *Journal of Economic Perspectives*.
- BAUM-SNOW, N. AND R. PAVAN (2011): “Understanding the City Size Wage Gap,” *The Review of Economic Studies*, 79, 88–127.
- BLOOM, N., R. HAN, AND J. LIANG (2022): “How Hybrid Working From Home Works Out,” Working Paper 30292, National Bureau of Economic Research.
- BLOOM, N., J. LIANG, J. ROBERTS, AND Z. J. YING (2015): “Does Working from Home Work? Evidence From a Chinese Experiment,” *The Quarterly Journal of Economics*, 130, 165–218.
- BRUECKNER, J., M. E. KAHN, AND G. C. LIN (2021): “A New Spatial Hedonic Equilibrium in the Emerging Work-from-Home Economy?” Working Paper 28526, National Bureau of Economic Research.
- BRYNJOLFSSON, E., J. J. HORTON, C. MAKRIDIS, A. MAS, A. OZIMEK, D. ROCK, AND H.-Y. TUYE (2023): “How Many Americans Work Remotely? A Survey of Surveys and Their Measurement Issues,” Working Paper 31193, National Bureau of Economic Research.

- BRYNJOLFSSON, E., J. J. HORTON, A. OZIMEK, D. ROCK, G. SHARMA, AND H.-Y. TUYE (2020): “COVID-19 and Remote Work: An Early Look at US Data,” Working Paper 27344, National Bureau of Economic Research.
- CAPPELLI, P. H. AND J. KELLER (2013): “A Study of the Extent and Potential Causes of Alternative Employment Arrangements,” *ILR Review*, 66, 874–901.
- CHAPPLE, K., H. MOORE, M. LEONG, D. HUANG, A. FOROUHAR, L. SCHMAHMANN, J. WANG, AND J. ALLEN (2023): “The Death of Downtown? Pandemic Recovery Trajectories across 62 North American Cities,” *Research Brief, School of Cities, University of Toronto and Institute of Governmental Studies, University of California, Berkeley*.
- CHOUDHURY, P., T. KHANNA, C. MAKRIDIS, AND K. SCHIRRMANN (2022): “Is Hybrid Work the Best of Both Worlds? Evidence from a Field Experiment,” *Harvard Business School Technology & Operations Mgt. Unit Working Paper*, No. 22-063.
- COMBES, P.-P., G. DURANTON, AND L. GOBILLON (2008): “Spatial wage disparities: Sorting matters!” *Journal of Urban Economics*, 63, 723–742.
- COMBES, P.-P., G. DURANTON, L. GOBILLON, D. PUGA, AND S. ROUX (2012): “The Productivity Advantages of Large Cities: Distinguishing Agglomeration From Firm Selection,” *Econometrica*, 80, 2543–2594.
- DALTON, M., M. DEY, AND M. LOEWENSTEIN (2022): “The Impact of Remote Work on Local Employment, Business Relocation, and Local Home Costs,” BLS Working Paper 553, U.S. Bureau of Labor Statistics.
- DAVIS, M. A., A. C. GHENT, AND J. GREGORY (2024): “The Work-From-Home Technology Boon and its Consequences,” *The Review of Economic Studies*, 91, 3362–3401.
- DAVIS, M. A. AND F. ORTALO-MAGNÉ (2011): “Household expenditures, wages, rents,” *Review of Economic Dynamics*, 14, 248–261.
- D’COSTA, S. AND H. G. OVERMAN (2014): “The urban wage growth premium: Sorting or learning?” *Regional Science and Urban Economics*, 48, 168–179.
- DE LA ROCA, J. AND D. PUGA (2016): “Learning by Working in Big Cities,” *The Review of Economic Studies*, 84, 106–142.
- DINGEL, J. I. AND B. NEIMAN (2020): “How Many Jobs Can be Done at Home?” Working Paper 26948, National Bureau of Economic Research.
- DURANTON, G. AND J. HANDBURY (2023): “Covid and Cities, Thus Far,” Working Paper 31158, National Bureau of Economic Research.

- DURANTON, G. AND D. PUGA (2019): “Urban Growth and its Aggregate Implications,” Working Paper 26591, National Bureau of Economic Research.
- EMANUEL, N., E. HARRINGTON, AND A. PALLAIS (2022): “The Power of Proximity: Office Interactions Affect Online Feedback and Quits, Especially for Women and Young Workers,” *Working Paper*.
- ETHERIDGE, B., Y. WANG, AND L. TANG (2020): “Worker productivity during lockdown and working from home: evidence from self-reports,” ISER Working Paper Series 2020-12, Institute for Social and Economic Research.
- GAUBERT, C. (2018): “Firm Sorting and Agglomeration,” *American Economic Review*, 108, 3117–53.
- GENNAIOLI, N., R. LA PORTA, F. LOPEZ-DE SILANES, AND A. SHLEIFER (2012): “Human Capital and Regional Development *,” *The Quarterly Journal of Economics*, 128, 105–164.
- GIBBS, M., F. MENGELO, AND C. SIEMROTH (2023): “Work from Home and Productivity: Evidence from Personnel and Analytics Data on Information Technology Professionals,” *Journal of Political Economy Microeconomics*, 1, 7–41.
- GLAESER, E. AND D. MARÉ (2001): “Cities and Skills,” *Journal of Labor Economics*, 19, 316–342.
- GUPTA, A., V. MITTAL, J. PEETERS, AND S. VAN NIEUWERBURGH (2021): “Flattening the Curve: Pandemic-Induced Revaluation of Urban Real Estate,” Working Paper 28675, National Bureau of Economic Research.
- GUPTA, A., V. MITTAL, AND S. VAN NIEUWERBURGH (2022): “Work From Home and the Office Real Estate Apocalypse,” Working Paper 30526, National Bureau of Economic Research.
- GYOURKO, J., A. SAIZ, AND A. SUMMERS (2008): “A New Measure of the Local Regulatory Environment for Housing Markets: The Wharton Residential Land Use Regulatory Index,” *Urban Studies*, 45, 693–729.
- HANSEN, S., P. J. LAMBERT, N. BLOOM, S. J. DAVIS, R. SADUN, AND B. TASKA (2023): “Remote Work across Jobs, Companies, and Space,” Working Paper 31007, National Bureau of Economic Research.
- HARRINGTON, E. AND N. EMANUEL (2022): “‘Working’ Remotely? Selection, Treatment, and Market Provision of Remote Work,” *Working Paper*.
- HENDERSON, J. (2003): “Marshall’s scale economies,” *Journal of Urban Economics*, 53, 1–28.

- KENNAN, J. AND J. R. WALKER (2011): “The Effect of Expected Income on Individual Migration Decisions,” *Econometrica*, 79, 211–251.
- KÜNN, S., C. SEEL, AND D. ZEGNERS (2020): “Cognitive Performance in the Home Office - Evidence from Professional Chess,” .
- LEE, S. AND J. LIN (2017): “Natural Amenities, Neighbourhood Dynamics, and Persistence in the Spatial Distribution of Income,” *The Review of Economic Studies*, 85, 663–694.
- LIPOWSKA, K., M. SMOTER, AND P. LEWANDOWSKI (2022): “Mismatch in preferences for working from home – evidence from discrete choice experiments: evidence from Poland,” .
- LIU, S. AND Y. SU (2021): “The impact of the COVID-19 pandemic on the demand for density: Evidence from the U.S. housing market,” *Economics Letters*, 207, 110010.
- (2023): “The Effect of Working from Home on the Agglomeration Economies of Cities: Evidence from Advertised Wages,” *SSRN*.
- LUTZ, C. AND B. SAND (2022): “Highly disaggregated land unavailability,” *Available at SSRN 3478900*.
- MANSON, S., J. SCHROEDER, D. V. RIPER, T. KUGLER, AND S. RUGGLES (2022): “IPUMS National Historical Geographic Information System: Version 17.0 [dataset],” <http://doi.org/10.18128/D050.V17.0>.
- MAS, A. AND A. PALLAIS (2017): “Valuing Alternative Work Arrangements,” *American Economic Review*, 107, 3722–3759, nBER Working Paper 22708.
- MATTHIES, B. AND A. KWAN (2022): “Measuring the Impact of Remote Work Using Big Data,” *Working Paper*.
- MONDRAGON, J. A. AND J. WIELAND (2022): “Housing Demand and Remote Work,” Working Paper 30041, National Bureau of Economic Research.
- MORETTI, E. (2004): “Estimating the social return to higher education: evidence from longitudinal and repeated cross-sectional data,” *Journal of Econometrics*, 121, 175–212, higher education (Annals issue).
- MUTH, R. F. (1969): *Cities and Housing*, Chicago: University of Chicago Press.
- OETTINGER, G. S. (2011): “The Incidence and Wage Consequences of Home-Based Work in the United States, 1980–2000,” *Journal of Human Resources*, 46, 237–260.
- OWENS, RAYMOND, I., E. ROSSI-HANSBERG, AND P.-D. SARTE (2020): “Rethinking Detroit,” *American Economic Journal: Economic Policy*, 12, 258–305.

- PARKHOMENKO, A. AND M. DELVENTHAL (2024): “Spatial Implications of Telecommuting,” *Working Paper*.
- RAMANI, A. AND N. BLOOM (2021): “The Donut Effect of Covid-19 on Cities,” Working Paper 28876, National Bureau of Economic Research.
- ROSSI-HANSBERG, E., P.-D. SARTE, AND F. SCHWARTZMAN (2019): “Cognitive Hubs and Spatial Redistribution,” Working Paper 26267, National Bureau of Economic Research.
- (2021): “Local Industrial Policy and Sectoral Hubs,” *AEA Papers and Proceedings*, 111, 526–31.
- SAIZ, A. (2010): “The Geographic Determinants of Housing Supply,” *The Quarterly Journal of Economics*, 125, 1253–1296.
- TRAIBERMAN, S. (2019): “Occupations and Import Competition: Evidence from Denmark,” *American Economic Review*, 109, 4260–4301.
- YANG, L., D. HOLTZ, S. JAFFE, S. SURI, S. SINHA, J. WESTON, C. JOYCE, N. SHAH, K. SHERMAN, B. HECHT, AND J. TEEVAN (2022): “The effects of remote work on collaboration among information workers,” 6, 43–54.

A Appendix

A.1 Data Sources

Cross-sectional Data on Remote Work Our first source of data to measure the prevalence of remote work in the U.S. economy and the earnings of remote workers are the decennial census between 1980 and 2000 and the American Community Survey thereafter. These surveys include a question asked of those ages 16 and over who were employed and at work in the previous week on the method of transportation usually used to get to work. We define as remote workers those who reported “work from home” on this question.¹ We measure the hourly earnings rate of workers by dividing the total pre-tax wage and salary income by the number of hours worked during the year.² This definition of remote work allows us to obtain a consistent measure of remote work and its compensation from 1980 to 2023 through repeated cross-sectional samples.³ On average, every year, about 5 million workers are listed as remote workers. However, the decennial census and the ACS do not contain information on the number of hours worked at home.

Longitudinal Data on Remote Work Our second source of data is the National Longitudinal Survey of Youth - 1979 Cohort (NLSY79), a nationally representative sample of 12,686 young men and women born between the years 1957 through 1964 in the United States. We focus on data reported from 1998 onward, a period through which the reporting of hours worked is consistent. Every two years, the survey reports the number of hours worked at home in a week. This allows us to observe variation in remote work on the intensive margin. We obtain workers’ hourly rates directly from the survey. Thanks to the longitudinal design of the survey, we can observe workers’ transitions into and out of remote work over time.

Foot Traffic Data We use data from a private provider, SafeGraph, which produces foot traffic information at the business place level by collecting anonymized phone GPS tracking from third-party applications. Specifically, we use the Neighborhood Patterns dataset, which contains information on foot traffic to census block groups every month. This dataset has several key advantages. First, it captures foot traffic at a fine geographical level.⁴ This allows us to specifically focus on mobility to cities’ CBDs. Second, it provides a count of individual visits by category of trip, including visits that are likely to be for work. We use this feature to define CBDs. Third, the visits to any block groups are disaggregated by block group of origin. This allows us to control

¹In the decennial census, the question on means of transportation to work was asked in the “long form” questionnaire, which was administered to approximately 1 out of every 6 housing units in the United States.

²The income variable is “incwage”. It includes wages, salaries, commissions, cash bonuses, tips, and other money income received from an employer. Payments-in-kind or reimbursements for business expenses are not included. The number of hours worked in the year is computed by multiplying the reported number of hours worked in a typical week by the number of weeks worked in the year.

³In 2023, no information on workers’ industry of work is available, so only include this year for the descriptive evidence in Section 3.

⁴There are 220,684 census block groups in the United States.

for unobserved permanent characteristics of origin block groups by studying mobility to the CBD from each block group separately.

Housing Prices and Rents We rely on house prices and rents aggregated at the zip code level by Zillow.⁵ Our measure of house prices is the Zillow House Value Index (ZHVI), which controls for common house characteristics and adjusts for seasonality. We measure rents with the Zillow Observed Rental Index (ZORI), an index of house rents obtained by averaging asking rents after controlling for house quality indicators. Both series include prices and rents of single- and multi-family units. These datasets have the advantage of being reported monthly before and during the COVID-19 pandemic, allowing us to track the changes in housing prices and rent gradients in about 200 CBSAs. While the monthly Zillow data is well suited for within-city comparison across time, the relatively low number of observed zip codes in smaller CBSAs makes it less amenable to comparisons across cities. To obtain more precise estimates of housing rent gradients for a larger number of CBSAs, we turn to data from the ACS at the census block group level.⁶ We use the median rent paid in a block group during the 2015-2019 period. This, along with other block group-level controls defined below, allows us to estimate housing rent gradients before the COVID-19 pandemic more precisely and for almost 300 CBSAs.

Local Housing Market Characteristics We collect zip code level variables to control for variation in housing market characteristics. From the Census Bureau, we obtain the median household income, the share of households in the top national income quintile, the median age, and the proportion of Black residents. There is significant variation in housing market characteristics at the CBSA level. We complement these measures with local geographic features collected by Lee and Lin (2018). We aggregate these census tract-level indicators at the zip code level.

A.2 Definitions of Data Samples

A.2.1 Census/ACS Sample

We combine the decennial census waves in 1980, 1990, and 2000 with the yearly waves of the American Community Survey between 2005 and 2023. We start from observations from all individuals recorded in each wave, weighted by their personal sampling weight. We only include workers who are employed, of age between 25 and 64, who do not work in agriculture or in the military, and who are not self-employed.⁷ We restrict our sample to individuals who have not moved to a different

⁵The datasets are publicly available from <https://www.zillow.com/research/data/>. [Ferdinando: should we state the date we have accessed the website here?](#)

⁶The data can be obtained from IPUMS' National Historical Geographic Information System (NHGIS) portal [Manson et al. \(2022\)](#).

⁷Specifically, we exclude workers in 1-digit industries 1 and 14 from the 1990 Census industry classification (“Agriculture, Forestry, and Fisheries” and “Active Duty Military/NA/NC”, respectively), workers in 1-digit occupations 4 and 7 from the 1990 Census occupation classification (“Agriculture, Forestry, and Fishing Occupations”

metropolitan area since the previous year in order to allocate the labor delivery, and earnings of the individual to the appropriate labor market. To limit measurement error in earnings, we further restrict our sample to only include full-time workers, employed for the full year. We only include individuals born in the United States. Finally, we only include individuals who reside in one of the Core-based Statistical areas in the United States.

We define the main variables of interest as follows. An individual is categorized as a remote worker if they answer “work from home” to the question “What is your means of transportation to work?”.⁸ Our main measure of earnings is log hourly wage. We compute it by dividing yearly wage income by the estimated number of hours worked in the year. To obtain the total number of hours worked per year, we multiply the usual number of hours worked per week by the total number of weeks worked in the year.⁹ For individuals located in small CBSAs (Micropolitan Statistical Areas), the CBSA is sometimes missing in IPUMS. We use a crosswalk from the PUMA (smallest geographical areas recorded in IPUMS) to CBSAs, by the intermediary of a crosswalk from PUMA to counties, and from counties to CBSAs.

Our final sample contains 22,789,086 observations, each corresponding to an individual in a given year. There are 637 distinct CBSAs covered by the sample. We report the number of observations, the share of remote workers, and the median hourly pay of commuters and remote workers per year in Table A1.

A.2.2 NLSY Sample

Our NLSY sample is constructed from the public use NLSY79 dataset.¹⁰ We only include individuals from the main sample.¹¹ Besides this restriction, we include all individuals.

We define the main variables of interest as follows. When estimating the remote work premium, we use a continuous measure of remote work based on the number of hours worked at home per week. When a discrete definition is necessary, for example, when determining transitions into and from remote work, we use 24 hours of work at home per week as the threshold. Our main measure of earnings is hourly rates of pay, reported directly in the data. The geographical location is coded by the region of the United States. The four regions are Northeast, North-Central, South, and West.

Our final sample comprises, on average, 30,548 observations per year, representing observations from 5,656 individuals. We report the number of observations, average number of hours worked at home, and median hourly pay of commuters and remote workers per year in Table A2.

and “Military Occupations/NA”, respectively), and workers whose reported “class” or worker is self-employed (variable `classwkr` equal to 1).

⁸This is coded as `tranwork` = 80 in IPUMS.

⁹The yearly income variable is `incwage`. The number of weeks is coded into bins by the variables `wkswork*`, and the usual number of hours is recorded in `uhrswork`.

¹⁰Note that there also exists the NLSY97, which follows individuals born between 1980 and 1984. Unfortunately, for the purposes of our analysis, the number of hours worked from home is not reported in this panel.

¹¹That is, we exclude individuals from the supplemental and military samples that disproportionately survey individuals in the military and economically disadvantaged non-black, non-Hispanic individuals.

Table A1: Summary Statistics for the Census/ACS Sample

Year	Number of Observations	Share of Remote Workers (pct)	Median Hourly Pay of Commuting Workers (2021 \$/hr)	Median Hourly Pay of Remote Workers (2021 \$/hr)
1980	1,112,304	0.42	29.3	19.0
1990	1,788,782	0.64	26.8	22.5
2000	2,178,352	1.31	26.9	32.5
2005	517,591	1.51	26.7	35.9
2006	543,922	1.65	26.1	36.3
2007	549,974	1.80	26.4	36.2
2008	593,101	2.00	25.6	37.0
2009	569,593	2.16	25.7	35.8
2010	560,349	2.33	26.0	34.7
2011	540,518	2.45	25.6	35.7
2012	557,632	2.56	25.1	35.4
2013	575,307	2.72	24.9	35.0
2014	579,939	2.86	25.0	35.5
2015	592,265	3.02	24.9	36.5
2016	602,106	3.38	25.2	36.7
2017	618,611	3.61	25.8	37.6
2018	627,578	3.79	26.0	37.9
2019	637,308	4.29	26.4	37.0
2020	482,726	18.53	26.0	39.0
2021	601,567	21.98	25.7	41.1
2022	646,785	17.94	25.8	39.2
2023	395,762	16.74	27.2	39.3

Data from the Census/ACS. Hourly pay is adjusted for the Consumer Price Index and defined as the total annual earnings divided by the total number of hours worked in the year.

A.2.3 SafeGraph Sample

We measure visits to CBSAs' CBDs with the Neighborhood Patterns dataset, which contains monthly data between January 2019 and July 2022. Every month, the data is reported in a table that lists the number of phone devices that stopped for a visit inside a census block group by block group of origin. A visit is defined as the recording of the same device inside a polygon identified as a "place of interest" (i.e., a place of business) for more than a minute. SafeGraph also reports for each block group and each month the number of devices with a primary nighttime location inside the specified block group. We refer to this number as the number of residing devices in a block group.

Visits are categorized based on the behavior associated with the visit. Our main category of interest is the one associated with visits featuring a "work" behavior. "Work" visits are those

Table A2: Summary Statistics for the NLSY Sample

Year	Number of Observations	Average Number of Hours Worked at Home	Median Hourly Pay of Commuting Workers (2021 \$/hr)	Median Hourly Pay of Remote Workers (2021 \$/hr)
2002	30,541	1.34	14.1	18.8
2004	30,548	1.64	15.2	19.7
2006	30,545	1.61	16.0	23.1
2008	30,548	2.07	16.8	23.2
2010	30,549	2.14	17.1	23.7
2012	30,540	2.61	18.0	25.6
2014	30,548	2.96	18.5	27.2
2016	30,549	3.45	19.2	28.6
2018	30,546	3.52	20.0	29.5
2020	30,544	7.90	20.0	31.5
2022	30,542	7.27	22.0	34.6

Data from the NLSY79. Hourly pay is adjusted for the Consumer Price Index and is reported for the main job during the specified two-year period.

recorded Monday through Friday between 7:30 am and 5:30 pm and that dwelled for at least six hours. Ideally, we would use “work” visits for all our analysis of visits to the CBD. However, this category only accounts for a small share of the total number of visits, leading the number of recorded “work” visits to be more volatile over time and less precisely measured.

For this reason, we use two different measures of visits in our analysis. First, we use the number of “work” visits from all block groups. We use the average number of monthly “work” visits in 2019 to define the location of the CBD. Second, we use the number of visits of any category by block group of origin. This is our preferred measure to study the variation over time of foot traffic patterns to the CBD.

Once the CBDs of each CBSA are defined according to the procedure defined in Section A.6, we define mobility to the CBD at the origin block group of level. For each block group i , month t , in a CBSA j , we compute the number of visits $N_{ii't}$ originating from block group i that have as destination a block group that is inside a CBD of CBSA j , divided by the number N_{it}^{res} of sampled devices residing in block group i at t :

$$sh_{it}^{CBD} = \frac{\sum_{i' \in CBD_j} N_{ii't}}{N_{it}^{res}}, \quad (37)$$

noting that we allow CBSAs to have multiple CBDs.

We exclude block groups with fewer than 300 residing devices in a month. Our sample contains data on 896 CBSAs, with 203,075 distinct census block groups. The median CBSA in the sample has 59 distinct block groups with available foot traffic data to the CBD.

A.2.4 ACS Housing Rents Sample

We assemble a dataset of housing rents and local market characteristics at the block group level from the 2015-2019 ACS. The main outcome variable in our sample of block group-level rents is the median rent paid in the block group.

Our controls include the percentage of dwellings by type of structure, number of bedrooms, and construction decade, all based on the 2015-2019 ACS data. Additionally, we include controls for block-group characteristics such as the percentage of Hispanic, Black, and Asian populations. We also include controls from [Lee and Lin \(2017\)](#) that are defined at the census tract level.¹² These include the average slope, the maximum temperature in July, the minimum temperature in January, annual precipitations, the distance to the closest port, the distance to the closest river, the distance to the closest lake, the distance to the closest shore, and the surface area of the block group.

Finally, we compute the distance of each block group to the closest CBD of the CBSA, using the latitude and longitude of the centroid of the block group.

A.3 Estimation of the Transition Elasticity and Transition Costs

A.3.1 Predicting Transition Shares

We estimate a probit model to control for individual characteristics in transition probabilities $\ell\ell'$:

$$Y_{i\ell\ell't} = \Phi \left(\delta_t^{r(i)} + X_{it}\beta \right),$$

where $Y_{i\ell\ell't}$ is an indicator of individual i transitioning from ℓ to ℓ' , $r(i)$ is individual i 's education-region group (among the eight possible groups), X_{it} contains individual i 's age, age squared, tenure at the job, tenure squared, occupation, industry. We define $\hat{\lambda}_{\ell\ell't}^r = \Phi \left(\hat{\delta}_t^r + \bar{X}_{it}\hat{\beta} \right)$ the predicted transition shares evaluated at mean values of X . The dependent variable in the estimation regression is then defined as

$$y_{\ell\ell't}^r \equiv \ln \frac{\hat{\lambda}_{\ell\ell't}^r (\hat{\lambda}_{\ell'\ell't+1}^r)^\beta}{\hat{\lambda}_{\ell\ell,t}^r (\hat{\lambda}_{\ell\ell't+1}^r)^\beta}.$$

We estimate the log hourly rates for each education group-region-year after controlling for individual characteristics

$$\ln w_{it} = X_{it}\beta + \zeta_i + \omega_{it}$$

where X_{it} contains individual i 's age, age squared, tenure at job, tenure squared, occupation, industry, and region. We define $\ln w_{\ell't+1}^r$ as the average value of $\hat{\omega}_{it+1}$ for individuals in education-region r . With 4 regions, 2 education groups, 9 periods (every two years from 2002 to 2018), 2 transition types, we obtain a maximum of $4 \times 2 \times 9 \times 2 = 144$ observations.

¹²We assign the same value of these geographic controls to all block groups inside the same tract.

A.3.2 Transitions by City Size

In this section, we conduct an alternative estimation of (21), with transition shares defined by subsets of CBSAs with similar population rather than by groups of region-educational attainment.

While the region-education groups used in our main specification allow for differences in transition patterns across broad geographical areas, they pool observations from many different cities in the same region. These cities may offer different conditions to remote workers. Pooling observations from CBSAs with similar population recognizes that larger cities may offer different remote work conditions than smaller cities—at the expense of pooling observations from different regions.

In order to partition cities into subsets with similar population, we first obtain information on the CBSA and county of each individual from the restricted-use NLSY Geocode dataset.¹³ When the CBSA information is missing, we infer it from the county FIPS code, if available. For each CBSA j , $j = 1, \dots, J$, we compute the average population \overline{pop}_j over the 2000-2018 period. Given a number of subsets K , we order CBSAs by increasing average population, such that the CBSAs indexed by j and $j + 1$ satisfy $\overline{pop}_j \leq \overline{pop}_{j+1}$ for any $j = 1, \dots, J - 1$. We then define the threshold indices $(\tau_k)_{k=0,\dots,K}$, such that $\tau_0 = 0$, $\tau_K = J$, and for $k = 1, \dots, K - 1$, τ_k is defined recursively as the smallest index such that all CBSAs indexed between τ_{k-1} and τ_k account for at least $1/K$ of the total average population across all CBSAs,

$$\tau_k = \min_{\tau=\tau_{k-1},\dots,J} \sum_{j=\tau_{k-1}}^{\tau} \overline{pop}_j \geq \frac{1}{K} \sum_j^J \overline{pop}_j, \quad k = 1, \dots, K - 1.$$

For each $k = 1, \dots, K$, we refer to the subset $\{j | \tau_{k-1} < j \leq \tau_k\}$ of CBSAs as subset k . We then define transition shares by counting the number of transitions into and out of remote work of individuals located in CBSAs that are part of the same subset k . By construction, subset $k = 1$ contains many small CBSAs, while subset K contains few large ones.

In Table A3, we describe the results from estimating (21) with $K = 5$ subsets of cities, defining remote work as spending either $d = 1$ or $d = 2$ days per week at home. We compare the OLS estimator with the Poisson Pseudo Maximum Likelihood (PPML) estimator. Given the limited number of remote workers observed per subset k and year t , the transition shares $\lambda_{\ell\ell't}^k$ are sometimes computed based on a small number of observations. We define a minimum threshold \bar{n}_{remote} of remote workers, such that observations $y_{\ell\ell't}^k$ are included in the estimation only if more than \bar{n}_{remote} remote workers are observed in subset k , year t . In the case where we define remote work as $d = 1$ day per week at home, we set $\bar{n}_{remote} = 20$, leaving 62 observations; with $d = 2$, we set $\bar{n}_{remote} = 10$, leaving 66 observations.

The estimates of s and F from the OLS and PPML estimator, with $d = 1$, are reported in Columns (1) and (2). The estimates of s are similar, and not significantly different from our main estimate of 0.3. The estimates of F are also close to our main estimate of 1.78. The estimates

¹³A description of the NLSY Geocode data is available at <https://www.bls.gov/nls/request-restricted-data/nlsy-geocode-data.htm>.

Table A3: Estimates of the Gravity Equation Based on City Size

	(1) Remote = 1 day	(2)	(3) Remote = 2 days	(4)
	OLS	PPML	OLS	PPML
$\ln \frac{w_{\ell t+1}^r}{w_{\ell t+1}^r}$	1.439 (0.380)	1.384 (0.389)	1.071 (0.482)	0.886 (0.460)
$d_{\ell \ell'}$	1.100 (0.686)	1.105 (0.661)	0.513 (0.933)	0.080 (0.764)
$d_{\ell \ell'}(t+1)$	-0.051 (0.046)	-0.060 (0.046)	0.133 (0.077)	0.027 (0.046)
$d_{\ell \ell'} L_{c,t+1}^r$	-0.152 (14.81)	-5.603 (14.71)	8.880 (17.19)	11.60 (14.73)
$d_{\ell \ell'} L_{t+1}^r$	0.103 (14.78)	5.546 (14.69)	-8.899 (17.16)	-11.60 (14.71)
$cons$	-0.339 (0.065)	-0.231 (0.060)	-0.406 (0.065)	-0.272 (0.060)
Implied parameters				
s	0.640 (0.169)	0.666 (0.187)	0.860 (0.387)	1.041 (0.540)
F	2.773 (0.910)	1.962 (0.780)	4.458 (2.020)	3.610 (2.158)
N	62	62	66	66
R^2	0.14		0.20	

Robust standard errors in parentheses. Structural parameters estimated with the Delta method.

obtained from defining remote work as $d = 2$ days or more per week are reported in Columns (3) and (4). The OLS and PPML yield slightly higher estimates of both s and F , although our main values of s and F are contained in the 95% confidence intervals of these estimates.

A.4 Occupations

We define 22 groups of occupations based on the occupation classification used in the 2000 decennial census, denoted OCC in IPUMS. From the 2000 decennial census until the latest ACS, the 2000 Census classification is available. For the decennial census waves in 1980 and 1990, the 1990 Census classification is available. We use a crosswalk between the 1990 and 2000 Census classifications to obtain a consistent definition of our occupation groups.

The NLSY uses the 2000 Census occupation classification from 2002 onward. Prior to 2002, the

Table A4: Summary Statistics for Occupation Groups

Code	Occupation	2019 Share of Total Employment	2019 Share That is Remote
43	Executive, Administrative, and Managerial Occupation	0.118	0.067
95	Management Related Occupations	0.050	0.088
124	Mathematical and Computer Scientists	0.041	0.106
156	Architecture and Engineering	0.025	0.041
196	Life, Physical, and Social Services	0.012	0.058
206	Community and Social Services	0.020	0.042
215	Legal	0.011	0.051
255	Education, Training, and Library	0.070	0.026
296	Art, Design, Entertainment, Sports and Media	0.016	0.083
354	Healthcare Practitioners and Technical	0.068	0.026
365	Healthcare Support	0.032	0.055
395	Protective Service	0.024	0.017
416	Food Preparation and Serving Related	0.047	0.012
425	Building and Grounds Cleaning and Maintenance	0.026	0.017
465	Personal Care and Service	0.017	0.031
496	Sales and Related	0.085	0.060
593	Office and Administrative Support	0.123	0.041
613	Farming, Forestry, and Fishing	0.002	0.073
694	Construction and Extraction	0.050	0.015
762	Installation, Repair, and Maintenance	0.032	0.017
896	Production	0.066	0.013
983	Transportation and Material Moving	0.064	0.016
999	Experienced Unemployed not Classified by Occupation	0.001	0.016

Occupation groups based on the occupation classification used in the 2000 decennial census, denoted OCC in IPUMS.

NLSY uses the 1970 Census occupation classification. We use a crosswalk from the 1970 Census to the 1990 Census classifications, then from the 1990 Census to the 2000 Census classifications to obtain a consistent definition.

We report descriptive statistics about these occupation groups in Table A4.

A.5 Remote Work Premium

A.5.1 Estimates from the ACS

In addition to our preferred estimation of the remote work premium based on individual longitudinal data in the NLSY, we also estimate here the remote work premium based on data from the American Community Survey. Hence, rather than defining remote work based on the num-

ber of hours worked at home, we define remote work as a binary variable. Specifically, we define $d_{remote_{it}}$ as an indicator that equals one if an individual reports “work at home” as their means of transportation to work, and then predict $\hat{d} = 1$ to represent remote work.

We then estimate the national trend and an intercept for each of the 22 occupation groups, denoted by o . Specifically, we estimate the following equation:

$$\ln w_{it} = (\psi_{o(i)}^0 + \psi^1 t) d_{remote_{it}} + X_{it} \beta_{o(i)} + \epsilon_{it},$$

where $\ln w_{it}$ is the log of the hourly wage for individual i at time t , $\psi_{o(i)}^0$ and ψ^1 represent the intercept and the national trend for occupation group o , respectively, and X_{it} is a vector of individual-level control variables, including age, age squared, tenure at the job, tenure squared, industry, marital status, race, education-year, number of children, metro area-year. We focus on full-time US-born workers in metropolitan areas observed between 2000 and 2018.

Finally, we estimate the remote work premium in city j as follows:

$$\psi_{jt} = \sum_o sh_{oj}^{2018} (\psi_o^0 + \psi^1 t) \hat{d},$$

where sh_{oj}^{2018} is the share of workers in city j working in occupation o in 2018.

A.5.2 Wage Premium of Remote Work by Occupations’ Teleworkable Index

Our theory predicts that cities’ heterogeneous paths in the wake of the pandemic lockdowns can be explained without large changes, or any change at all, in the productivity of remote work—a feature that we view as appealing.

However, there may have been some changes in the productivity of remote work, and these changes may have been heterogeneous across cities. One possibility is that occupations that offer a high potential for telework may have experienced larger increases in productivity, leading CBSAs with higher employment shares in those occupations to experience higher average increases in remote work productivity.

We investigate this possibility by plotting a version of Figure 1b for two groups of occupations in the ACS: those above and below the median share of teleworkable index, according to [Dingel and Neiman \(2020\)](#).

The occupation groups above the median value of teleworkable index are “Executive, Administrative, and Managerial Occupation”, “Management Related Occupations,” “Mathematical and Computer Scientists,” “Architecture and Engineering,” “Life, Physical, and Social Services,” “Community and Social Services,” “Legal,” “Education, Training, and Library,” “Art, Design, Entertainment, Sports and Media,” “Sales and Related,” and “Office and Administrative Support.”

Those below the median value of teleworkable index are “Healthcare Practitioners and Technical,” “Healthcare Support,” “Protective Services,” “Food Preparation and Serving Related,” “Building and Grounds Cleaning and Maintenance,” “Personal Care and Service,” “Farming,

Table A5: Remote Work Premium for Occupation Groups

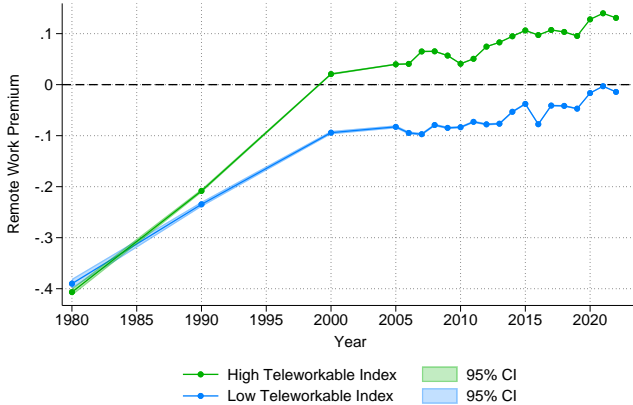
	(1) NLSY Log Hourly Wage	(2) ACS Log Hourly Wage
Remote	-0.006 (0.001)	0.029 (0.000)
Remote × Year	0.001 (0.000)	0.006 (0.000)
Management Related Occupations × Remote	0.000 (0.001)	-0.058 (0.000)
Mathematical and Computer Scientists × Remote	0.002 (0.001)	-0.021 (0.000)
Architecture and Engineering × Remote	0.000 (0.001)	-0.009 (0.000)
Life, Physical, and Social Services × Remote	-0.002 (0.004)	0.013 (0.001)
Community and Social Services × Remote	-0.001 (0.003)	-0.190 (0.001)
Legal × Remote	0.002 (0.002)	-0.060 (0.001)
Education, Training, and Library × Remote	0.003 (0.002)	-0.064 (0.000)
Art, Design, Entertainment, Sports × Remote	-0.003 (0.003)	-0.080 (0.001)
Healthcare Practitioners and Technical × Remote	-0.001 (0.002)	-0.151 (0.000)
Healthcare Support × Remote	-0.002 (0.003)	-0.373 (0.001)
Protective Service × Remote	-0.000 (0.003)	-0.086 (0.001)
Food Preparation and Serving Related × Remote	-0.004 (0.003)	-0.153 (0.001)
Building Cleaning and Maintenance × Remote	-0.003 (0.003)	-0.198 (0.001)
Personal Care and Service × Remote	-0.003 (0.002)	-0.325 (0.001)
Sales and Related × Remote	0.002 (0.001)	0.140 (0.000)
Office and Administrative Support × Remote	-0.002 (0.001)	-0.050 (0.000)
Farming, Forestry, and Fishing × Remote	-0.009 (0.004)	-0.038 (0.001)
Construction and Extraction × Remote	-0.003 (0.004)	-0.111 (0.001)
Installation, Repair, and Maintenance × Remote	-0.002 (0.001)	-0.125 (0.001)
Production × Remote	-0.001 (0.003)	-0.069 (0.001)
Transportation and Material Moving × Remote	-0.009 (0.007)	-0.141 (0.001)
Indiv. Controls	Yes	Yes
Year FE	Yes	Yes
Occ. & Ind. FE	Yes	Yes
Indiv. FE	Yes	No
Observations	40,385	15,872,072

Robust standard errors in parentheses. Occupation groups based on the occupation classification used in the 2000 decennial census, denoted OCC in IPUMS.

Forestry, and Fishing,” “Construction and Extraction,” “Installation, Repair, and Maintenance,” “Production,” “Transportation and Material Moving,” and “Experienced Unemployed not Classified by Occupation.”

We report the results in Figure A1. The two series show that, expectedly, the premium for remote work has been higher for occupations with high teleworkable index. However, both groups

Figure A1: Remote Work Hourly Wage Premium – Low vs. High Teleworkable Index Occupations



This figure reports the coefficients of yearly remote work indicators from the regression of log hourly wages, including the same controls as in Panel (b) of Figure 1b, for two subsamples: individuals working in occupation groups with above and below median teleworkable index, as defined by [Dingel and Neiman \(2020\)](#). The shaded areas represent the 95 confidence interval around the estimates.

have experienced parallel upward trends since 2005, with not clear sign of differential growth including after 2020. We view this as another sign that large heterogeneous changes in the productivity of remote work of specific occupations is unlikely to be the main driver of the large divergence in city structure since the COVID-19 pandemic.

subsec:mobility

A.6 Defining Central Business Districts

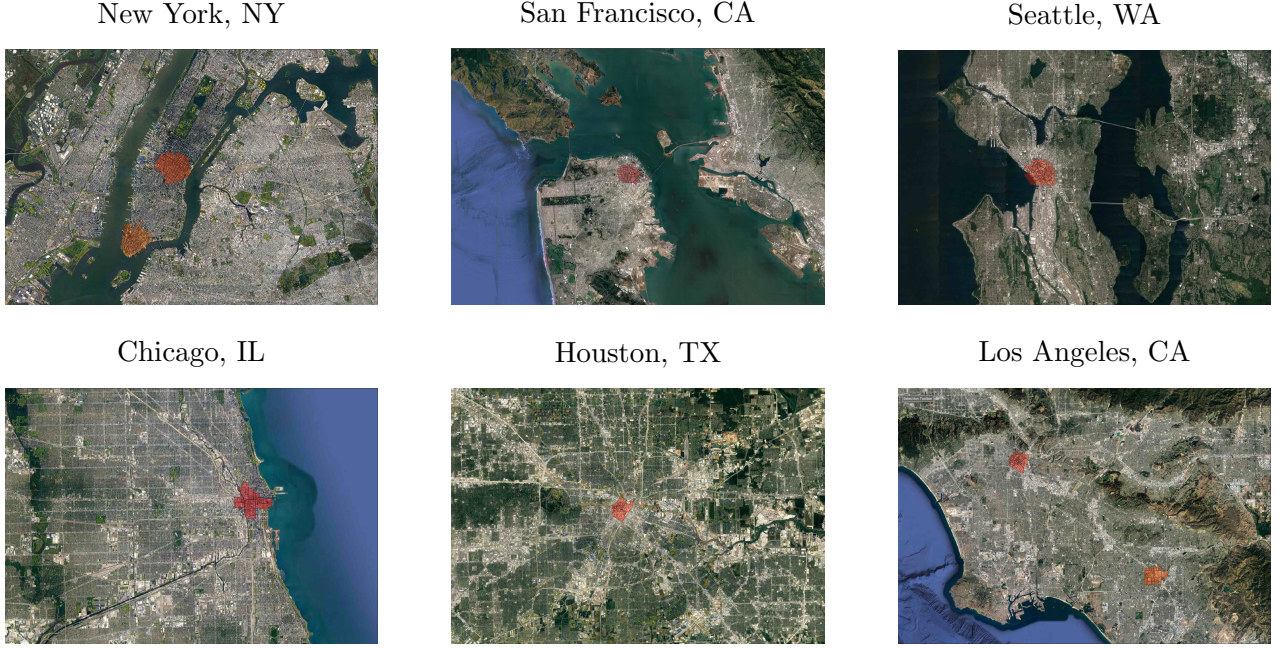
For each CBSA j , chosen radius r , we define the geographic coordinates of the k^{th} CBD of j as

$$z_{cbd,j}^{(1)}(r) = \arg \max_z \sum_{i \in cbsa_j} \mathbb{1}\{dist(z_i, z) \leq r\} \frac{N_{commute\ i2019}}{land_area_i}, \quad (38)$$

where i is a block group, z_i its coordinates (latitude and longitude), $dist(\cdot, \cdot)$ the geodesic distance, $N_{commute\ i2019}$ the total number of work-related visits recorded in block group i during the year 2019 from SafeGraph.

For $k \geq 2$, we impose that the center of the k^{th} CBD is not inside previous CBDs. We retain the k^{th} CBD if it attracts at least 80% as many commuters as the main CBD and if it does not overlap with CBDs 1 to $k-1$. We define the distance of each zip code to the CBD as the distance to the nearest CBD.

Figure A2: Central Business Districts of Selected Large Cities



A.7 Change in Visits to the CBD for Selected Cities

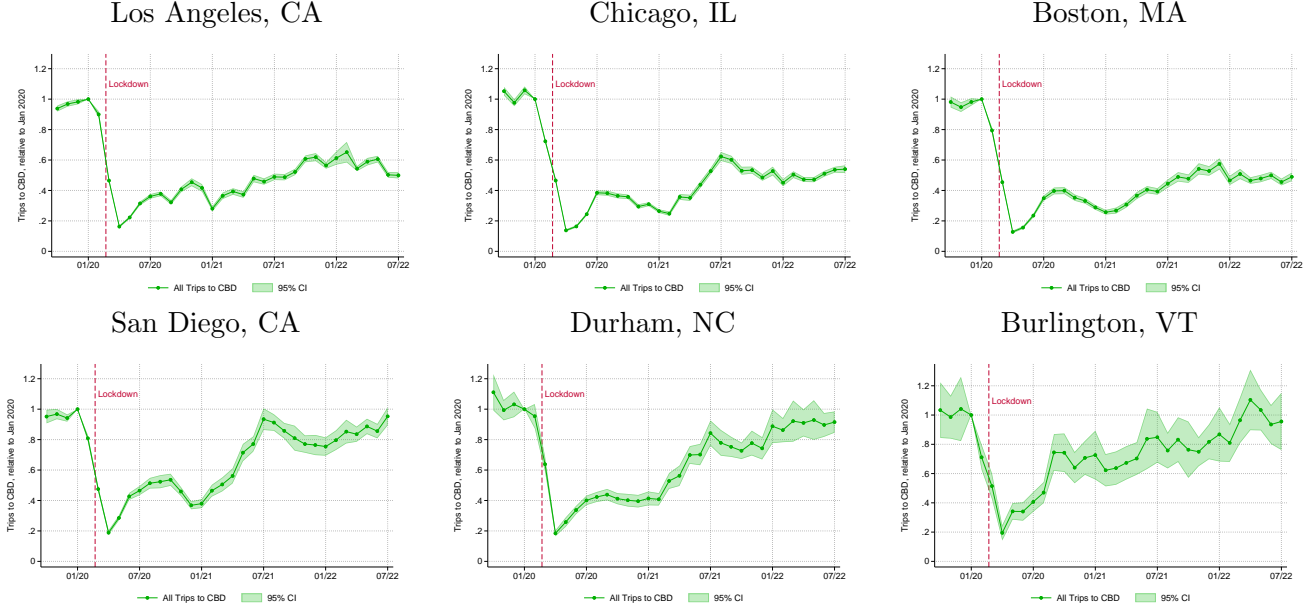
In Figure A4, we report the time series of visits to the CBD of six selected cities. The estimates are the coefficients for monthly indicators in a regression at the block group-month level. The outcome variable is the number of visits to the CBD of the CBSA from the specified block group, divided by the number of residing devices in that block group, as defined in (37), scaled by the value of this ratio in January 2020. That is, our outcome variable is $y_{it} = sh_{it}^{CBD}/sh_{it_0}^{CBD}$, where i is a block group, t is a month, and t_0 is set to January 2020. We then estimate the following regression for each CBSA:

$$y_{it} = \sum_{s=s_0}^S \beta_s \mathbf{1}\{t = s\} + \epsilon_{it},$$

where $s_0 = 1$ for October 2019, and $S = 34$ for July 2022. We restrict the sample to block groups that are located less than 50 kilometers away from the CBD, and cluster standard errors at the census tract level, which contains 3.4 block groups on average.

Figure A4 reports the estimates of β_s for the CBSAs of Los Angeles, CA, Chicago, IL, Boston, MA, San Diego, CA, Durham, NC, and Burlington, VT, along with the 95 percent confidence interval around each estimate. All six CBSAs experience a sudden drop in visits to the CBD in March-April 2020, corresponding to the period of nation-wide stay-at-home orders at the onset of the COVID-19 pandemic. The share of visits to the CBD drops to about 20 percent of their value just three months earlier. The patterns in the following months are similar for the three cities in the top panel. After some ebbs and flows likely explained by the various waves of COVID-19

Figure A4: Change in Visits to the CBD for Selected Cities



Estimates of monthly indicators in a separate regression for each CBSA of visits to the CBD at the block group-month level. The outcome variable is the number of visits to the CBD from the specified block group, divided by the number of residing devices in that block group, as defined in (37), scaled by the value of this ratio in January 2020. The shaded areas represent the contour delimited by the consecutive 95 percent confidence intervals of each monthly indicator. Standard errors are clustered at the census tract of origin.

infections, visits to the CBD in these CBSAs stabilize at, or below, 50 percent of January 2020 levels. In the three cities in the lower panel, however, the patterns of visits to the CBD is starkly different: after a small temporary upset in the winter of 2021, visits to the CBD continue to increase and return to pre-pandemic levels, or close to, by the end of the sample period.

A.8 Office Trips for Selected Cities

In Section 3.1, we measure trips to the CBD as the share of *all* trips originating from a census block group and ending in the CBD, averaged across all block groups. This measure, therefore, captures not only workers' trips to the office, but also non-work-related trips, such as visits to retail stores, restaurants, and other amenities.

In this section, we confirm that, for the CBSAs for which they are available, office trips to the CBD follow the same patterns as all other trips. We use an alternative measure of trips to the CBD based only on the subset of trips that are labeled as *workplace* trips in the Neighborhood Patterns dataset. Workplace visits are defined by SafeGraph as those recorded Monday through Friday between 7:30 am and 5:30 pm and that dwelled for at least six hours. Workplace visits are recorded less consistently than all trips and are less often reported in smaller CBSAs. For the nine CBSAs analyzed in Figures 2 and A4, however, workplace visits are reported consistently.

We report the monthly estimates of *office* trips to these CBSA's CBDs in Figure A5.

Figure A5 reveals the same patterns as those observed in Figures 2 and A4. For all cities, the first months of the pandemic saw a drastic drop in trips to around 20 percent of their initial value. The recovery, however, has been quite different. While Madison, San Diego, Durham, and Burlington essentially went back to their pre-pandemic levels by the end of our sample period, CBD office trips for New York, San Francisco, Los Angeles, Chicago, and Boston have stabilized at around 40 percent of their pre-pandemic levels.

A.9 Evidence of Population Changes Across CBSAs

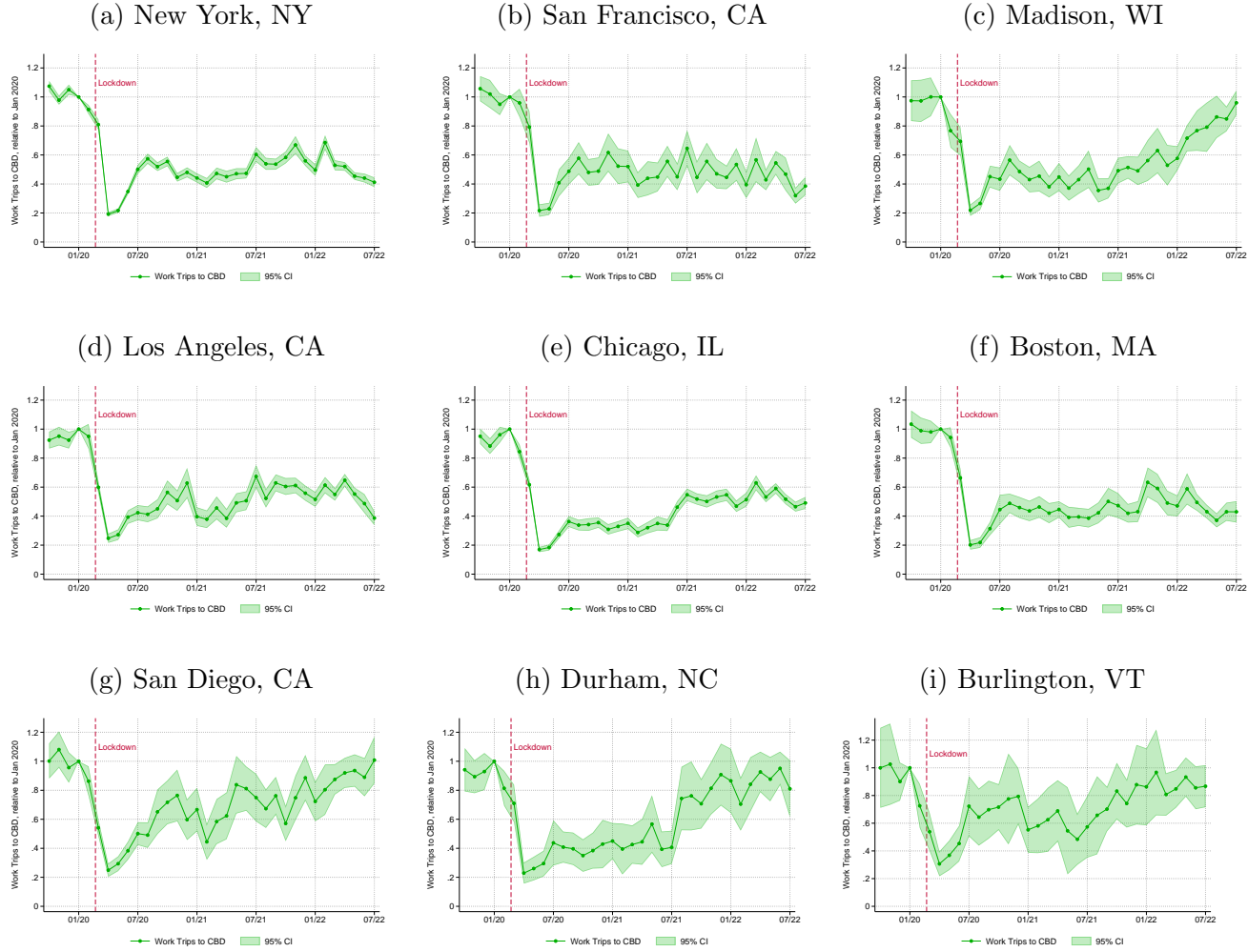
In this section, we motivate our choice of considering a closed-city model by documenting that, while there have been noticeable changes in CBSAs' populations since 2019, those changes are small in comparison to the large shifts in remote work, trips to CBD, and house price gradients documented in Sections 2 and 3.

We look at estimates of CBSAs' population published by the US Census Bureau. We build a yearly time series from 2015 to 2023 by appending a file with estimates from 2015 to 2020, included, and one from 2020, included, to 2023. Some CBSAs' delineations changed in 2020, leading to two different population estimates for that same year, one for each delineation. To avoid jumps due to these delineation changes, we adjusted the estimates in 2020-2023 by the difference in the two estimates in 2020. In Figure A6, we start by documenting the changes in population for the nine cities used as examples throughout the paper. Several cities, particularly those that experienced large decreases in trips to CBD, have also seen their population decline between 2019 and 2023. New York City's population declined by 3.1 percent, while San Francisco's population declined by 4.3 percent, the strongest decline in that group. CBSAs that returned to pre-pandemic levels of trips to CBD, such as Madison, WI, Durham, NC, Burlington, VT, and San Diego, CA, appear to be following their pre-pandemic trends. Note that the decline in population in the largest cities is consistent with our findings that these cities offer lower levels of welfare in the low-commuting equilibrium.

In Figure A7a, we show that this deviation from trend of the CBSA population for large cities, but not for smaller cities, appears to be systematic. Large CBSAs with employment above 1.5 million grew on average by 3.7 percent between 2015 and 2019, but only by 1.9 percent between 2019 and 2023. Small CBSAs with employment below 150 thousand, however, grew almost at the same rate between 2015 and 2019 (0.4 percent) and between 2019 and 2023 (0.5 percent). Hence, on average, small CBSAs on average grew at the same rate in the four years preceding and following the COVID-19 pandemic, while large CBSAs grew by 1.8 percentage points less. In comparison, these large CBSAs saw a decrease in trips to CBD by at least 40 percent.

In Figure A7b, we find that, even though larger cities appear to have experienced larger deviation from their population trends since the pandemic, there is little, if any, correlation between the population change between 2019 and 2023 and the change in trips to CBD between January 2020 and July 2022. We view this as further evidence that the reallocation of workers across

Figure A5: Office Trips to CBD relative to January 2020



Estimates of monthly indicators in a separate regression for each CBSA of *workplace* visits to the CBD—those recorded Monday through Friday between 7:30 am and 5:30 pm that dwelled for at least six hours—at the block group-month level. The outcome variable is the number of visits to the CBD from the specified block group, divided by the number of residing devices in that block group, as defined in (37), scaled by the value of this ratio in January 2020. The shaded areas represent the contour delimited by the consecutive 95 percent confidence intervals of each monthly indicator. Standard errors are clustered at the census tract of origin.

CBSAs is unlikely to be the essential driving force behind the dramatic changes in city structure we document in Sections 2 and 3.

A.10 Evidence on Remote Work, Agglomeration Externalities and Transportation Elasticities

In this subsection we ask what determines, empirically, whether a city is inside its cone. The several dimensions of heterogeneity that we have exploited to quantify the cities' parameters, like industrial and occupational composition and the rent gradients, all jointly contribute to this position. To organize our discussion, we leverage our theory, which indicates that the position of a city with respect to its cone is influenced by the city's size, agglomeration and transportation cost elasticities, and the relative productivity of remote work.

The left side of Figure A8 reports the relationship between the change in visits to the CBD and our estimates of agglomeration externalities, δ_j , transportation elasticities γ_j , and relative remote productivity z_j/A_j . Each bubble represents a city of population proportional to the bubble area. The right side of Figure A8 reports the share of cities that are predicted to be in their cone of multiplicity as a function of the same parameters. Blue dots indicate the fraction of cities in the cone in the calibrated model for 20 quantiles of the variable indicated on the horizontal axis.

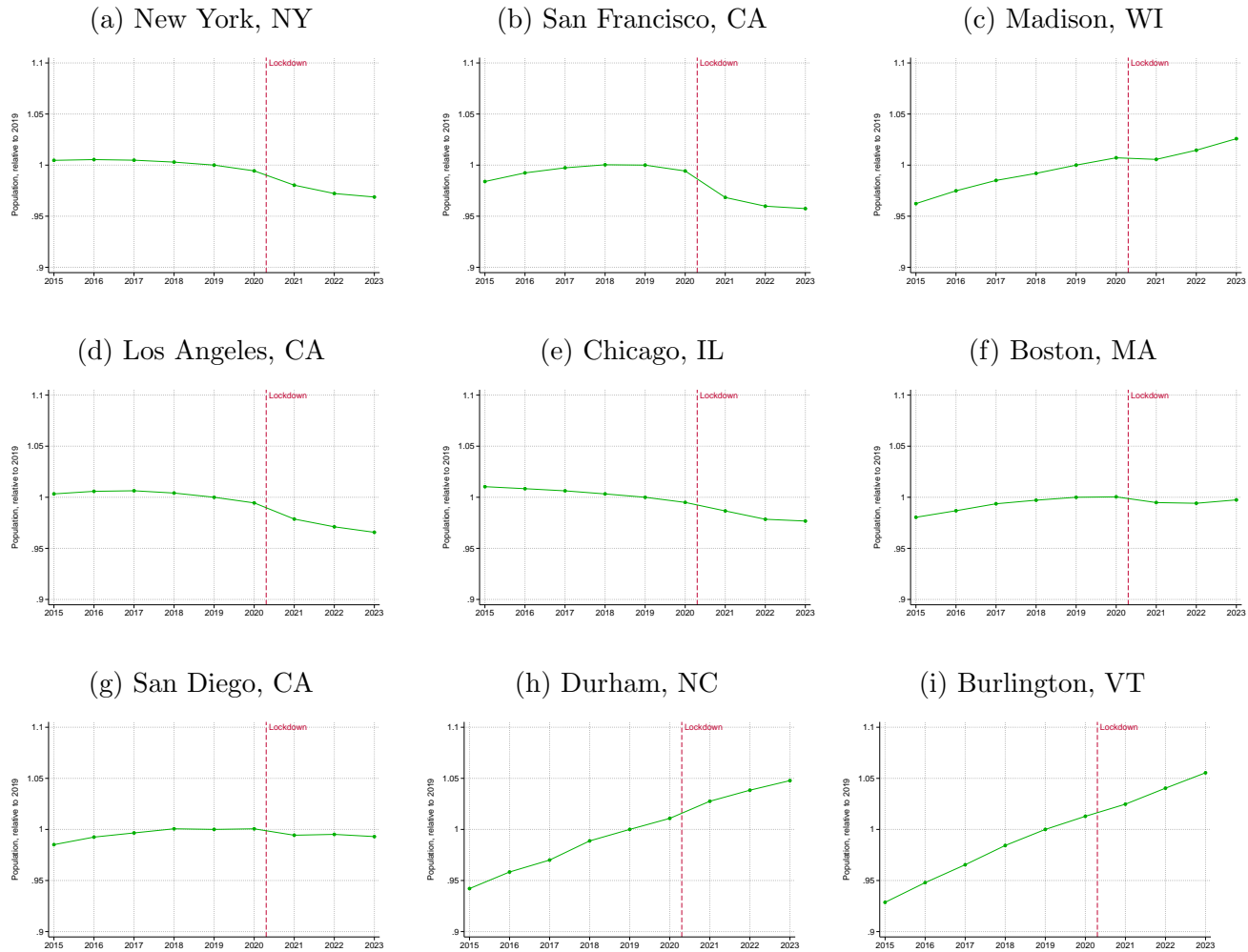
The left side of the figure shows that cities that experienced larger declines in visits to the CBD are those that have a larger agglomeration externality, a smaller transportation cost elasticity, and a higher relative productivity of remote work. These relationships are quite strong, as indicated by the magnitude and significance of the population-weighted linear fit in the figures and values of R^2 between 0.08 and 0.41.

The right side of the figure shows that the relationship between the drop in visits to the CBD and the key agglomeration parameters is rooted in the workings of the model. The figures show that calibrated cities with higher agglomeration externalities δ_j , lower transportation elasticities γ_j , and higher relative productivity of remote work z_j/A_j are those that are the most likely to be inside the cone of multiplicity.¹⁴ Therefore, our model predicts that these are the cities that are the most likely to remain in a low-commuting equilibrium after a temporary shock such as a lockdown.

In Table A6, we explore the relative ability of these factors to relate to CBD trips, and their contribution to whether each city is inside or outside its cone – the multivariate versions of the left and right columns of Figure A8. We note that these partial correlations should be interpreted with caution, since it is their joint combination that determines whether or not a city exhibits multiple stationary equilibria. In particular, in Column (1) we run a linear regression of the shortfall in trips to the CBD on standardized values of L_j , z_j/A_j , δ_j , and γ_j . We find that the variation in agglomeration elasticity and the relative remote work productivity are the most strongly associated

¹⁴Panel (d) in this figure excludes some large outliers focusing on $\gamma_j < 0.1$. This choice is made for the visibility of the graph, and the estimates return unchanged messages without these restrictions.

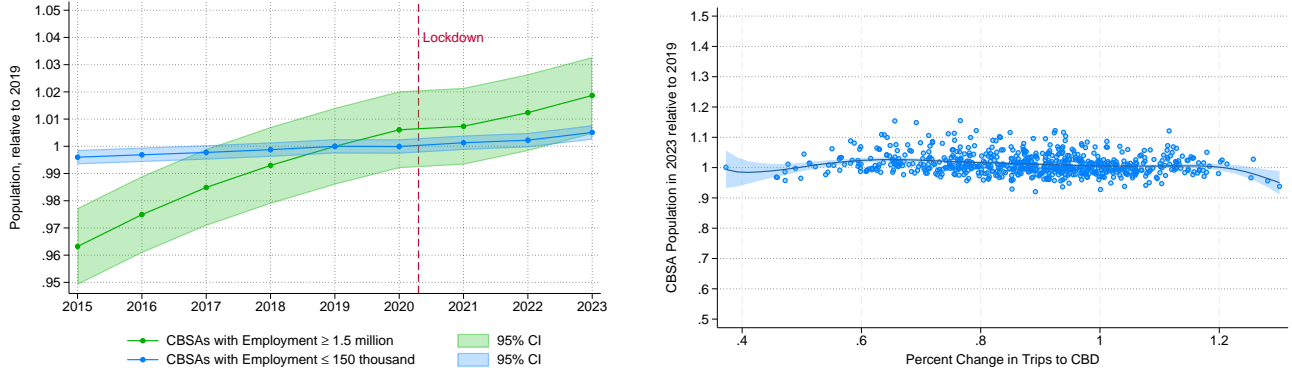
Figure A6: Change in Total Population Relative to 2019



Population estimates from “Annual Resident Population Estimates and Estimated Components of Resident Population Change for Metropolitan and Micropolitan Statistical Areas and Their Geographic Components for the United States,” available at <https://www.census.gov/data/tables/time-series/demo/popest/2020s-total-metro-and-micro-statistical-areas.html>.

Figure A7: Change in Total Population Relative to 2019

(a) Change in Population in Large vs. Small CBSAs (b) Population Change vs. Change in CBD Trips



Population estimates from “Annual Resident Population Estimates and Estimated Components of Resident Population Change for Metropolitan and Micropolitan Statistical Areas and Their Geographic Components for the United States,” available at <https://www.census.gov/data/tables/time-series/demo/popest/2020s-total-metro-and-micro-statistical-areas.html>. Panel (a) represents the average CBSA population relative to 2019 for i) CBSAs with total employment above 1.5 million (25 largest CBSAs), ii) CBSAs with total employment below 150,000 (663 smallest CBSAs). The shaded areas represent the consecutive 95 percent confidence intervals of each yearly estimate. Panel (b) reports the change in CBSA population between 2019 and 2023 against the change in visits to the CBD in July 2022 relative to January 2020. Each marker represents a CBSA. The solid line represents a fitted kernel-weighted local polynomial smoothing, with the shaded area corresponding to the 95 percent confidence interval around the fitted value.

to the drop in trips to CBD. In column (2), we estimate a probit regression of the indicator of whether the city is inside its cone on standardized values of L_j , z_j/A_j , δ_j , and γ_j . Empirically, we find a large role for the distance elasticity of transportation costs, γ_j , which is natural given the large variability we find in the data, followed by the relative productivity of remote work. The high pseudo- R^2 suggests that there is little residual variation to be explained by the interactions of these factors.

A.11 Establishment Employment Concentration by City Size

Our theory considers a competitive production sector in which no single firm is large enough to affect the equilibrium selection through its own demand for in-person and remote workers. In practice, however, some CBSAs host large establishments that can represent a substantial share of that CBSA’s employment. If smaller CBSAs are more likely to host such large establishments, they may be more likely to return to high levels of commuting if those establishments participate in bringing workers back to the office.

In this section, we show that, perhaps surprisingly, smaller MSAs (the subset of CBSAs for which we can perform the exercise) are *less* likely to host establishments that account for a large

Figure A8: Visits to CBD and Share of Cities in the Cone vs. City Parameters

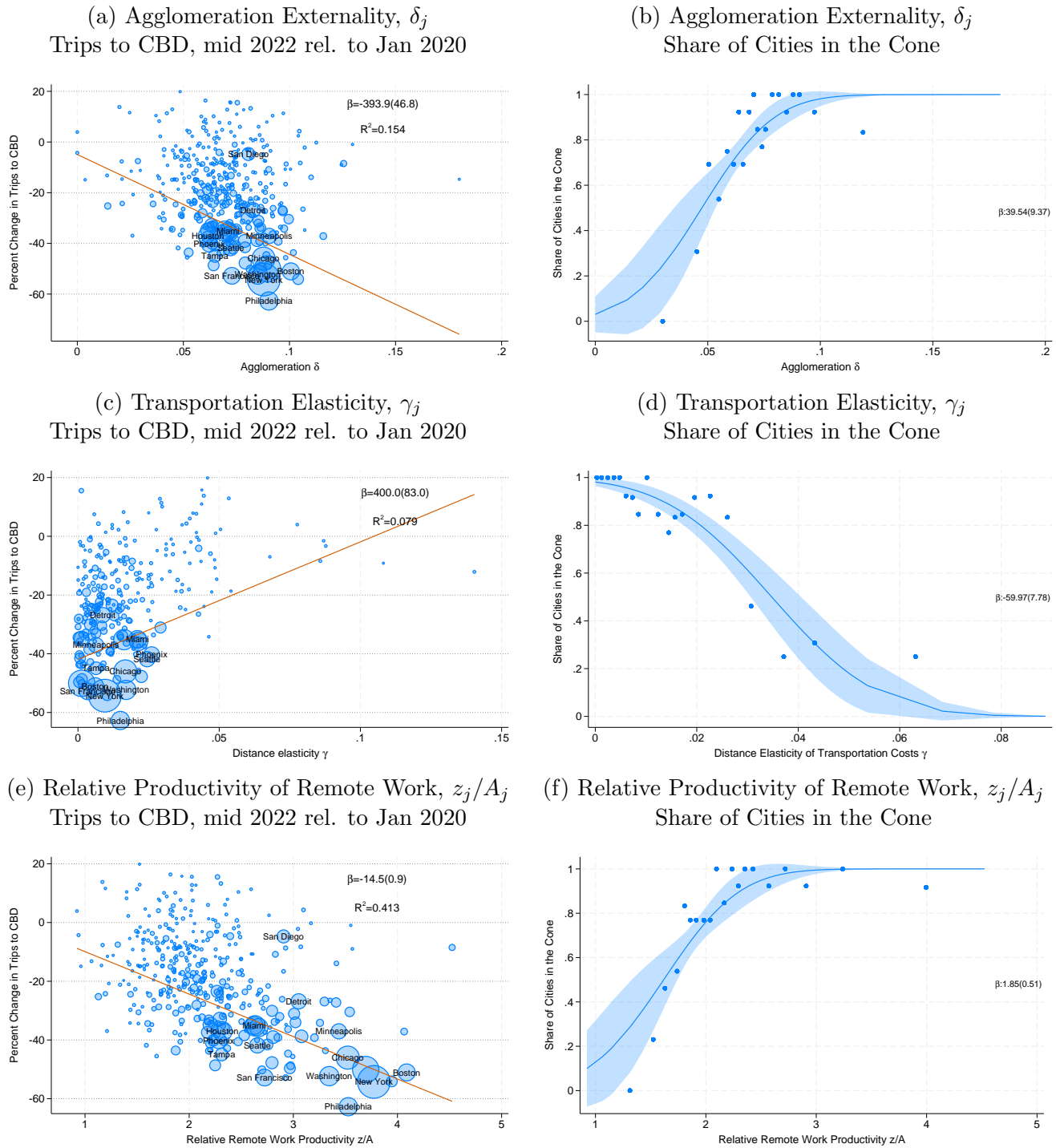


Table A6: Probit Regression of Cone Indicator on Model-Predicted CBSA Characteristics

	(1) Trip shortfall	(2) $\mathbb{1}_j^{\text{cone}}$
Employment	-2.37 (1.74)	-4.87 (1.17)
Relative Remote Productivity, z_j/A_j	-16.48 (4.07)	18.51 (3.57)
Agglomeration Externality, δ_j	12.63 (3.24)	7.29 (2.20)
Transportation Cost Elasticity, γ_j	1.58 (0.92)	-58.37 (12.87)
Constant	-19.13 (0.79)	13.96 (2.99)
Observations	274	274
R^2	0.334	
Pseudo R^2		0.974

Column (1) of this table shows the results of a linear regression of the shortfall of trips in July 2022 relative to January 2020, as described in the main text, on $\mathbb{1}_j^{\text{cone}}$ on $L_j, z_j/A_j, \delta_j$, and γ_j . Column (2) shows the results of a probit regression on the same set of variables. All the regressors have been standardized. Robust standard errors in parentheses.

share of their employment. We interpret this finding as indicative that the differential rates of return to the office between large and small CBSAs are unlikely to be facilitated by the idiosyncratic decisions of the largest establishments.

We examine the empirical relationship between the MSA-level concentration of employment in large establishments and the total employment size of the MSA. To this aim, we estimate, for each MSA j , the share of employment accounted for by the fraction p of largest establishments, $\chi_j(p) \in (0, 1)$, and relate it to the log employment in the MSA j , $\log(\text{emp}_j)$.

We start by constructing a Lorenz curve for the total MSA j 's employment in 2019. The curve maps the share $e_j(s) \in (0, 1)$ of MSA j 's establishments smaller than s into the share of employment $\zeta_j(s) \in (0, 1)$ accounted for by those establishments. The 2019 County Business Patterns' MSA file (CBP) contains, for each MSA j , the total employment in the MSA E_j , the total number of establishments N_j , and the number of establishments $n_j(r)$ in each of 11 different employment brackets $[t_l(r), t_u(r)]$, for $r = 1, \dots, 11$, plus a residual category $t_l(12)$ with employment above 5,000. With these data, we seek to 1) estimate employment in each bracket with an appropriate weight between the lower and upper end, 2) estimate employment in the top bracket where we only know the lower end, 3) to minimize the sum of squared deviations between estimated and actual employment across CBSAs. We address each of these points as follow:

1. We approximate employment in brackets size $[t_l(r), t_u(r)]$, for $r \leq 11$, with

$$emp(r; \omega, b) = t_u(r) [\omega \cdot \varphi(t_u(r); b)] + t_l(r) [1 - \omega \cdot \varphi(t_u(r); b)] \quad (39)$$

where $\omega \in [0, 1]$ is a weight common across all ranges, and $\varphi(t_u(r); b) \in [0, 1]$ is a “bending” function that shifts the common weight differentially across ranges as a function of a parameter $b \in [0, 1]$. The values of ω and b will be chosen optimally, as described below. Note that if $\omega = 0.5$, $\varphi(t_u(r); b) = 1$ for all r , the approximation is simply the average of the brackets’ endpoints; since the establishment size distribution is not uniform, one might conjecture that the appropriate midpoint varies across the intervals. In particular, if the establishment size is Pareto, the appropriate midpoint is closer to the left end for lower employment ranges than it is for higher employment ranges. We then seek a function $\varphi(t_u(r); b)$ that assumes values between 0 and 1, is increasing in the endpoint $t_u(r)$, and admits “no bending” as a possibility, that is, $\varphi(t_u(r); b) = 1$ for all $t_u(r)$. One such function is:

$$\varphi(x; b) = b + (1 - b) \left(\frac{x - 4}{4995} \right)^{1/2} \quad (40)$$

defined between the values of $x = 4$ (the upper end of the lowest employment bracket, 1 to 4) and $x = 4999$ (the upper end of the highest employment bracket, from 2,500 to 4,999 employees), and $b \in [0, 1]$. This function approaches a flat line at 1, and the heterogeneity among midpoints becomes less extreme, as $b \rightarrow 1$.

2. With regard to the second constraint, we parameterize employment in the residual interval as $emp(12; m) = 5,000m$, with $m \geq 1$. The total imputed employment in a CBSA can then be written as:

$$\tilde{e}_j(\omega, b, m) = \sum_{r=1}^{11} emp_j(r; \omega, b) n_j(r) + emp_j(12; m) n_j(12) \quad (41)$$

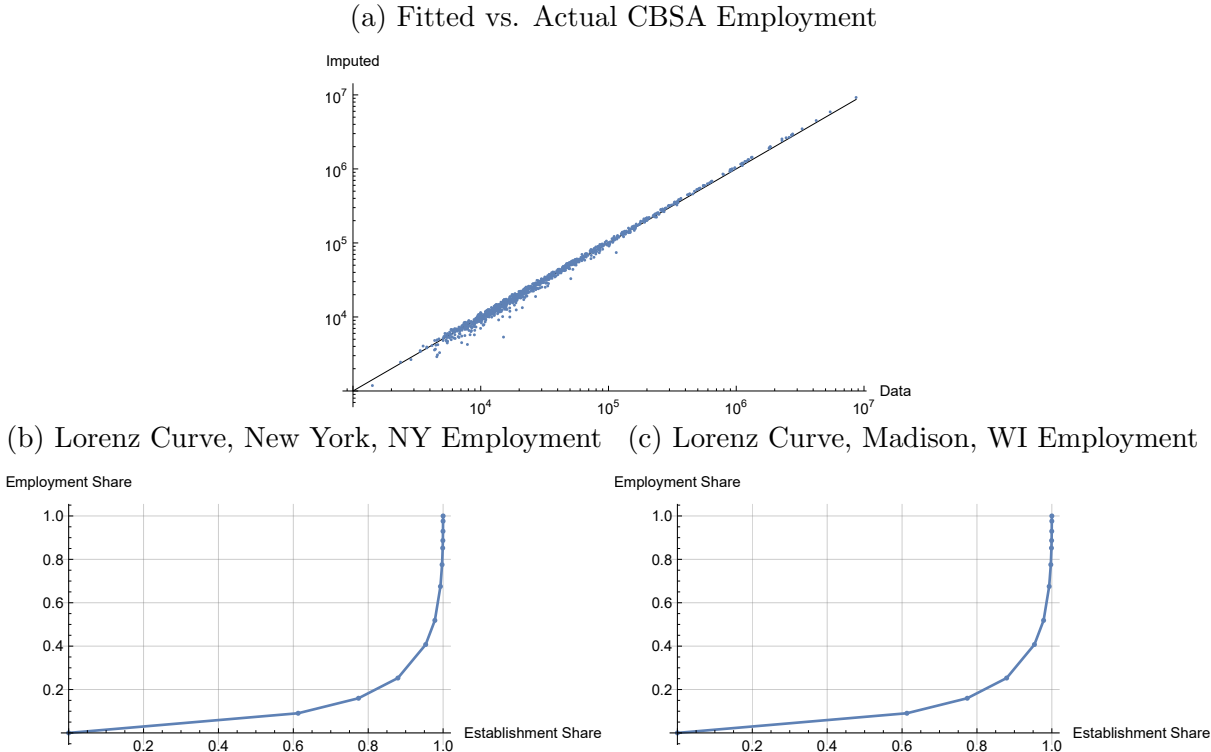
3. We then minimize

$$\rho(\omega, b, m) = \sum_j \left(\frac{\tilde{e}_j(\omega, b, m)}{E_j} - 1 \right)^2 \quad (42)$$

under the constraints that $\omega \in [0, 1]$, $b \in [0, 1]$, $m \geq 1$.

The best fit for our procedure is $b = 1$, $\omega = 0.4475$, $m = 1$, which rejects heterogeneous weights and suggests a common weight higher than 0.5 on the highest end of each bracket. Panel (a) of figure A9 reports a comparison between data and fitted CBSA employment, across CBSAs. This procedure delivers data on the number of establishments and an estimate of the total employment in each of the brackets, $emp_j(r; 0.447, 1) n_j(r)$, for each bracket and CBSA. We build the Lorenz curve for each MSA by computing the share of establishments up to a given size bin s , $e_j(s) = \sum_{r=1}^s n_j(r)/N_j$, and

Figure A9: Estimating employment by bracket size from CBSA County Business Patterns

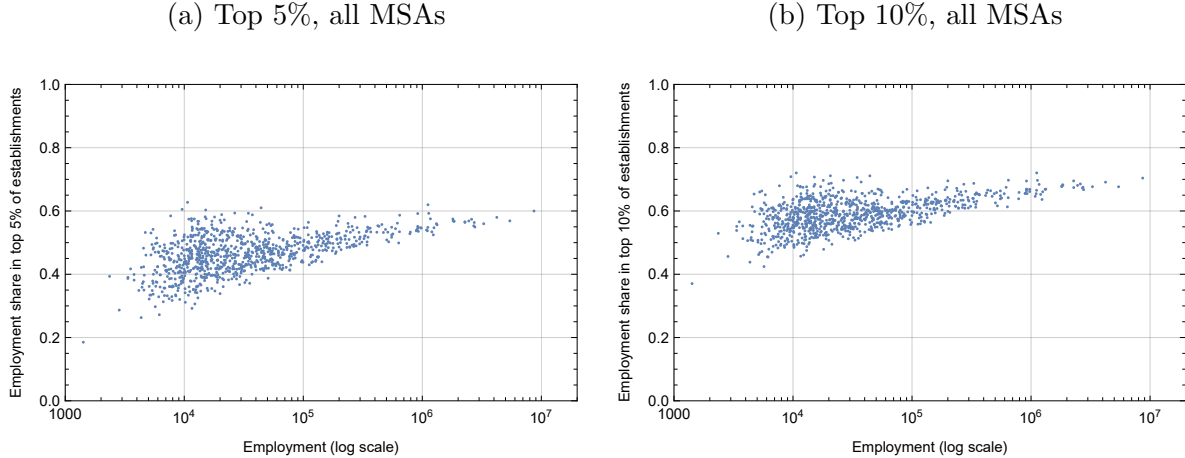


Panel (a) of this figure shows the relationship between actual CBSA employment on the x axis, and estimated employment after recovering the optimal weights ω, b, m from equation 42, on the y axis; the black line is the 45 degree line. Panels (b) and (c) show the implied Lorenz curves for the metro areas of New York, NY and Madison, WI.

the cumulative employment share accounted for by these establishments, $\zeta_j(s) = \sum_{r=1}^s emp_j(r)/E_j$. For each MSA j , we then linearly interpolate the set of points $(e_j(s), \zeta_j(s))$ to obtain the function $\tilde{\zeta}_j(s)$, giving, for each $s \in (0, 1)$, the share of employment accounted for by the $100e$ percent smallest establishments in that MSA. Finally, for a chosen share of top establishments p , we compute the share of employment accounted for by the $100p$ percent largest establishments in MSA j as $\chi_j(p) = 1 - \tilde{\zeta}_j(1 - p)$. Two examples of the function $\chi_j(p)$ for New York and Madison, WI, are reported in panels (b) and (c) of Figure A9.

Figure A10 shows the relationship between city size and the share of employment accounted for by the largest 5% and 10% of establishments, respectively. We find that smaller cities tend to have employment less concentrated in a few large establishments. We interpret this finding as indicative that the return to the office in smaller cities is less likely to be triggered by the decision of a few large employers mandating a return to the office.

Figure A10: Employment Concentration in Largest Establishments by MSA Size



Estimated share of employment accounted for by the top 5 and 10 percent establishments in size. Each dot represents a Metropolitan Statistical Area. The MSA employment is obtained from the 2019 County Business Patterns. The share of employment in the top establishments is obtained by constructing the Lorenz curve of employment share by establishment size for each MSA.

A.12 Changes in CBSAs' Teleworkable Employment

Our theory considers workers in a representative occupation with in-person and remote productivities that are calibrated as the employment-weighted average of our occupation-specific productivity estimates. This assumption abstracts from the possibility for workers to change their occupations over time. However, shifts in cities' occupational composition could partly explain their diverging trajectories if, in response to the pandemic lockdowns, workers in large cities decided to transition in large numbers to occupations more amenable to remote work, while workers in smaller cities did not.

In this section, we show that this was not the case. First, while there is a noticeable transition toward occupations with higher teleworkable index, it is of much lower magnitude than the shift in trips to CBD. Second, that shift is slightly more pronounced in *smaller* CBSAs, indicating that the dramatic switch to remote work in large cities is not explained by a disproportional shift toward teleworkable occupations.

In Figure A11, we report the evolution of the share of teleworkable employment, computed as the employment-weighted average of the time-invariant measures of occupational teleworkable index by Dingel and Neiman (2020). In New York City, we observed a marked, but limited, increase in teleworkable employment. The share increased by 2.3 percent between 2015 and 2019 and by 5.0 percent between 2019 and 2023. In San Francisco, the share of teleworkable employment has increased on average at a rate comparable to pre-pandemic. Our measure of teleworkable employment is more volatile in Madison; on average, it also increased at a similar rate to pre-pandemic.

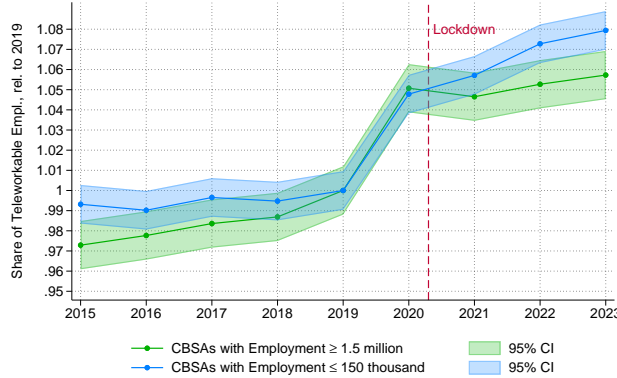
Figure A11: Change in Share of Teleworkable Employment for Selected Cities



Estimates are constructed by computing CBSAs' yearly occupational composition from the ACS, and multiplying each occupational share by the teleworkable index from [Dingel and Neiman \(2020\)](#).

We investigate these patterns systematically across large and small CBSAs in Figure A12. On average, the share of teleworkable employment increased by 5 percent between 2019 and 2020 in small and large CBSAs. By 2023, the increase was 7.9 percent in small CBSAs, and 5.8 percent in large CBSAs. We view this finding as indicating that changes in CBSAs' occupational composition are unlikely to be a key driver of the heterogeneous responses described in Section 3.

Figure A12: Change in Share of Teleworkable Employment in Large vs. Small CBSAs



Plotted coefficients represent the average share of teleworkable employment in a CBSA relative to 2019 for i) CBSAs with total employment above 1.5 million (25 largest CBSAs), ii) CBSAs with total employment below 150,000 (663 smallest CBSAs). The shaded areas represent the consecutive 95 percent confidence intervals of each yearly estimate.

A.13 Estimates of the Elasticity of Substitution Between Remote and In-Person Workers

A.13.1 Model with Multi-Sector CES Production and Inelastic Labor Supply

The model in Section 4 focuses on a representative production sector that implicitly assumes a linear production function in remote and in-person workers, such that the relative wage of remote

and in-person workers is independent of their relative labor supply. These assumptions translate into a simple strategy for estimating the remote work premium based on the relative wages of remote and in-person workers.

In this Section, we provide evidence in support of these assumptions. We develop an alternative model that allows for multiple sectors and a CES production in remote and in-person workers. We derive estimating equations for the elasticity of substitution between remote and in-person workers and find very large values that do not reject the linear specification in the main model. For that reason, we maintain the linear production model as our main model.

Consider a disk-shaped city with an exogenous population of size L . There are two final goods in the economy: consumption and housing. The final consumption good Q , the price of which we normalize to 1, is produced according to a Cobb-Douglas function over intermediate sectoral goods,

$$Q = \prod_{s=1}^S q_s^{\beta_s}, \quad \beta_s \in (0, 1), \quad s = 1, \dots, S, \quad \sum_{s=1}^S \beta_s = 1. \quad (43)$$

Sectoral goods are produced in the CBD by profit-maximizing firms under constant returns to scale according to a CES production function combining in-person and remote workers,

$$q_s = A_s [A_{cs} L_{cs}^\theta + A_{ms} L_{ms}^\theta]^{1/\theta}, \quad \theta \leq 1, \quad (44)$$

where L_{cs} is the number of in-person workers, L_{ms} is the number of remote workers, and $\theta = (\rho - 1)/\rho$, where ρ is the elasticity of substitution between remote and in-person workers. The efficiency of in-person and remote workers in sector s depends on the total economic activity that takes place in the city center across all sectors, which we measure, as in Section 4, by defining

$$\tilde{L}_c \equiv L_c^\mu L^{1-\mu}, \quad (45)$$

a function of the current number of commuters $L_c = \sum_{s=1}^S L_{cs}$, the total city size $L = L_c + L_m$, and the fraction of days per week a remote worker spends at home, μ . We postulate that the factor shares for each type of labor are given by

$$A_{cs} \equiv \frac{(A_s \tilde{L}_c^\delta)^\mu}{z_s^\mu + (A_s \tilde{L}_c^\delta)^\mu}, \quad A_{ms} \equiv \frac{z_s^\mu}{z_s^\mu + (A_s \tilde{L}_c^\delta)^\mu}. \quad (46)$$

The productivity of a commuting worker depends on the in-office productivity in that sector $A_s > 0$, and on how many workers are on average in the CBD, \tilde{L}_c , with an elasticity $\delta > 0$. Similarly, the productivity of a remote worker depends on the remote work productivity in that sector z_s . Hence, the optimal ratio of remote workers increases in their productivity, the more so as they spend a higher share of the week at home. The wage for workers in mode ℓ in sector s resulting from profit

maximization is given by

$$w_{\ell s} = p_s A_s^\theta A_{\ell s} L_{\ell s}^{\theta-1} q_s^{1-\theta}, \quad (47)$$

where p_s is the price of sectoral good s . The wage of commuters relative to remote workers in sector s is therefore given by

$$\frac{w_{ms}}{w_{cs}} = \left(\frac{z_s}{A_s \tilde{L}_c^\delta} \right)^\mu \left(\frac{L_{ms}}{L_{cs}} \right)^{\theta-1}. \quad (48)$$

Absentee landlords invest their effort to produce housing on their unit-size plot and receive $r(d)$ per unit of housing. Land has an alternative use that yields r_a .

Equation (48) will be the basis of our estimation strategy of the elasticity of substitution between remote and in-person workers. We aim to estimate $\phi \equiv \theta - 1 = -1/\rho$.

A.13.2 Estimates of the Elasticity of Substitution Between Remote and In-Person

Consider equation (48) for different cities $j = 1, \dots, J$ and different periods $t = 1, \dots, T$. Let δ_j be the agglomeration externality in city j . We assume that the technology z_{st} is constant across cities and let in-office productivity be the product of sector-year, city-year terms, and a residual $A_{sjt} = \bar{A}_{st} \bar{a}_{jt} \tilde{a}_{sjt}$. Taking logs and adding time and city indices, equation (48) writes

$$\log \frac{w_{msjt}}{w_{csjt}} = D_{st} + G_{jt} + \phi \log \frac{L_{msjt}}{L_{csjt}} + \epsilon_{sjt}, \quad (49)$$

where $D_{st} \equiv \mu \log \frac{z_{st}}{A_{st}}$, $G_{jt} \equiv -\mu \bar{a}_{jt} - \mu \delta_j \log \tilde{L}_{cj t}$, $\phi \equiv \theta - 1$, and the error term $\epsilon_{sjt} = -\mu \log \tilde{a}_{sjt}$ captures unobserved productivity shocks specific to each sector-city-year.

A threat to identification in (49) is the presence of contemporaneous unobserved innovations to the productivity of any sector s in a city j . These innovations are likely to affect both the relative wages and labor supply of remote workers. We estimate ϕ using past ratios of the relative labor supply, $L_{msjt'}/L_{csjt'}$, with $t' < t$, as instrument for the ratio in period t , under the exclusion restriction that those past ratios are orthogonal to the contemporaneous innovations in the sector-city component of productivity.

We estimate Equation (49) with the ACS data, using all years between 1980 and 2022, 638 CBSAs, and 33 distinct industry groups. In an alternative specification, we replace industry groups with the 22 occupation groups defined in Section A.4. We define the dependent variable as the residual remote work premium for a sector-CBSA-year ψ_{sjt} estimated from the regression of all workers' hourly wage on individual characteristics and indicators of being remote in each sector and CBSA, and year t ,

$$\log w_{it} = \sum_{s=1}^S \mathbb{1}_{sec_{it}=s} \left(\gamma_{st} X_{it} + \sum_{j=1}^J \mathbb{1}_{cbsa_{it}=j} (\beta_{jst} + \psi_{jst} \mathbb{1}_{remote_{it}=1}) \right) + u_{it}, \quad (50)$$

where the vector of individual covariates X_{it} contains a constant and worker i 's log of the levels

and squares of their work experience and age, and indicators for levels of educational attainment, part-year work status, marital status, race, number of children, and gender.

We report the estimates of ϕ from equation (49) in Table A7. Recall that $\phi = -1/\rho$, so for any value of $\rho \in [0, \infty)$, $\phi \in (-\infty, 0)$, and values of ϕ close to zero correspond to very high values of the elasticity of substitution ρ .

The exclusion restriction in our estimation of Equation (49) is that the levels of the innovations in city-sector productivity are independent over time. Next, we consider a different exclusion restriction and assume that the changes in innovations are independent over time. This allows for the estimation of ϕ in time differences. For any $\tau \in \mathbb{N}$, define $\Delta x_t = x_t - x_{t-\tau}$ for any variable x . Then, a consistent estimate of ϕ can be obtained using past values of the change in the relative supply of remote workers, $\Delta \log L_{msjt'}/L_{csjt'}$, with $t' < t$,

$$\Delta \log \frac{w_{msjt}}{w_{csjt}} = d_{st} + g_{jt} + \phi \Delta \log \frac{L_{msjt}}{L_{csjt}} + \varepsilon_{sjt}, \quad (51)$$

where $d_{st} \equiv \Delta D_{st}$, $g_{jt} \equiv \Delta G_{jt}$, and $\varepsilon_{sjt} \equiv \Delta \epsilon_{sjt}$. We report the estimates of ϕ from equation (51) in Table A7, where instruments are defined for a reference period $t' = t - 3$ and time differences are defined with $\tau = 3$. In all our specifications, whether dividing workers by occupation or industry groups, estimating the elasticity of substitution using levels or time differences, with OLS or instrumental variables, the estimates are consistently centered on zero, implying a near-infinite elasticity of substitution between remote and in-person workers.

From Table A7, we conclude that the association between the relative labor supply of remote workers and their compensation is consistent with a very large elasticity of substitution, and with setting $\phi = 0$, i.e., $\theta = 1$ in Equation (44), implying that the production function is well represented by a linear function as in the paper.

A.14 Estimation Details for the Agglomeration Externalities

A.14.1 Main Specification

The dependent variable in Equation (28) is the log change in the hourly wages of commuters in each CBSA and year. We build it using our ACS sample and a similar approach to the one taken in Section A.13.2, but focusing on city-wide wages of commuters only instead of sector-specific wages of all workers.

Namely, we define the dependent variable as the residual commuter wages for a CBSA-year \bar{w}_{jt} estimated from the regression of all commuters' hourly wage on individual characteristics and for each CBSA, and year t ,

$$\log w_{it} = \sum_{j=1}^J \mathbb{1}_{cbsa_{it}=j} (\gamma_{jt} X_{it} + \bar{w}_{jt}) + u_{it}, \quad (52)$$

Table A7: Estimates of Substitution Parameter Between Remote and In-Person

	By Occupation				By Industry			
	Levels		Time Diff.		Levels		Time Diff.	
	(1) OLS	(2) IV	(3) OLS	(4) IV	(5) OLS	(6) IV	(7) OLS	(8) IV
$\log \frac{L_{msjt}}{L_{csjt}}$	0.005 (0.002)	-0.000 (0.015)			-0.001 (0.002)	-0.016 (0.014)		
$\Delta \log \frac{L_{msjt}}{L_{csjt}}$			0.003 (0.003)	0.006 (0.008)			-0.003 (0.003)	0.005 (0.008)
CBSA-Year FE	Yes	Yes	Yes	Yes	Yes	Yes	Yes	Yes
Group-Year FE	Yes	Yes	Yes	Yes	Yes	Yes	Yes	Yes
Observations	104501	44094	44094	25156	102371	41334	41334	23756

Estimates of $\phi = -1/\rho$, where ρ is the elasticity of substitution between remote and in-person workers. Columns (1)-(4) define worker groups as the 22 occupation groups in Section A.4; Columns (5)-(8) define worker groups as the 33 two-digit 1990-industry codes in the ACS. Columns (1)-(2) and (5)-(6) estimate Equation (49); Columns (3)-(4) and (7)-(8) estimate Equation (51). The dependent variable is the estimated remote work hourly wage premium, in levels or in time-difference, from Equation (50). The period of reference for the definition of instrumental variables is $t' = t - 3$, and time differences are defined with $\tau = 3$.

where the vector of individual covariates X_{it} contains a constant and worker i 's log of the levels and squares of their work experience and age, and indicators for each occupation, levels of educational attainment, part-year work status, marital status, race, number of children, and gender.

We specify δ_j as a linear combination of CBSA j 's labor-value-added employment shares in each of the four industry groups. We use estimates of the labor-value-added shares γ_s , $s = 1, \dots, 22$, of each of the 1997-NAICS 2-digit industries from [Rossi-Hansberg et al. \(2021\)](#) and compute the employment shares $shemp_{sj0}$ of each industry s in each CBSA j in 1980 in our ACS sample. We then compute the labor-value-added employment share in each industry group as,

$$s_{gj0} \equiv \sum_{s \in g} \gamma_s shemp_{sj0}, \quad (53)$$

where $s \in g$ indicates that industry s is part of the industry group g .

Table A8 reports the results. In Panel (A), for each industry group $g \geq 1$, β_g represents the agglomeration strength in sector g , relative to nontradable industries (RUC), $g = 0$. Focusing on the IV estimates in column (2), we find that all industry groups have a higher agglomeration strength than nontradables, with the highest value for manufacturing, followed by accommodation, trade, and transportation. In Panel (B), the industry-specific coefficients are combined with each CBSA j 's labor-value-added adjusted employment shares by group, s_{gj0} to form estimates δ_j . Our

Table A8: Estimates of Agglomeration Externalities by Industry Group and CBSA

(A) Agglomeration Externality by Industry Group	Parameter	(1) OLS	(2) IV
Health and education (HE)	β_1	0.967 (0.166)	0.613 (0.099)
Professional and other services (PS)	β_2	2.015 (0.586)	0.512 (0.522)
Manufacturing (M)	β_3	0.749 (0.833)	1.166 (0.549)
Accommodation, trade, and transportation (ATT)	β_4	0.897 (2.259)	0.786 (2.364)
	β_0	-0.412 (0.228)	-0.149 (0.254)
Observations		9,152	9,152
First Stage Within- R^2			0.48
<hr/>			
(B) Agglomeration Externality by CBSA			
Mean		0.043	0.067
Standard deviation		0.045	0.022

Panel (A) reports estimates of industry-group agglomeration externalities from Equation (28), with an intercept and slope of $\Delta \log L_{jt}$ for each CBSA, and year fixed effects. The dependent variable is the log time difference of commuter wages in each CBSA-year according to Equation (52) in Appendix A.14.1. The instrumental variables are the predicted changes in the number of commuters, defined in (27). The regression is based on observations for 622 CBSAs and 15 years. Robust standard errors in parentheses. We confirm the strength of the first stage by reporting the R^2 of the regression of $\Delta \log S_{cjt}$ on IV_{jt} after residualizing each on an intercept and slope of $\Delta \log L_{jt}$ for each CBSA, and year fixed effects. Panel (B) reports the first two moments of the distribution of positive CBSA-specific estimates of agglomeration externalities, computed as $\delta_j = \beta_0 + \sum_{g=1}^4 \beta_g s_{gj0}$.

preferred IV estimates in column (2) indicate a mean value of δ_j of 0.067 and a standard deviation of 0.022 across the 622 CBSAs in the sample. In Appendix A.14.2, we perform robustness exercises for the specifications of Equation (28); in Appendix A.14.3, we define agglomeration externalities using only industry estimates from Rossi-Hansberg et al. (2021). We find similar qualitative results in both exercises.

A.14.2 Robustness of the Main Specification

We test the robustness of our main specification for the estimation of agglomeration externalities by leaving out each year from the sample alternatively. The results are summarized in Table A9. They indicate that while the estimated agglomeration parameters vary somewhat if we drop one

year, the mean value remains within an interval of 0.06 and 0.09.

Table A9: Robustness Exercises for the Estimation of Agglomeration Externalities

Year Excluded	$p_{50}(\hat{\delta})$	$sd(\hat{\delta})$
2007	0.071	0.022
2008	0.065	0.025
2009	0.082	0.025
2010	0.086	0.032
2011	0.081	0.032
2012	0.073	0.024
2013	0.060	0.026
2014	0.073	0.022
2015	0.090	0.021
2016	0.060	0.017
2017	0.053	0.021
2018	0.061	0.029
2019	0.089	0.017
2020	0.084	0.032
2021	0.097	0.051

The table report robustness exercises in the estimation of the agglomeration externality from Equation (28). In particular, each row repeats our estimation excluding one year at a time from the sample, and reports the mean and standard deviation of δ_j across 622 CBSAs.

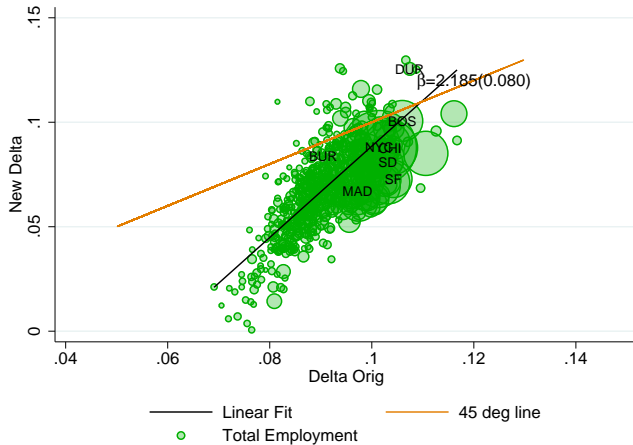
A.14.3 Alternative Estimates of Agglomeration Externalities

In this section, we construct alternative estimates of agglomeration externalities and test the robustness of our quantification. We build city-specific estimates relying on industry-specific estimates of agglomeration externalities obtained by Rossi-Hansberg et al. (2021). They specify a production function featuring labor productivity that is influenced by external effects stemming from the local composition of labor. They recover the endogenous levels of local productivity that rationalize observed data on wages, employment, and input-output linkages as an equilibrium. Given their measures of productivity, they estimate the degree of local externalities for four industry groups and two broad occupational categories.¹⁵

We construct our alternative measure of city-specific agglomeration externalities by computing the average of the four industry-specific externality parameters weighted by each city's employment shares in the four industries. We compute these industry shares using the County Business Patterns

¹⁵The industry groups, based on the NAICS 1997 classification, are Health and education (HE), Professional and other services (PS), Manufacturing (M), Accommodation, trade, and transportation (ATT). The two occupational categories are Cognitive Non-Routine (CNR) and non Cognitive Non-Routine (non-CNR). They define CNR occupations as all those with SOC-2 classifications 11 to 29 and non-CNR occupations as all other occupations.

Figure A13: Agglomeration Externalities from Main Specification vs. Constructed from Rossi-Hansberg et al. (2021)



This figure reports the CBSA-specific values of δ_j implied by our main specification on the y axis and by the alternative method described in Section A.14.3 on the x axis.

in 2019.¹⁶ Specifically, we compute the city-specific averages of the externality parameters τ_L in Table 1 of Rossi-Hansberg et al. (2021). The average value of the agglomeration externality across 624 CBSAs is 0.089, which is close to estimates obtained in different contexts by other studies.¹⁷ Figure A13 compares our main estimates to those from this alternative method, revealing a good correlation between the two methods. The R^2 is 0.23.

A.15 Transportation Cost Elasticity and City Size

In this section, we report the relation between the estimated distance elasticity of transportation cost, γ , and CBSA size, across the 622 cities in our sample. This relation is depicted in Figure A14, where we exclude a few outliers for visibility. We estimate that a doubling of city size is associated to a distance that is 0.001 smaller, relative to a sample mean of 0.026.

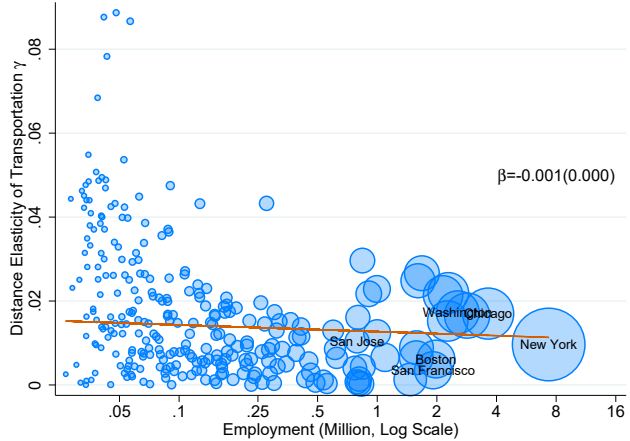
A.16 Change in Trips to CBD and Welfare Change from Switching to Remote Equilibrium for Largest Cities

In Table A10, we report the values of our estimates for the change in visits to the CBD and the welfare of the low-commuting stationary equilibrium relative to the high-commuting stationary

¹⁶We use the crosswalk provided by Rossi-Hansberg et al. (2021) to map the four groups of industries defined by NAICS 1997 into the industries used by the County Business Patterns. See Appendix Table A.16 page 80 of Rossi-Hansberg et al. (2019).

¹⁷Duranton and Puga (2019) estimate an overall agglomeration externality of 0.08 in the United States, once adding the static and dynamic effects of city size on individual productivity.

Figure A14: Transportation Cost Elasticity, γ , and CBSA size



This figure reports the city-specific γ_j against the CBSA's BEA employment. Each γ_j is estimated as described in Section 5.4. The size of the circles represents CBSA's employment.

equilibrium. Our sample is the largest 45 U.S. cities for which we can compute the relevant parameters and the commuting trips to the CBD.

In the table, Column 2 reports the employment from the 2019 Census that we use in our calibrations, as described in Appendix A.18. Column 3 reports the change in visits to the CBD for each city from January 2020 to July 2022, as described in Appendix A.7.¹⁸ Column 4 reports the welfare ratio $\mathcal{W}(L_{c \text{ low}}^{ss})/\mathcal{W}(L_{c \text{ high}}^{ss})$, defined in Section 7. These values are only computed for the CBSAs that are in their cone of multiplicity according to our estimation. We indicate by “U” the CBSAs that are outside their cone, for which there exists no low-commuting stationary equilibrium.

Figure A15 shows correlates of $\hat{\mathcal{W}}$, the welfare in the low-commuting relative to the high-commuting stationary equilibrium. These scatterplots can only be computed for the set of cities in the cone of multiplicity. The left panel shows a scatterplot between $\hat{\mathcal{W}}$ and the net strength of agglomeration externalities, $\delta - \gamma/(2\mu)$. The right panel shows a scatterplot between $\hat{\mathcal{W}}$ and the share of trips to the CBD in July 2022, relative to January 2020. The marker size is proportional to total city employment.

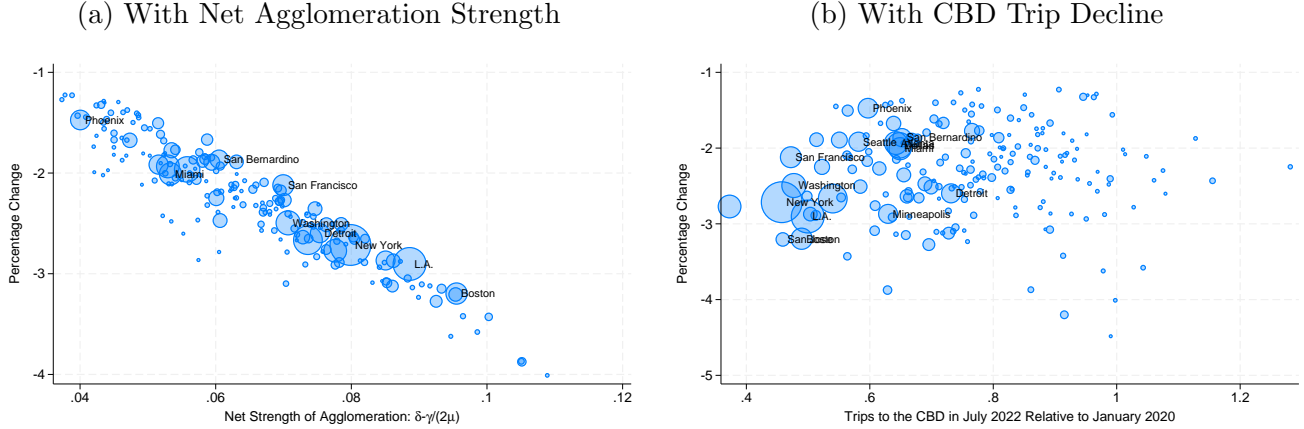
¹⁸These values are a simple transformation of those plotted on the y axis of Panel (b) of Figure 4 (the complement to 100).

Table A10: Change in Trips to CBD and Welfare Loss in Remote Equilibrium for a Group of 45 Cities

CBSA	2019 Census Employment	Trips to CBD Jul'22 / Jan'20	Welfare Change $\mathcal{W}(L_{c \text{ low}}^{ss})/\mathcal{W}(L_{c \text{ high}}^{ss})$
New York-Northern New Jersey-Long Island, NY-NJ-PA	7,334,144	0.457	0.968
Los Angeles-Long Beach-Santa Ana, CA	4,748,281	0.499	0.962
Chicago-Joliet-Naperville, IL-IN-WI	3,630,720	0.540	0.967
Dallas-Fort Worth-Arlington, TX	2,842,177	0.648	0.972
Washington-Arlington-Alexandria, DC-VA-MD-WV	2,548,552	0.477	0.974
Atlanta-Sandy Springs-Marietta, GA	2,284,940	0.642	0.974
Philadelphia-Camden-Wilmington, PA-NJ-DE-MD	2,270,070	0.373	0.969
Miami-Fort Lauderdale-Pompano Beach, FL	2,149,512	0.649	0.972
Boston-Cambridge-Quincy, MA-NH	1,979,049	0.490	0.965
San Francisco-Oakland-Fremont, CA	1,914,574	0.472	0.972
Phoenix-Mesa-Glendale, AZ	1,680,550	0.597	0.980
Seattle-Tacoma-Bellevue, WA	1,606,160	0.582	0.977
Detroit-Warren-Livonia, MI	1,578,962	0.732	0.968
Minneapolis-St. Paul-Bloomington, MN-WI	1,575,451	0.630	0.966
Riverside-San Bernardino-Ontario, CA	1,468,173	0.652	0.968
Tampa-St. Petersburg-Clearwater, FL	1,095,802	0.551	0.975
Charlotte-Gastonia-Rock Hill, NC-SC	999,016	0.766	0.974
Portland-Vancouver-Hillsboro, OR-WA	996,704	0.523	0.972
Austin-Round Rock-San Marcos, TX	906,522	0.639	0.977
Cincinnati-Middletown, OH-KY-IN	845,880	0.699	0.966
Pittsburgh, PA	841,832	0.689	0.974
Kansas City, MO-KS	832,707	0.655	0.967
Sacramento-Arden-Arcade-Roseville, CA	811,475	0.514	0.973
Las Vegas-Paradise, NV	807,521	0.504	0.953
Nashville-Davidson-Murfreesboro-Franklin, TN Are	798,725	0.660	0.967
San Jose-Sunnyvale-Santa Clara, CA	791,561	0.459	0.964
Columbus, OH	791,421	0.585	0.967
Indianapolis-Carmel, IN	771,329	0.615	0.968
Virginia Beach-Norfolk-Newport News, VA-NC	624,538	0.669	0.973
Providence-New Bedford-Fall River, RI-MA	612,059	0.696	0.961
Richmond, VA	534,987	0.564	0.977
Salt Lake City, UT	488,013	0.596	0.970
Hartford-West Hartford-East Hartford, CT	451,318	0.680	0.968
New Orleans-Metairie-Kenner, LA	434,260	0.498	0.963
Buffalo-Niagara Falls, NY	412,839	0.609	0.966
Grand Rapids-Wyoming, MI	412,449	0.513	0.964
Rochester, NY	395,591	0.608	0.966
Worcester, MA	346,749	0.658	0.963
Bridgeport-Stamford-Norwalk, CT	331,525	0.554	0.970
Albany-Schenectady-Troy, NY	320,810	0.662	0.970
Albuquerque, NM	313,814	0.572	0.970
New Haven-Milford, CT	310,423	0.629	0.959
Allentown-Bethlehem-Easton, PA-NJ	303,219	0.637	0.964
Tucson, AZ	301,333	0.563	0.971
Madison, WI	276,371	0.959	U
Baton Rouge, LA	270,329	0.748	U

The letter “U” in Column 4 indicates that the CBSA is outside the multiplicity cone according to our estimates.

Figure A15: Correlates of Welfare Change \hat{W}



A.17 Endogenous housing supply

In this subsection we study the consequences on the total housing supply of assuming that the density of housing (and hence, of population) respond to the rent level. Assume that housing supply $h(d)$ at distance d from the CBD on each ray is governed by the following relationship:

$$h(d) = ar(d)^\eta, \quad a > 0, \quad \eta \geq 0. \quad (54)$$

Hence, the number of housing units increases with the market rent with elasticity η . When $\eta = 0$, housing supply is inelastic. Agents optimizing by choosing consumption and housing at any distance from the CBD, and then choosing the optimal distance. The equilibrium rent function is,

$$r(x) = \begin{cases} r_a (\bar{d}^\mu \bar{D}^{1-\mu})^{\gamma/(1-\alpha)} x^{-\gamma/(1-\alpha)} & \text{if } x < \bar{d} \\ r_a \bar{D}^{(1-\mu)\gamma/(1-\alpha)} x^{-(1-\mu)\gamma/(1-\alpha)} & \text{if } x \geq \bar{d} \end{cases}. \quad (55)$$

In this circular city, the total number of units in the disk of radius \bar{d} must equal the total number of households in that disk, namely,

$$L_c = \int_0^{\bar{d}} h(x) 2\pi x dx = (\bar{D}^{1-\mu} \bar{d}^\mu)^{\eta\gamma/(1-\alpha)} r_a^\eta 2\pi a \frac{\bar{d}^{2-\eta\gamma/(1-\alpha)}}{2 - \eta\gamma/(1-\alpha)}. \quad (56)$$

In the inelastic housing supply case, this equation implies $L_c = 2\pi a \bar{d}^2$. In the elastic housing supply this expression is in general different; however, empirically, $\bar{D} \approx \bar{d}$ since the number of commuters pre-pandemic is small, and remote workers live on the widest circles in the disk city. Hence, $L_c \approx \bar{d}^{\eta\gamma/(1-\alpha)} r_a^\eta 2\pi a \frac{\bar{d}^{2-\eta\gamma/(1-\alpha)}}{2 - \eta\gamma/(1-\alpha)} = r_a^\eta 2\pi a \frac{\bar{d}^2}{2 - \eta\gamma/(1-\alpha)}$, which is proportional in \bar{d} to the inelastic housing supply case.

A.18 Descriptive Evidence Using Census Employment

A.18.1 Individual Mobility

In Section 3, we characterize CBSAs by their total non-farm employment in 2019, published by the BEA. While this variable provides a measure of city size for all CBSAs, it is distinct from the measure of city size that we use in the quantification of the model in several ways. First, it is based on counting the number of jobs in the CBSAs, rather than on the number of workers, as is the case in our Census data. Since some workers hold more than one job, the BEA measure is typically larger than our Census measure. Second, because the Census data is based on individual records, we can count the number of commuters and calibrate our model to workers who are more likely to face the trade-off between remote work and commuting that our theory speaks to. For example, the Census allows us to focus on workers between 25 and 64 years of age and to exclude self-employed workers. As a result, our Census-based measure of CBSA employment is 56 percent lower than the BEA measure on average. The correlation between the log of the two employment measures is 0.89.

Using the Census individual data to measure commuting decisions, we can compute total employment for 598 out of the 847 CBSAs represented in Figure 3. In Figure A16 and A17, we reproduce the analogous figures to Figures 3 and 4 with this smaller sample of CBSAs. In Figure A16, we use lower thresholds of employment (1 million for “large” CBSAs, 100,000 for “small” CBSAs) to reflect the fact that our measure of employment from the Census is lower than the BEA measure on average. These thresholds of Census employment reproduce the partition of CBSAs in Figure 3, with the first group containing the top 3 percent of CBSAs in terms of employment, the second containing the bottom 75 percent of CBSAs.

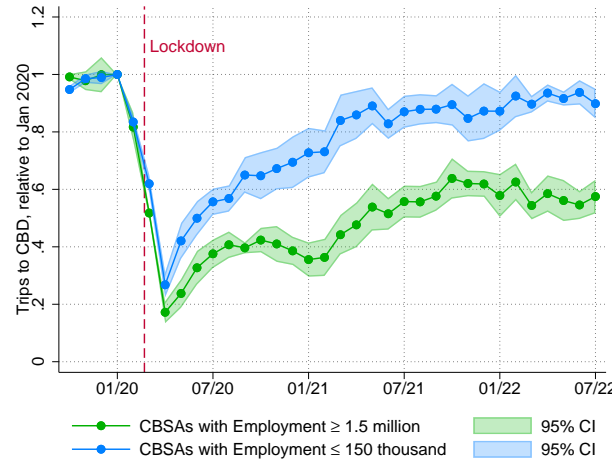
The patterns of trips to CBD over time are very similar to those described in Section 3.1. Namely, CBSAs of all sizes experience a large decline of trips to CBD of 70 to 80 percent during the stay-at-home policies in 2020, with larger CBSAs only recovering to 60 percent of their pre-pandemic values, while smaller CBSAs return at least to 90 percent on average. Figure A17 confirm that the relationship between the size of the drop in trips to CBD and CBSA employment became stronger by July 2022 than in April 2020.

A.18.2 Distance Gradients in House Prices

Figure A18 shows that the divergence in the average distance elasticity of house prices relative to January 2020 between smaller and larger cities is visible also when we measure size with Census employment.

Panel (a) of Figure A19 confirms that the flattening of the housing price gradients occurs in similar magnitude for cities of all sizes in January 2021. Panel (b) confirms that even in the sample of cities ordered by Census employment, the drop in the gradient is more strongly related to city size by December 2022.

Figure A16: Visits to the CBD Relative to January 2020, Census Employment



The figure reports the estimates of the average volume of visits to the CBD from block groups located in i) CBSAs with total Census employment above 1 million (19 largest CBSAs), ii) CBSAs with total employment below 100,000 (450 smallest CBSAs) expressed as a share of their values in January 2020.

A.19 Empirical Determinants of Multiplicity and Change in CBD Trips

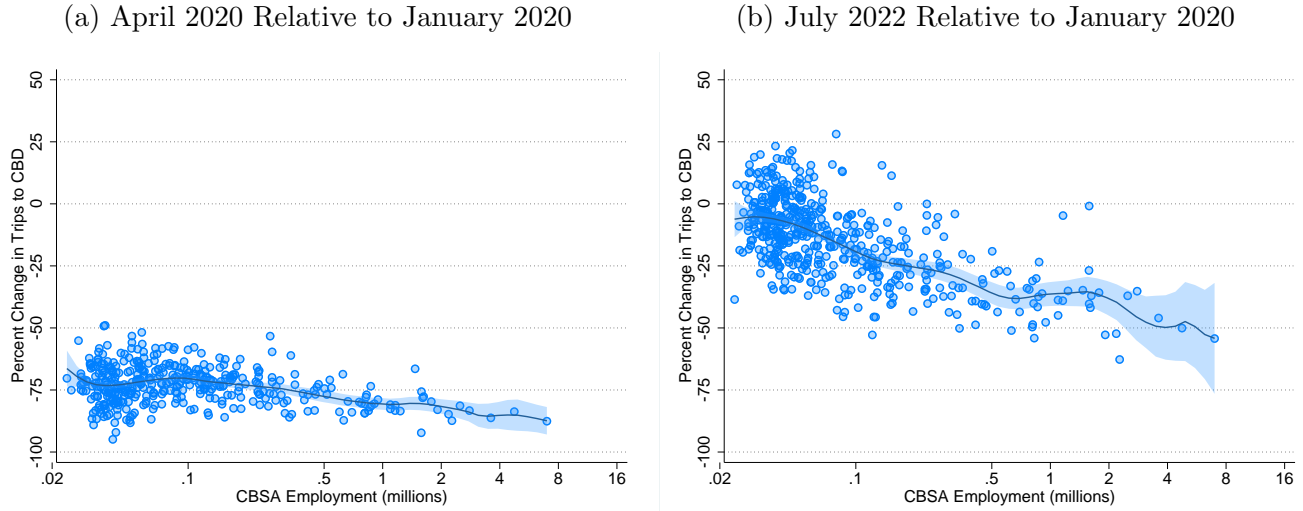
In this subsection, we explore the relation between drop in CBD trips, the position of a city relative to its cone, and other pre-pandemic cities' characteristics.

Our explanation of the post-pandemic empirical patterns rests on a theory where the full set of a city's characteristics jointly determines the recovery (or lack thereof) of trips to the CBD, as summarized by the indicator variable $\mathbf{1}_j^{cone}$. Still, one may ask whether this summary measure has power in explaining the post-pandemic behavior of cities, on top of other controls that approximate alternative plausible explanations of the return to office. A note of caution is that these alternative variables also determine the value of the parameters that determine $\mathbf{1}_j^{cone}$. Still, as a way of exploring this question, Table A11 relates the shortfall in trips in a city to its cone indicator and other pre-pandemic characteristics, like the share of employment with above-median teleworkable index, the value added share of employment in the four industries that we use to quantify agglomeration externalities, and the pre-pandemic share of trips to the CBD, a proxy for pre-pandemic congestion.

Column (1) reports the results of a linear regression of the percentage difference in trips to the CBD in July 2022, relative to January 2020, on the indicated regressors. We find that the cone indicator variable is strongly negatively associated with the change in trips, even after controlling for plausible alternative explanations.

Note that, since the left-hand side in column (1) is a continuous measure, it embodies information both about the switch, and about the location of the new equilibrium. To circumvent this feature, we construct a variable that approximates a binary measure of the switching behavior. In particular, we construct an indicator variable that is equal to 1 if the city's trips in July do

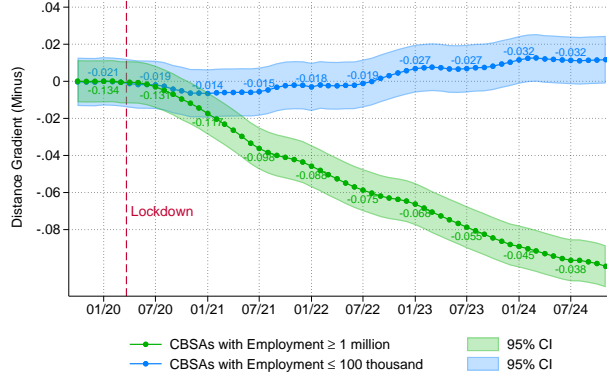
Figure A17: Response of Trips to the CBD, Census Employment



Panel (a) reports the change in the average level of visits to each CBSA's CBD between January 2020 and April 2020, against our measure of employment from the Census. Panel (b) reports the change in visits to the CBD in July 2022 relative to January 2020. Each marker represents a CBSA. The solid line represents a fitted kernel-weighted local polynomial smoothing, with the shaded area corresponding to the 95 percent confidence interval around the fitted value.

not drop more than 5% (indicating that the city's pre-pandemic trips are back to where they used to be), and 0 if the trips drop more than 20% (indicating the city's trips have not returned to their initial levels). Column (2) runs a probit regression of this indicator, $\mathbb{1}_j^{back(5,20)}$, on the same set of right-hand side variables. We find that the cone indicator continues to have strong predictive power beyond controls for alternative explanations. Column (3) further sharpens our indicator for return to the high commuting equilibrium, distinguishing cities where the trips are exactly at, or above, pre-pandemic levels, and cities where trips fell more than 30% (denoted with $\mathbb{1}_j^{back(0,30)}$), with similar results. In all cases, the cone indicator is the most significant variable in the regression. Taken together, these findings are suggestive that a city's position relative to its cone of multiplicity continues to hold explanatory power relative to proxies for plausible alternative explanations.

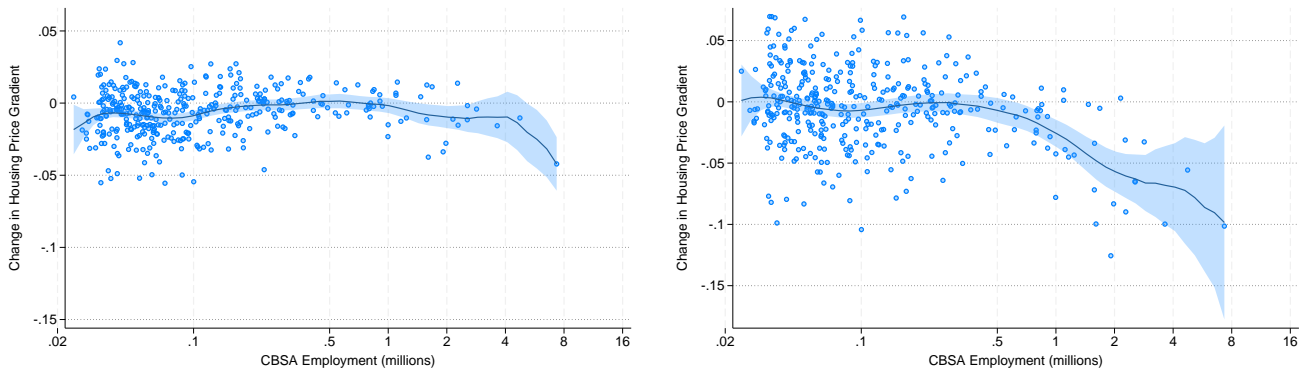
Figure A18: Distance Gradient of Housing Prices Relative to January 2020, Census Employment



This figure reports the difference between the average housing price gradients in January 2020 and each following month, using the same Census employment thresholds as in Figure A16. A negative value for the difference in housing price gradients implies a lower premium for housing located close to the CBD. The value of the average housing price gradient in each group is reported next to the marker of the associated group every six months. In total, 19 CBSAs have employment above 1 million and 166 have employment below 100,000. The shaded areas represent the contour delimited by the consecutive 95 percent confidence intervals of each monthly indicator.

Figure A19: Response of House Price Gradients, Census Employment

(a) January 2021 Relative to January 2020 (b) December 2022 Relative to January 2020



This figure reports the difference between the housing price gradients in January 2020 and December 2022, against our measure of employment from the Census. Each marker represents a CBSA. The gradients are estimated using zip code level data from Zillow for 210 CBSAs. A negative value for the difference implies a lower premium for housing located close to the CBD. The solid line represents a fitted kernel-weighted local polynomial smoothing, with the shaded area corresponding to the 95 percent confidence interval around the fitted value.

Table A11: Determinants of CBSAs' Changes in Trips to CBD: Observable Characteristics

	(1) Trip shortfall	(2) $\mathbb{1}_j^{\text{back}(5,20)}$	(3) $\mathbb{1}_j^{\text{back}(0,30)}$
$\mathbb{1}_j^{\text{cone}}$	-8.03 (0.00)	-1.19 (0.00)	-1.38 (0.01)
Share of Teleworkable Employment	-37.12 (0.04)	-5.73 (0.07)	-2.06 (0.76)
V.A. Sh. Emp. Health and education	-3.81 (0.93)	6.24 (0.44)	0.09 (0.99)
V.A. Sh. Emp. Professional and other services	-286.44 (0.00)	-16.43 (0.11)	-39.13 (0.04)
V.A. Sh. Emp. Manufacturing	82.15 (0.39)	39.99 (0.04)	45.56 (0.10)
V.A. Sh. Emp. Accommodation, trade, and transport.	-82.81 (0.41)	4.91 (0.71)	-7.05 (0.74)
Share of Trips to CBD in 2019	-0.79 (0.60)	-0.27 (0.36)	-0.53 (0.46)
Constant	31.05 (0.06)	2.24 (0.37)	4.52 (0.19)
Observations	275	188	99
R^2	0.422		
Pseudo R^2		0.394	0.578

Column (1) reports the results of a linear regression of the percentage drop in the number of trips to the CBDs in July 2022, relative to January 2020, on $\mathbb{1}_j^{\text{cone}}$ and other controls described in Appendix A.19. Column (2) reports the results of a probit regression of $\mathbb{1}_j^{\text{back}(5,20)}$ on the same set of regressors; column (3) reports a similar probit regressor with dependent variable $\mathbb{1}_j^{\text{back}(0,30)}$. Robust p-values in parentheses.

B Theory

B.1 Rewriting the average value of a worker

By adding and subtracting the continuation value in the current labor delivery mode, the equation for U_ℓ can be rewritten as

$$\begin{aligned} U_\ell (\{\varepsilon_{ct}, \varepsilon_{mt}\}; L_{ct}, \omega^t) &= u_\ell (L_{ct}; A_t, T_t, z_t) + \max_{\ell'} \left\{ \beta V_{\ell'} (L_{ct+1}; \omega^{t+1}) - F_{\ell\ell't} + \varepsilon_{\ell't} \right\} \\ &= u_\ell (L_{ct}; A_t, T_t, z_t) + \beta V_\ell (L_{ct+1}; \omega^{t+1}) - F_{\ell\ell,t} + \\ &\quad \max_{\ell'} \left\{ \beta [V_{\ell'} (L_{ct+1}; \omega^{t+1}) - V_\ell (L_{ct+1}; \omega^{t+1})] - (F_{\ell\ell't} - F_{\ell\ell t}) + \varepsilon_{\ell't} \right\} \\ &= u_\ell (L_{ct}; A_t, T_t, z_t) + \beta V_\ell (L_{ct+1}; \omega^{t+1}) - F_{\ell\ell t} + \max_{\ell'} \left\{ \bar{\varepsilon}_t^{\ell\ell'} + \varepsilon_{\ell't} \right\} \end{aligned} \quad (57)$$

where

$$\bar{\varepsilon}_t^{\ell\ell'} (L_{ct+1}) \equiv \beta [V_{\ell'} (L_{ct+1}; \omega^{t+1}) - V_\ell (L_{ct+1}; \omega^{t+1})] - (F_{\ell\ell't} - F_{\ell\ell t}) \quad (58)$$

is the average value of switching from ℓ to ℓ' . Taking the expectation of U_ℓ with respect to ε_t ,

$$\begin{aligned} V_\ell (L_{ct}; z_t) &= u_\ell (L_{ct}; A_t, T_t, z_t) + \beta V_\ell (L_{ct+1}; \omega^{t+1}) - F_{\ell\ell t} + E_t \max_{\ell'} \left\{ \bar{\varepsilon}_t^{\ell\ell'} + \varepsilon_{\ell't} \right\} \equiv \\ &\equiv u_\ell (L_{ct}; A_t, T_t, z_t) + \beta V_\ell (L_{ct+1}; \omega^{t+1}) - F_{\ell\ell t} + \Omega (\bar{\varepsilon}_t^\ell) \end{aligned} \quad (59)$$

where $\bar{\varepsilon}_t^\ell \equiv \{\bar{\varepsilon}_t^{\ell c}, \bar{\varepsilon}_t^{\ell m}\}$. $\Omega (\bar{\varepsilon}_t^\ell)$ is the value of the option of being able to move out of ℓ if circumstances require, or the “option value” of ℓ .

Under our distributional assumption for ε_t we can write the share of workers in ℓ state transitioning to ℓ' as

$$\lambda_t^{\ell\ell'} = \frac{\exp (\bar{\varepsilon}_t^{\ell\ell'} (L_{ct+1}) / s)}{\exp (\bar{\varepsilon}_t^{\ell c} (L_{ct+1}) / s) + \exp (\bar{\varepsilon}_t^{\ell m} (L_{ct+1}) / s)} \quad (60)$$

We can use this expression to obtain the average expected switching values. In fact,

$$\frac{\lambda_t^{\ell\ell'}}{\lambda_t^{\ell\ell}} = \exp \left(\bar{\varepsilon}_t^{\ell\ell'} / s - \bar{\varepsilon}_t^{\ell\ell} / s \right) \implies s \ln \frac{\lambda_t^{\ell\ell'}}{\lambda_t^{\ell\ell}} = \bar{\varepsilon}_t^{\ell\ell'} - \bar{\varepsilon}_t^{\ell\ell} \implies \bar{\varepsilon}_t^{\ell\ell'} = s \ln \frac{\lambda_t^{\ell\ell'}}{\lambda_t^{\ell\ell}} \quad (61)$$

To obtain the option value of being in ℓ , recall that

$$\Omega (\bar{\varepsilon}_t^\ell) = s \log [\exp (\bar{\varepsilon}_t^{\ell c} / s) + \exp (\bar{\varepsilon}_t^{\ell m} / s)] \quad (62)$$

Since $\log \lambda_t^{\ell\ell} = \bar{\varepsilon}_t^{\ell\ell} / s - \log [\exp (\bar{\varepsilon}_t^{\ell c} / s) + \exp (\bar{\varepsilon}_t^{\ell m} / s)] = -\log [\exp (\bar{\varepsilon}_t^{\ell c} / s) + \exp (\bar{\varepsilon}_t^{\ell m} / s)]$, we have that

$$\Omega (\bar{\varepsilon}_t^\ell) = -s \ln \lambda_t^{\ell\ell} \quad (63)$$

B.2 Existence of a stationary equilibrium

To prove that a stationary equilibrium always exists, we proceed in steps. First, Lemma B.1 shows that the characterization of a stationary equilibrium can be reduced to the zeros of one equation in one unknown, the share of commuters who remain commuters next period, λ^{cc} . Lemma B.2 establishes a useful property of one component in such equation. Finally, Proposition B.1 shows that this equation always has at least one solution.

In a stationary equilibrium, the system is characterized by 11 unknowns, $u_c, u_m, L_c, V_c, V_m, \lambda^{cc}, \lambda^{mm}, \bar{\varepsilon}^{cc}, \bar{\varepsilon}^{cm}, \bar{\varepsilon}^{mc}, \bar{\varepsilon}^{mm}$, and 11 equations: the flow utility values that account for the relation between d, \bar{D} , and L_c, L :

$$u_c = \log r_a^{\alpha-1} \bar{\alpha} \frac{B(\tilde{L}_c)}{\tau(\tilde{L}_c)} \frac{w_c}{\left(\tilde{L}_c/\pi\right)^{\gamma/2}} \quad (64)$$

$$u_m = \log r_a^{\alpha-1} \bar{\alpha} T^\mu \left(\frac{B(\tilde{L}_c)}{\tau(\tilde{L}_c)} \right)^{1-\mu} \frac{w_m}{(L/\pi)^{\gamma(1-\mu)/2}} \quad (65)$$

the law of motion for L_c ,

$$L_c = L_c \lambda^{cc} + (L - L_c) (1 - \lambda^{mm}) \quad (66)$$

the average value functions by mode,

$$V_c = u_c + \beta V_c - s \ln \lambda^{cc} - F_{cc} \quad (67)$$

$$V_m = u_m + \beta V_m - s \ln \lambda^{mm} - F_{mm} \quad (68)$$

the transition probabilities,

$$\lambda^{cc} = \frac{\exp(\bar{\varepsilon}^{cc}/s)}{\exp(\bar{\varepsilon}^{cc}/s) + \exp(\bar{\varepsilon}^{cm}/s)} \quad (69)$$

$$\lambda^{mm} = \frac{\exp(\bar{\varepsilon}^{mm}/s)}{\exp(\bar{\varepsilon}^{mc}/s) + \exp(\bar{\varepsilon}^{mm}/s)} \quad (70)$$

and the expected values from switching

$$\bar{\varepsilon}^{cc} = 0 \quad (71)$$

$$\bar{\varepsilon}^{mm} = 0 \quad (72)$$

$$\bar{\varepsilon}^{cm} = \beta (V_m - V_c) - (F_{cm} - F_{cc}) \quad (73)$$

$$\bar{\varepsilon}^{mc} = \beta (V_c - V_m) - (F_{mc} - F_{mm}) \quad (74)$$

The following lemma shows that we can always reduce this system of equations to one equation in one unknown.

Lemma B.1 *The characterization of the stationary equilibrium (64)-(74) can be reduced to one equation in one unknown,*

$$f(\lambda^{cc}) \equiv \frac{1}{1 + \exp(\bar{\varepsilon}^{cm}(\lambda^{cc})/s)} - \lambda^{cc} = 0 \quad (75)$$

where

$$\bar{\varepsilon}^{cm}(\lambda^{cc}) \equiv \frac{\beta}{1-\beta} [e_f(\lambda^{cc}) + e_o(\lambda^{cc}) - (F_{mm} - F_{cc})] - F_{cm} + F_{cc} \quad (76)$$

is the value of switching from c to m ; the function

$$e_o(\lambda^{cc}) \equiv s \ln \lambda^{cc} \frac{1 - \phi \lambda^{cc}}{1 - \lambda^{cc}} \quad (77)$$

is the difference in the option values of staying in m versus staying in c ; and the function

$$e_f(\lambda^{cc}) \equiv u_m(L_c(\lambda^{cc})) - u_c(L_c(\lambda^{cc})) \quad (78)$$

is the difference in the flow value of utilities, with

$$L_c(\lambda^{cc}) = \frac{(1-\phi)\lambda^{cc}}{(1-\lambda^{cc})(1-\phi\lambda^{cc}) + (1-\phi)\lambda^{cc}} L \equiv \sigma(\lambda^{cc}) L \quad (79)$$

$$\phi \equiv \left[1 - \exp \left(\frac{F_{cc} + F_{mm} - F_{cm} - F_{mc}}{s} \right) \right] \leq 1 \quad (80)$$

Proof. Rearrange the value of switching from c to m (eq. (73)) as $\beta(V_c - V_m) = -\bar{\varepsilon}^{cm} - F_{cm} + F_{cc}$. Substitute this expression into eq. (74) for $\bar{\varepsilon}^{mc}$ to obtain

$$\bar{\varepsilon}^{mc} = \beta(V_c - V_m) - F_{mc} + F_{mm} \quad (81)$$

$$= -\bar{\varepsilon}^{cm} - F_{cm} + F_{cc} - F_{mc} + F_{mm} \quad (82)$$

Rearranging the average value functions (67)-(68), one can write

$$\begin{aligned} V_c &= (u_c - s \ln \lambda^{cc} - F_{cc}) / (1 - \beta) \\ V_m &= (u_m - s \ln \lambda^{mm} - F_{mm}) / (1 - \beta) \end{aligned}$$

and use these expressions into (73) to obtain

$$\begin{aligned} \bar{\varepsilon}^{cm} &= \beta(V_m - V_c) - F_{cm} + F_{cc} = \frac{\beta}{1-\beta} [u_m - s \ln \lambda^{mm} - F_{mm} - (u_c - s \ln \lambda^{cc} - F_{cc})] - F_{cm} + F_{cc} = \\ &= \frac{\beta}{1-\beta} [u_m - u_c + s \ln \lambda^{cc}/\lambda^{mm} - F_{mm} + F_{cc}] - F_{cm} + F_{cc} \end{aligned} \quad (83)$$

We want to express the right-hand side of this expression only as a function of λ_{cc} .

To do that, note that eq. (69) and (71) together imply

$$\lambda^{cc} = \frac{1}{1 + \exp(\bar{\varepsilon}^{cm}/s)} \implies \exp(-\bar{\varepsilon}^{cm}/s) = \lambda^{cc}/(1 - \lambda^{cc}) \quad (84)$$

Use (72) and (82) into eq. (70) for λ^{mm} ,

$$\lambda^{mm} = \frac{1}{\exp((- \bar{\varepsilon}^{cm} - F_{cm} + F_{cc} - F_{mc} + F_{mm})/s) + 1} \quad (85)$$

We can then use eq. (84) in (85) to obtain,

$$\begin{aligned} \lambda^{mm} &= \frac{1}{\exp(-\bar{\varepsilon}^{cm}/s) \exp((-F_{cm} + F_{cc} - F_{mc} + F_{mm})/s) + 1} = \\ &= \frac{1}{\lambda^{cc}/(1 - \lambda^{cc}) \exp((-F_{cm} + F_{cc} - F_{mc} + F_{mm})/s) + 1} = \\ &= \frac{(1 - \lambda^{cc})}{\lambda^{cc} \exp((-F_{cm} + F_{cc} - F_{mc} + F_{mm})/s) + (1 - \lambda^{cc})} = \\ &= \frac{(1 - \lambda^{cc})}{1 - \lambda^{cc} [1 - \exp((-F_{cm} + F_{cc} - F_{mc} + F_{mm})/s)]} \implies \\ \lambda^{mm} &= \frac{1 - \lambda^{cc}}{1 - \phi \lambda^{cc}} \end{aligned} \quad (86)$$

$$\text{with } \phi \equiv \left[1 - \exp\left(\frac{F_{cc} + F_{mm} - F_{cm} - F_{mc}}{s}\right) \right] \leq 1 \quad (87)$$

Use (86) to write the stationary equilibrium value of L_c (from eq. (66)) as

$$\begin{aligned} L_c &= L_c \lambda^{cc} + (L - L_c)(1 - \lambda^{mm}) \\ L_c - L_c \lambda^{cc} + L_c(1 - \lambda^{mm}) &= L(1 - \lambda^{mm}) \\ L_c \left(1 - \lambda^{cc} + \frac{(1 - \phi) \lambda^{cc}}{1 - \phi \lambda^{cc}}\right) &= L \frac{(1 - \phi) \lambda^{cc}}{1 - \phi \lambda^{cc}} \\ L_c ((1 - \lambda^{cc})(1 - \phi \lambda^{cc}) + (1 - \phi) \lambda^{cc}) &= L(1 - \phi) \lambda^{cc} \\ L_c &= \frac{(1 - \phi) \lambda^{cc}}{(1 - \lambda^{cc})(1 - \phi \lambda^{cc}) + (1 - \phi) \lambda^{cc}} L \equiv \sigma(\lambda^{cc}) L \end{aligned} \quad (88)$$

Making use of (86) and (88), we can then rewrite (83) as

$$\begin{aligned} \bar{\varepsilon}^{cm} &= \frac{\beta}{1 - \beta} [u_m(L_c(\lambda^{cc})) - u_c(L_c(\lambda^{cc})) + s \ln \lambda^{cc}/\lambda^{mm} - F_{mm} + F_{cc}] - F_{cm} + F_{cc} \\ &= \frac{\beta}{1 - \beta} \left[u_m(L_c(\lambda^{cc})) - u_c(L_c(\lambda^{cc})) + s \ln \lambda^{cc} \frac{1 - \phi \lambda^{cc}}{1 - \lambda^{cc}} - F_{mm} + F_{cc} \right] - F_{cm} + F_{cc} \end{aligned} \quad (89)$$

■

Lemma B.2 *The function $e_o(\lambda)$ in eq. (77) increases from $-\infty$ to $+\infty$ as $\lambda \in (0, 1)$.*

Proof. *The derivative of $e_o(\lambda) = s \ln(\lambda^{\frac{1-\phi\lambda}{1-\lambda}})$ with respect to λ is*

$$\begin{aligned} s \left[\frac{1}{\lambda} - \frac{\phi}{1-\phi\lambda} + \frac{1}{1-\lambda} \right] &= s \left[\frac{1}{\lambda} + \frac{-\phi(1-\lambda) + (1-\phi\lambda)}{(1-\phi\lambda)(1-\lambda)} \right] = s \left[\frac{1}{\lambda} + \frac{1-\phi}{(1-\phi\lambda)(1-\lambda)} \right] = \\ &= s \left[\frac{(1-\phi\lambda)(1-\lambda) + (1-\phi)\lambda}{(1-\phi\lambda)(1-\lambda)\lambda} \right] = s \frac{1-2\phi\lambda + \phi\lambda^2}{(1-\phi\lambda)(1-\lambda)\lambda} \end{aligned} \quad (90)$$

This function is always positive because the numerator is a convex parabola in λ , and the minimum is reached at $\lambda = 2\phi/(2\phi) = 1$, where the numerator is equal to $1 - 2\phi + \phi = 1 - \phi > 0$. Note that $\lim_{\lambda \rightarrow 0} \lambda^{\frac{1-\phi\lambda}{1-\lambda}} = 0$, and $\lim_{\lambda \rightarrow 1} \lambda^{\frac{1-\phi\lambda}{1-\lambda}} = +\infty$, so that the function $\lim_{\lambda \rightarrow 0} e_o(\lambda) = -\infty$ and $\lim_{\lambda \rightarrow 1} e_o(\lambda) = +\infty$. ■

Recall that $e_o(\lambda^{cc})$ is the option value of a remote worker minus the option value of a commuting worker. Lemma B.2 says that: 1) as the equilibrium number of commuters grows, the relative option value of being a remote worker grows; 2) as we approach a purely remote equilibrium ($\lambda^{cc} \rightarrow 0$), switching from c to m implies a loss in option values that approaches $+\infty$; as we approach a purely commuting equilibrium ($\lambda^{cc} \rightarrow 1$), switching from c to m implies a gain in the option values that approaches $+\infty$. In this sense, $e_o(\lambda)$ acts as a dynamic congestion force, always increasing the value of becoming a remote worker when there are more commuters.

Proposition B.1 *There exists at least one stationary equilibrium $L_{c,ss}$.*

Proof. *Consider the equation $f(\lambda) = 0$ characterizing stationary equilibria from (75). $f(\lambda)$ is continuous over $\lambda \in (0, 1)$. We aim at showing that $\lim_{\lambda \rightarrow 0} f(\lambda) > 0$ and $\lim_{\lambda \rightarrow 1} f(\lambda) < 0$, so that $f(\lambda) = 0$ (and there exists at least one stationary equilibrium) for some $\lambda \in (0, 1)$ by the intermediate value theorem.*

Consider the behavior of

$$\bar{\varepsilon}^{cm}(\lambda^{cc}) \equiv \frac{\beta}{1-\beta} [e_f(\lambda^{cc}) + e_o(\lambda^{cc}) - (F_{mm} - F_{cc})] - F_{cm} + F_{cc}$$

from (76). The difference in the option values $e_o(\lambda^{cc})$ behaves as $\lim_{\lambda \rightarrow 0} e_o(\lambda^{cc}) = -\infty$ and $\lim_{\lambda \rightarrow 1} e_o(\lambda^{cc}) = +\infty$ from Lemma B.2.

Using the functional forms in Assumption 1 in the indirect utility functions (64) and (65), we can write

$$\begin{aligned} e_f(\lambda^{cc}) &\equiv u_m(\lambda^{cc}) - u_c(\lambda^{cc}) = \mu \left(\log T - \log \frac{\bar{B}}{\bar{\tau}} - (\delta + \xi - \theta - \gamma/2) \log L - \frac{\gamma}{2} \log \pi + \log \frac{Z}{A} \right) \\ &\quad - \mu^2 (\delta + \xi - \theta - \gamma/(2\mu)) \log \sigma(\lambda^{cc}) \end{aligned} \quad (91)$$

As $\lambda \rightarrow 1$, this difference approaches a finite number. When $\lambda \rightarrow 0$, this difference approaches $-\infty$ if $\delta + \xi < \theta + \gamma/(2\mu)$, and $+\infty$ if $\delta + \xi > \theta + \gamma/(2\mu)$,

These observations imply that $\lim_{\lambda^{cc} \rightarrow 1} \bar{\varepsilon}^{cm}(\lambda^{cc}) = +\infty$. Moreover, Assumption 2 guarantees that $\lim_{\lambda^{cc} \rightarrow 0} \bar{\varepsilon}^{cm}(\lambda^{cc}) = -\infty$. It follows that $\lim_{\lambda \rightarrow 0} f(\lambda) = 1$ and $\lim_{\lambda \rightarrow 1} f(\lambda) = -1$. Hence, eq. (75) always has at least one solution. ■

B.3 Sufficient conditions for a unique stationary equilibrium

In this subsection, we show sufficient conditions for the stationary equilibrium to be unique and how this stationary equilibrium changes with some of the model's parameters. The proof of this result in Proposition B.2 is based on establishing conditions for the monotonicity of $f(\lambda)$ in eq. (75). Lemma B.3 below preliminarily establishes the monotonicity of L_c in the share of commuters that remain commuters, λ^{cc} .

Lemma B.3 *The function $\sigma(\lambda)$ in eq. (79) is monotonically increasing from 0 to 1 when $\lambda \in [0, 1]$.*

Proof. Computing the derivative,

$$\begin{aligned}\sigma'(\lambda) &= \frac{(1-\phi)[(1-\lambda)(1-\phi\lambda)+(1-\phi)\lambda] - (1-\phi)\lambda[(1-\phi)-(1-\phi\lambda)-\phi(1-\lambda)]}{[(1-\lambda)(1-\phi\lambda)+(1-\phi)\lambda]^2} = \\ &= (1-\phi) \frac{(1-\lambda)(1-\phi\lambda)+(1-\phi)\lambda - \lambda(1-\phi)+\lambda(1-\phi\lambda)+\phi\lambda(1-\lambda)}{[(1-\lambda)(1-\phi\lambda)+(1-\phi)\lambda]^2} = \\ &= \frac{(1-\phi)(1-\lambda^2\phi)}{[(1-\lambda)(1-\phi\lambda)+(1-\phi)\lambda]^2}\end{aligned}\tag{92}$$

which is always positive. ■

Proposition B.2 *Assume $\delta+\xi < \theta+\gamma/(2\mu)$. Then there is a unique stationary equilibrium value of the commuting population $L_{c,ss}$. This stationary equilibrium value monotonically increases with A and \bar{B} , and monotonically falls with Z , T and $\bar{\tau}$.*

Proof. Recall eq. (91), stating that

$$\begin{aligned}e_f(\lambda^{cc}) &\equiv u_m(\lambda^{cc}) - u_c(\lambda^{cc}) = \mu \left(\log T - \log \frac{\bar{B}}{\bar{\tau}} - (\delta + \xi - \theta - \gamma/2) \log L - \frac{\gamma}{2} \log \pi + \log \frac{Z}{A} \right) \\ &\quad - \mu^2(\delta + \xi - \theta - \gamma/(2\mu)) \log \sigma(\lambda^{cc})\end{aligned}\tag{93}$$

When $\delta + \xi < \theta + \gamma/(2\mu)$, this difference is increasing in λ^{cc} from Lemma B.3 and it follows that $\bar{\varepsilon}^{cm}(\lambda^{cc})$ in eq. (76) is monotonically increasing in λ^{cc} , mapping the interval $(0, 1)$ into $(-\infty, +\infty)$. Hence, the function $f(\lambda^{cc})$ in (75) is monotonically decreasing in λ^{cc} and maps the interval $(0, 1)$ into itself. Equation (75) has then a unique solution for λ^{cc} , which maps into a unique value for $L_c = \sigma(\lambda^{cc})L$.

Note also that A , Z , T , \bar{B} and $\bar{\tau}$ only affect the value of $\bar{\varepsilon}^{cm}(\lambda^{cc})$ in (76) through $u_m - u_c$; in particular, $\bar{\varepsilon}^{cm}(\lambda^{cc}; A, \bar{B}, Z, T, \tau)$ grows with Z , T , and $\bar{\tau}$ while falling with A and \bar{B} for any

given λ^{cc} . Hence, $f(\lambda^{cc})$ in (75) shifts uniformly down with Z , T , $\bar{\tau}$ and up with A and \bar{B} in its domain $\lambda^{cc} \in (0, 1)$. This implies that the solution to (75) and $L_c = \sigma(\lambda_{cc})L$ also moves in the same direction with these parameters. ■

B.4 Necessary and sufficient conditions for multiple stationary equilibria

In Proposition B.1 we have shown that there is always at least one stationary equilibrium because $f(\lambda)$ starts positive, ends negative, and is continuous. In Proposition B.3, we show that for any level of (sufficiently strong) agglomeration forces, there is a range of values z/A where the economy exhibits multiple stationary equilibria. Proposition B.3 makes use of the following four lemmas. Lemma B.4 characterizes necessary and sufficient conditions for multiplicity in terms of the function $f(\lambda)$ in eq. (75): multiple stationary equilibria exist if $f'(\lambda) > 0$ at a stationary equilibrium, which can be restated into a condition on $\partial\bar{\varepsilon}^{cm}(\lambda)/\partial\lambda$, the slope of the expected value of switching from c to m with respect to λ . Lemma B.5 considers such slope and it shows that, at a candidate $\hat{\lambda}$, one can always make $\partial\bar{\varepsilon}^{cm}(\lambda)/\partial\lambda$ arbitrarily negative by choosing an externality term δ above a threshold δ^* . This fact is useful because the slope of $\bar{\varepsilon}^{cm}$ can be used to control the slope of $f(\lambda)$. Lemma B.6 characterizes some properties of this threshold δ^* . Lemma B.7 shows that for any level of δ , we can always find a ratio of the exogenous remote work to in-office productivity, z/A , that makes an arbitrary $\hat{\lambda}$ a stationary equilibrium. Proposition B.3 uses these lemmas to show that for a high enough δ , we can always find a z/A that makes some $\hat{\lambda}$ a stationary equilibrium where $f'(\hat{\lambda}) > 0$.

Lemma B.4 Consider an economy Ω . The economy has multiple stationary equilibria if and only if there exist one $\hat{\lambda}$ such that

$$f(\hat{\lambda}) = 0 \tag{94}$$

$$\left. \frac{\partial f(\lambda)}{\partial \lambda} \right|_{\lambda=\hat{\lambda}} > 0 \tag{95}$$

Moreover, if such $\hat{\lambda}$ exists, then it holds true that:

$$\left. \frac{\partial \bar{\varepsilon}^{cm}(\lambda)}{\partial \lambda} \right|_{\lambda=\hat{\lambda}} < -\frac{s}{\hat{\lambda}(1-\hat{\lambda})} \tag{96}$$

Proof. From Lemma B.1, a stationary equilibrium is characterized by $f(\hat{\lambda}) = 0$. Suppose

$$\left. \frac{\partial f(\lambda)}{\partial \lambda} \right|_{\lambda=\hat{\lambda}} > 0 \tag{97}$$

Since $f(\lambda)$ always starts at +1 and ends at -1, $f(\lambda)$ will cross zero at least two more times, one

to the left and one to the right of $\hat{\lambda}$. In other words, the equation $f(\lambda)$ has more than one solution, that is, the economy exhibits multiple stationary equilibria.

Note that, using the definition of f in eq. (75),

$$\begin{aligned}\frac{\partial f(\lambda)}{\partial \lambda} &= -\frac{\exp(\bar{\varepsilon}^{cm}(\lambda)/s)}{(1+\exp(\bar{\varepsilon}^{cm}(\lambda)/s))^2} \frac{1}{s} \frac{\partial \bar{\varepsilon}^{cm}(\lambda)}{\partial \lambda} - 1 > 0 \\ \frac{\partial \bar{\varepsilon}^{cm}(\lambda)}{\partial \lambda} &< -s \frac{(1+\exp(\bar{\varepsilon}^{cm}(\lambda)/s))^2}{\exp(\bar{\varepsilon}^{cm}(\lambda)/s)}\end{aligned}\quad (98)$$

Additionally, using the same definition, at a stationary equilibrium it holds true that

$$f(\hat{\lambda}) \equiv \frac{1}{1+\exp(\bar{\varepsilon}^{cm}(\hat{\lambda})/s)} - \hat{\lambda} = 0 \implies \frac{1}{1+\exp(\bar{\varepsilon}^{cm}(\hat{\lambda})/s)} = 1/\hat{\lambda} \quad (99)$$

$$1 + \exp(\bar{\varepsilon}^{cm}(\hat{\lambda})/s) = 1/\hat{\lambda} \quad (100)$$

$$\exp(\bar{\varepsilon}^{cm}(\hat{\lambda})/s) = (1 - \hat{\lambda})/\hat{\lambda} \quad (101)$$

Hence, using equations (100) and (101) in eq. (98), we have

$$\left. \frac{\partial \bar{\varepsilon}^{cm}(\lambda)}{\partial \lambda} \right|_{\lambda=\hat{\lambda}} < -\frac{s}{\hat{\lambda}(1-\hat{\lambda})} \quad (102)$$

■

Lemma B.5 $\forall \hat{\lambda} \in (0, 1), K > 0, \exists \delta^*(\hat{\lambda}, K) > 0 :$

$$\left. \frac{\partial \bar{\varepsilon}^{cm}(\lambda, \delta)}{\partial \lambda} \right|_{\lambda=\hat{\lambda}} < -K \iff \delta + \xi > \delta^*(\hat{\lambda}, K)$$

Proof. Consider the expression for $\bar{\varepsilon}^{cm}(\lambda)$ from (76):

$$\bar{\varepsilon}^{cm}(\lambda) \equiv \frac{\beta}{1-\beta} [e_f(\lambda) + e_o(\lambda) - (F_{mm} - F_{cc})] - F_{cm} + F_{cc}$$

The first derivative of this function with respect to λ is

$$\frac{\partial \bar{\varepsilon}^{cm}(\lambda)}{\partial \lambda} = \frac{\beta}{1-\beta} [e'_f(\lambda) + e'_o(\lambda)]$$

We know that $e'_o(\lambda) > 0$. From eq. (91), we can easily compute e'_f so that our condition becomes

$$\begin{aligned} \frac{\partial \bar{\varepsilon}^{cm}(\lambda)}{\partial \lambda} \Big|_{\lambda=\hat{\lambda}} &< -K \iff e'_f(\lambda) \Big|_{\lambda=\hat{\lambda}} < -e'_o(\lambda) \Big|_{\lambda=\hat{\lambda}} - \frac{1-\beta}{\beta} K \iff \\ \delta + \xi &> \frac{1}{\mu^2} \left[\frac{\sigma(\lambda)}{\sigma'(\lambda)} \left(e'_o(\lambda) + \frac{1-\beta}{\beta} K \right) \right]_{\lambda=\hat{\lambda}} + \frac{\gamma}{2\mu} + \theta \equiv \delta^*(\hat{\lambda}, K) \end{aligned} \quad (103)$$

■

Lemma B.6 Define

$$\hat{\delta}(\lambda) \equiv \frac{1}{\mu^2} \left[\frac{\sigma(\lambda)}{\sigma'(\lambda)} \left(e'_o(\lambda) + \frac{1-\beta}{\beta} \frac{s}{\lambda(1-\lambda)} \right) \right] + \frac{\gamma}{2\mu} + \theta \quad (104)$$

as the threshold function $\delta^*(\lambda, K)$ for $K = \frac{s}{\lambda(1-\lambda)}$ in eq. (103). Then, $\hat{\delta}(\lambda)$ reaches a minimum value of $\eta_{min} > \gamma/(2\mu) + \theta$. If $\phi \in (0, 1)$, then $\hat{\delta}(\lambda)$ is convex in λ .

Proof. The function $\hat{\delta}(\lambda)$ is defined for $\hat{\lambda} \in (0, 1)$, is continuous, and differentiable. Since the term in the square brackets is always positive, the function is also always positive. To further characterize $\hat{\delta}(\lambda)$, we study its limiting properties. To compute $\lim_{\hat{\lambda} \rightarrow 0} \hat{\delta}(\hat{\lambda})$, we substitute the expressions for $\sigma(\lambda)$, $e'_o(\lambda)$ and $\sigma'(\lambda)$ from equations (88), (90), and (92) and obtain

$$\lim_{\hat{\lambda} \rightarrow 0} \hat{\delta}(\hat{\lambda}) = \frac{s}{\mu^2 \beta} + \frac{\gamma}{2\mu} + \theta \equiv \hat{\delta}_0 > 0$$

Further, $\lim_{\hat{\lambda} \rightarrow 1} \hat{\delta}(\hat{\lambda}) = +\infty$ since, from (88) and (92), $\lim_{\hat{\lambda} \rightarrow 1} \sigma(\hat{\lambda}) = 1$ and $\lim_{\hat{\lambda} \rightarrow 1} \sigma'(\hat{\lambda}) = 1$; and from Lemma B.2, $\lim_{\hat{\lambda} \rightarrow 1} e'_o(\hat{\lambda}) = +\infty$.

The first derivative of $\hat{\delta}(\lambda)$, after some algebra, is given by:

$$\begin{aligned} \hat{\delta}'(\lambda) = & - \frac{s}{\mu^2} \frac{4\phi(1-2\phi\lambda+\phi\lambda^2)}{(1-\phi\lambda^2)(1-\phi\lambda)} \\ & + \frac{s}{\mu^2} \frac{(1-2\phi\lambda+\phi\lambda^2)^2(1-3\phi^2\lambda^2-3\phi\lambda^2+4\phi^2\lambda^3+\phi)}{(1-\phi\lambda^2)^2(1-\phi\lambda)^2(1-\lambda)^2} \\ & + \frac{s}{\mu^2} \frac{1-\beta}{\beta} \frac{1+2\phi(2\lambda-2\lambda^2-1)-\phi^2\lambda^2(2-4\lambda+\lambda^2)}{(1-\phi\lambda^2)^2(1-\lambda)^2} \end{aligned} \quad (105)$$

Moreover,

$$\lim_{\hat{\lambda} \rightarrow 0} \hat{\delta}'(\lambda) < 0 \iff \phi > \frac{1}{2+\beta} \quad (106)$$

Hence, the function begins by sloping down if ϕ is large enough. Assume that $\hat{\delta}(\lambda)$ is convex, which

we will prove right below. In this case, the (unique) minimum is achieved for a $\eta_{min} : \gamma/(2\mu) + \theta < \eta_{min} < \hat{\delta}_0$. If the function begins by sloping up, then $\eta_{min} \equiv \hat{\delta}_0$.

It remains to be proven that $\hat{\delta}(\lambda)$ is convex. To this end, it is thus sufficient to prove the convexity of the simplified function $\hat{\delta}(\lambda)_{simple}$, which takes out the constant term $\frac{\gamma}{\mu} + \theta$ and the positive multiplicative term $\frac{s}{\mu^2}$:

$$\begin{aligned}\hat{\delta}(\lambda)_{simple} &= \frac{\lambda(1 - 2\phi\lambda + \phi\lambda^2)}{1 - \phi\lambda^2} \left[\frac{1 - 2\phi\lambda + \phi\lambda^2}{(1 - \phi\lambda)(1 - \lambda)\lambda} + \frac{1 - \beta}{\beta} \frac{1}{\lambda(1 - \lambda)} \right] \\ &= \frac{(1 - 2\phi\lambda + \phi\lambda^2)}{(1 - \phi\lambda^2)(1 - \lambda)} \left[\frac{1 - 2\phi\lambda + \phi\lambda^2}{(1 - \phi\lambda)} + \frac{1 - \beta}{\beta} \right] \\ &= \underbrace{\frac{(1 - 2\phi\lambda + \phi\lambda^2)^2}{(1 - \phi\lambda^2)(1 - \lambda)(1 - \phi\lambda)}}_{\text{first term } \Xi_1} + \underbrace{\frac{1 - \beta}{\beta} \frac{(1 - 2\phi\lambda + \phi\lambda^2)}{(1 - \phi\lambda^2)(1 - \lambda)}}_{\text{second term } \Xi_2}.\end{aligned}$$

We argue that each of the terms Ξ_1 and Ξ_2 is convex, which will prove the convexity of their sum.

The second derivative of Ξ_1 is:

$$\frac{d^2\Xi_1}{d\lambda^2} = \frac{2}{(1 - \lambda)^3} + \phi^2 \left(\frac{2}{(1 - \phi\lambda)^3} - \frac{8x(\phi\lambda^2 + 3)}{(1 - \phi\lambda^2)^3} \right)$$

We prove by contradiction that $\frac{d^2\Xi_1}{d\lambda^2}$ cannot be negative. Recall that the range of values for ϕ, λ is $\phi \in (0, 1), \lambda \in (0, 1)$. The first term of the expression $\frac{2}{(1 - \lambda)^3}$, is always positive. If $\frac{d^2\Xi_1}{d\lambda^2}$ is negative at any value of λ , then the term $\left(\frac{2}{(1 - \phi\lambda)^3} - \frac{8x(\phi\lambda^2 + 3)}{(1 - \phi\lambda^2)^3} \right)$ must be negative. If this is so, then:

$$\begin{aligned}\frac{d^2\Xi_1}{d\lambda^2} &= \frac{2}{(1 - \lambda)^3} + \phi^2 \left(\frac{2}{(1 - \phi\lambda)^3} - \frac{8x(\phi\lambda^2 + 3)}{(1 - \phi\lambda^2)^3} \right) \\ &\geq \frac{2}{(1 - \lambda)^3} + \left(\frac{2}{(1 - \phi\lambda)^3} - \frac{8x(\phi\lambda^2 + 3)}{(1 - \phi\lambda^2)^3} \right) \\ &\geq \frac{2}{(1 - \lambda)^3} + \left(\frac{2}{(1 - \lambda)^3} - \frac{8x(\phi\lambda^2 + 3)}{(1 - \phi\lambda^2)^3} \right) \\ &\geq \frac{2}{(1 - \lambda)^3} + \left(\frac{2}{(1 - \lambda)^3} - \frac{8x(\lambda^2 + 3)}{(1 - \lambda^2)^3} \right) \\ &= \frac{4}{(1 + \lambda)^3} \\ &\geq 0\end{aligned}$$

The fourth line follows because $\frac{d}{da} = -\frac{8x(\phi\lambda^2 + 3)}{(1 - \phi\lambda^2)^3} = -\frac{16\lambda^3(5 + \phi\lambda^2)}{(-1 + \phi\lambda^2)^4} \leq 0$, so the term is most

negative at $\phi = 1$. We have shown that $\frac{d^2\Xi_1}{d\lambda^2}$ is weakly positive. Thus, Ξ_1 is convex.

We now move on to the second term term. The second derivative of Ξ_2 is:

$$\frac{d^2\Xi_2}{d\lambda^2} = \frac{2(1 - \phi\lambda^2)^3 - 4\phi^2\lambda(\phi\lambda^2 + 3)(1 - \lambda)^3}{(1 - \lambda)^3(1 - \phi\lambda^2)^3}$$

The denominator is obviously positive for $\phi \in (0, 1), \lambda \in (0, 1)$. We want to prove that the numerator is positive. Let us observe so the numerator, which we denote as $N_2(\lambda)$:

$$N_2(\lambda) = 2(1 - \phi\lambda^2)^3 - 4\phi^2\lambda(\phi\lambda^2 + 3)(1 - \lambda)^3$$

By inspection, $N_2(\lambda)$ is decreasing in ϕ for $\phi \in (0, 1)$. As such we only need to prove that $N_2(\lambda)$ is positive for $\phi = 1$ to show that $N_2(\lambda)$ is always positive.

$$\begin{aligned} N_2(\lambda) &= 2(1 - \phi\lambda^2)^3 - 4\phi^2\lambda(\phi\lambda^2 + 3)(1 - \lambda)^3 \\ &\geq 2(1 - \lambda^2)^3 - 4\lambda(\lambda^2 + 3)(1 - \lambda)^3 \\ &= 2(1 - \lambda)^6 \\ &\geq 0 \text{ for } \lambda \in (0, 1) \end{aligned}$$

We have shown that both the numerator and denominator of the second derivative of Ξ_2 are positive. As such, Ξ_2 is convex.

We have shown that Ξ_1 and Ξ_2 are convex, their sum $\hat{\delta}(\lambda)_{simple}$ is also convex, which in turn implies that our original function $\hat{\delta}(\lambda)$ is convex.

■

Lemma B.6 essentially states what is the minimum level of agglomeration forces that overcomes dynamic congestion forces if at a candidate λ we want $f'(\lambda) > 0$, a necessary condition for such λ to be an unstable equilibrium in a multiple equilibrium configuration.

Lemma B.7 *For each $\hat{\lambda}$ and δ , there exists a ratio z/A such that $f(\hat{\lambda}; \delta, z/A) = 0$. This ratio is described by the function*

$$\begin{aligned} \rho(\hat{\lambda}) &= \exp \left\{ \frac{1}{\mu} \left[\frac{1 - \beta}{\beta} (F_{cm} - F_{cc}) + F_{mm} - F_{cc} \right] \right\} \times \pi^{\gamma/2} \frac{\bar{B}}{\bar{\tau}T} \\ &\times \frac{\sigma(\hat{\lambda})^{\mu(\xi+\delta-\theta)-\gamma/2}}{(1 - \phi\hat{\lambda})^{s/\mu}} \times \left(\frac{1 - \hat{\lambda}}{\hat{\lambda}} \right)^{s/(\beta\mu)} \times L^{\xi+\delta-\theta-\gamma/2} \end{aligned} \quad (107)$$

Proof. Using the definition of $\bar{\varepsilon}^{cm}(\hat{\lambda})$ from eq. (76) in the condition for a stationary equilibrium from (75),

$$\begin{aligned}\hat{\lambda} &= \frac{1}{1 + \exp(\bar{\varepsilon}^{cm}(\hat{\lambda})/s)} \implies s \ln \frac{1 - \hat{\lambda}}{\hat{\lambda}} = \bar{\varepsilon}^{cm}(\hat{\lambda}) \\ s \ln \frac{1 - \hat{\lambda}}{\hat{\lambda}} &= \frac{\beta}{1 - \beta} [e_f(\hat{\lambda}) + e_o(\hat{\lambda}) - (F_{mm} - F_{cc})] - F_{cm} + F_{cc}\end{aligned}$$

Using $e_f \equiv u_m - u_c$ and the result in eq. (91), after some manipulation, we obtain

$$\begin{aligned}\frac{Z}{A} &= \exp \left\{ \frac{1}{\mu} \left[\frac{1 - \beta}{\beta} (F_{cm} - F_{cc}) + F_{mm} - F_{cc} \right] \right\} \times \pi^{\gamma/2} \frac{\bar{B}}{\bar{T}} \\ &\times \frac{\sigma(\hat{\lambda})^{\mu(\xi+\delta-\theta)-\gamma/2}}{(1 - \phi\hat{\lambda})^{s/\mu}} \times \left(\frac{1 - \hat{\lambda}}{\hat{\lambda}} \right)^{s/(\beta\mu)} \times L^{\xi+\delta-\theta-\gamma/2} \equiv \rho(\hat{\lambda})\end{aligned}\quad (108)$$

L_c is a function of $\hat{\lambda}$ and is bounded between 0 and L . One can verify using eq. (77) that the sum in the curly bracket $-e_o(\hat{\lambda}) + \frac{1-\beta}{\beta}s \ln \frac{1-\hat{\lambda}}{\hat{\lambda}}$ goes to $+\infty$ for $\hat{\lambda} \rightarrow 0$ and to $-\infty$ for $\hat{\lambda} \rightarrow 1$. Hence, the image of \hat{z} spans $(0, +\infty)$ as $\hat{\lambda}$ varies in $(0, 1)$.

■

Proposition B.3 Assume $F_{cc} = F_{mm} = 0$. Then, there exist a finite threshold $\eta_{min} > \theta + \gamma/(2\mu)$, and a set $\mathcal{Z} \subset \mathbb{R}_{++}$, such that:

- i) for $\delta + \xi > \eta_{min}$, \mathcal{Z} is a non-empty interval (Z_{min}, Z_{max}) and there are multiple stationary equilibria if $z/A \in \mathcal{Z}$; further, Z_{min} and Z_{max} grow with L and \bar{B} and fall with T and $\bar{\tau}$.
- ii) there is a unique stationary equilibrium in all other cases.

Proof. From Lemma B.4, we know that equations (94) and (96) characterize an economy with multiple stationary equilibria. We seek necessary and sufficient conditions for those equations to hold.

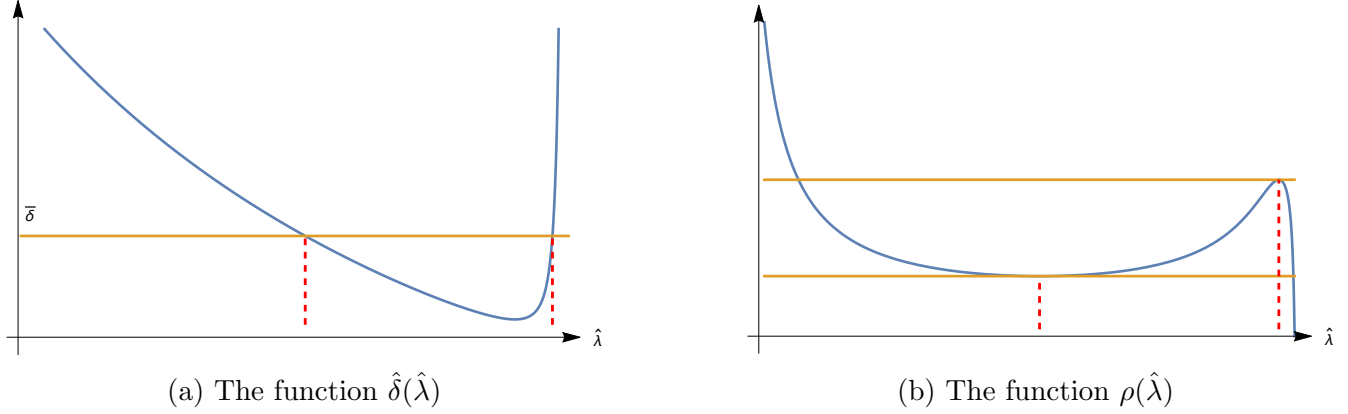
Consider the equation $\hat{\delta}(\hat{\lambda})$ in Lemma B.6. From Lemmas B.4 and B.5, $f'(\hat{\lambda}) > 0$ if and only if we pick a $\bar{\delta} : \bar{\delta} + \xi \geq \hat{\delta}(\hat{\lambda})$. Note that $\hat{\delta}(\hat{\lambda})$ is defined for $\hat{\lambda} \in (0, 1)$, is continuous, and differentiable. Also, from Lemma B.6, it is convex in $\hat{\lambda}$ and it reaches a global minimum value of $\hat{\delta}_{min}$. An example of this function is plotted in Panel (a) of Figure A20.

Our proof proceeds with a taxonomic discussion of the implications of different values of $\bar{\delta}$. This discussion can be organized around features of the set

$$\Lambda(\bar{\delta}) \equiv \{\hat{\lambda} : \hat{\delta}(\hat{\lambda}) \leq \bar{\delta} + \xi\} \quad (109)$$

Note that by construction, for each $\hat{\lambda} \in \Lambda(\bar{\delta})$, eq. (96) is satisfied if $f(\hat{\lambda}, \bar{\delta}, z/A) = 0$.

Figure A20: Identifying the Range of Parameters for Multiple Stationary Equilibria



Consider part *i*) of the proposition, and fix a $\bar{\delta} : \bar{\delta} + \xi > \hat{\delta}_{min} > \gamma/(2\mu) + \theta$. Then, the set $\Lambda(\bar{\delta})$ is non-empty; moreover, since $\hat{\delta}$ is convex from Lemma B.6, the set $\Lambda(\bar{\delta})$ is an interval of the form $\Lambda(\bar{\delta}) = (\lambda_{min}(\bar{\delta}), \lambda_{max}(\bar{\delta}))$. Consider then the set

$$\mathcal{Z}(\bar{\delta}) = \{z/A : z/A = \rho(\hat{\lambda}) \text{ for some } \hat{\lambda} \in \Lambda(\bar{\delta})\} \quad (110)$$

The set \mathcal{Z} is the image of the set Λ in z/A (see Panel (b) of Figure A20). By construction, for any z/A in this set, there is some $\hat{\lambda}$ for which $\hat{\lambda}, z/A$ is a stationary equilibrium, that is, eq. (94) holds. Since at the same $\hat{\lambda}$ eq. (96) also holds, the economy exhibits multiple stationary equilibria. Note also that since $\rho(\lambda)$ is continuous and Λ is an interval, $\mathcal{Z}(\bar{\delta})$ is also an interval and can be written as

$$\begin{aligned} \mathcal{Z}(\bar{\delta}) &= (Z_{min}(\bar{\delta}), Z_{max}(\bar{\delta})) \\ Z_{min}(\bar{\delta}) &= \min_{\lambda \in \Lambda(\bar{\delta})} \rho(\lambda) \\ Z_{max}(\bar{\delta}) &= \max_{\lambda \in \Lambda(\bar{\delta})} \rho(\lambda) \end{aligned}$$

To show how $Z_{min}(\bar{\delta}), Z_{max}(\bar{\delta})$ vary with L , we consider the expression for $\rho(\lambda)$ in eq. (108). If λ^- is the minimizer when the total city size is L , then λ^- is also the minimizer when the total city size is kL , for $k > 0$; additionally, $\rho(\lambda, kL) = k^{\bar{\delta}+\xi-\theta-\gamma/2}\rho(\lambda, L)$. Since $\bar{\delta} + \xi - \theta - \gamma/2 > 0$ is satisfied whenever \mathcal{Z} is non-empty, then Z_{min} grows with L . A similar argument shows that Z_{max} also grows with L . Further, similar arguments can be made to show that these boundaries grow with \bar{B} and fall with $\bar{\tau}$ and T .

To prove part *ii*), note that if $\bar{\delta} + \xi > \hat{\delta}_{min}$ but $z/A \notin \mathcal{Z}(\bar{\delta})$, then by construction none of the $\hat{\lambda} \in \Lambda(\bar{\delta})$ are a stationary equilibrium where (96) holds; however, since a stationary equilibrium always exists, the equilibrium must be unique. Similarly, if $\bar{\delta} + \xi < \hat{\delta}_{min}$, then the set $\Lambda(\bar{\delta})$ in eq. (109) is empty; hence, there is no $\hat{\lambda}$ for which eq. (94) holds at a candidate stationary equilibrium.

Again, since a stationary equilibrium always exists, it must be unique. \blacksquare

Proposition 4.3 then follows from the fact that L_c is monotone increasing in λ^{cc} by Lemma B.3.

B.5 Relative Transition Shares

Lemma B.8 Suppose $F_{cc} = F_{mm} = 0$ and that $F_{cm} = F_{mc} = F$. Then

$$y_{\ell\ell't} \equiv \ln \frac{\lambda_{\ell\ell't} \lambda_{\ell'\ell't+1}^\beta}{\lambda_{\ell\ell't} \lambda_{\ell\ell't+1}^\beta} = \frac{\beta}{s} (u_{\ell't+1} - u_{\ell't}) - \frac{(1-\beta)F}{s}. \quad (111)$$

Proof.

Combining (18) and (17), the share of workers in state ℓ transitioning to ℓ' is given by

$$\lambda_{\ell\ell't} = \frac{\exp(\beta V_{\ell't+1} - F_{\ell\ell',t})^{1/s}}{\exp(\beta V_{ct+1} - F_{\ell ct})^{1/s} + \exp(\beta V_{mt+1} - F_{\ell mt})^{1/s}}, \quad (112)$$

where we denote $V_{\ell t+1} = V_\ell(L_{ct+1}; \omega^{t+1})$. We first obtain an expression of $\lambda_{\ell\ell't}$ as a function of $V_{\ell t}$, $V_{\ell't+1}$ and transition costs only by re-writing (59) with time indices only,

$$V_{\ell t} = u_{\ell t} + \beta V_{\ell t+1} - F_{\ell\ell t} + \Omega_{\ell t}, \quad (113)$$

and re-writing (63) after replacing the transition share by its expression in (112):

$$\Omega_{\ell t} = -s \ln \left(\frac{\exp(\beta V_{\ell t+1} - F_{\ell\ell t})^{1/s}}{\exp(\beta V_{ct+1} - F_{\ell ct})^{1/s} + \exp(\beta V_{mt+1} - F_{\ell mt})^{1/s}} \right). \quad (114)$$

Substituting for $\Omega_{\ell t}$ in (113), we get the following expression for the value of labor delivery mode ℓ :

$$V_{\ell t} = u_{\ell t} + s \ln \left(\exp(\beta V_{ct+1} - F_{\ell ct})^{1/s} + \exp(\beta V_{mt+1} - F_{\ell mt})^{1/s} \right), \quad (115)$$

or equivalently,

$$\exp(\beta V_{ct+1} - F_{\ell ct})^{1/s} + \exp(\beta V_{mt+1} - F_{\ell mt})^{1/s} = \exp(V_{\ell t} - u_{\ell t})^{1/s}. \quad (116)$$

Recognizing the left hand side as the denominator in (112), we obtain the following expressions for the share of workers in state ℓ transitioning to ℓ' at t , in state ℓ transitioning to ℓ at t , in state ℓ' transitioning to ℓ' at $t+1$ and in state ℓ transitioning to ℓ' at $t+1$, respectively, as:

$$\lambda_{\ell\ell't} = \exp(\beta V_{\ell't+1} - F_{\ell\ell't} + u_{\ell t} - V_{\ell t})^{1/s}. \quad (117)$$

$$\lambda_{\ell\ell t} = \exp(\beta V_{\ell t+1} - F_{\ell\ell t} + u_{\ell t} - V_{\ell t})^{1/s}, \quad (118)$$

$$\lambda_{\ell'\ell't+1} = \exp(\beta V_{\ell't+2} - F_{\ell'\ell't+1} + u_{\ell't+1} - V_{\ell't+1})^{1/s}, \quad (119)$$

$$\lambda_{\ell\ell't+1} = \exp(\beta V_{\ell't+2} - F_{\ell\ell't+1} + u_{\ell't+1} - V_{\ell't+1})^{1/s}. \quad (120)$$

We get the following expression for the ratio of the discounted probabilities:

$$\frac{\lambda_{\ell\ell't} (\lambda_{\ell'\ell't+1})^\beta}{\lambda_{\ell\ell t} (\lambda_{\ell\ell't+1})^\beta} = \exp(\beta(u_{\ell't+1} - u_{\ell t+1}) + F_{\ell\ell t} - F_{\ell\ell't} + \beta(F_{\ell\ell't+1} - F_{\ell'\ell't+1}))^{1/s}. \quad (121)$$

Using the assumption imposed in Proposition 4.3 that $F_{\ell\ell t} = 0$ for all t and $\ell \in \{m, c\}$, and that $F_{lm} = F_{ml} = F$, the logarithm of this ratio can be written as

$$\ln \frac{\lambda_{\ell\ell't} (\lambda_{\ell'\ell't+1})^\beta}{\lambda_{\ell\ell t} (\lambda_{\ell\ell't+1})^\beta} = \frac{\beta}{s}(u_{\ell't+1} - u_{\ell t+1}) - \frac{1-\beta}{s}F. \quad (122)$$

■

B.6 Testing for multiple equilibria

It is in principle possible for models like ours to exhibit multiple equilibria, not only multiple stationary equilibria. For example, a city could start in an initial condition with low commuting, but individual expectations of a return to high commuting might put the system on a self-fulfilling path. In this subsection, we describe how we test – and find no evidence of – this possibility.

In particular, let us examine first a case where, starting from an initial condition that we expect to converge toward the high-commuting equilibrium, the system might actually converge toward the low commuting one. For cities with multiple stationary equilibria, we have always found 2 stable and one unstable stationary equilibrium. We therefore start by setting an initial condition for L_{c0} above the unstable equilibrium. The top panels of Figure A21 set $L_{c0}/L = 0.15$ for the metro area of New York, which is above the unstable stationary equilibrium (dashed red line).

In Panel (a), we set as initial guesses for the time path of the value functions V_c and V_m their respective value in the high-commuting stationary equilibrium. We require, as a convergence criterion, both that the sup-norm relative distance between successive guesses of the value functions is less than a given threshold and that the terminal value of these value functions is within the same relative tolerance from the high-commuting stationary equilibrium value. We set this threshold to 10^{-6} . The panel shows successive time paths of L_c/L at the indicated iteration number. In this exercise, our value function iteration algorithm converges to a solution in a little more than 4,000 iterations.

Starting from the same $L_{c0}/L = 0.15$, Panel (b) sets as initial guesses for the time path of the value functions V_c and V_m their respective value in the low-commuting stationary equilibrium. We impose the same convergence criterion, requiring this time that the terminal value of the value functions converge to the low-commuting stationary equilibrium. In this case, our value function iteration algorithm does not converge within 40,000 iterations. Panel (b) shows that along the

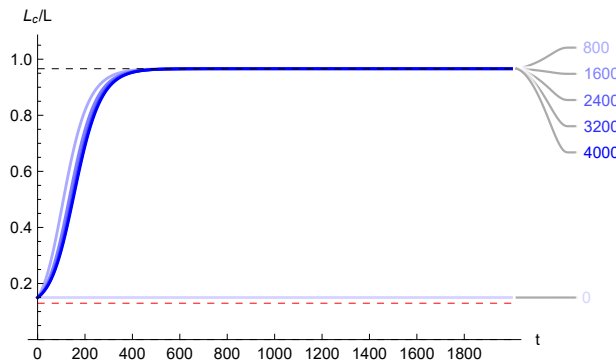
iteration process, the guesses attempt to reach the low commuting equilibrium, but they move progressively away from it.

The bottom panels of Figure A21 report analogous exercises where we instead start from an initial condition below the unstable equilibrium, namely $L_{c0}/L = 0.10$. In Panel (c), we again attempt to converge toward the high-commuting equilibrium, with no success. In Panel (d), we successfully converge towards the low-commuting equilibrium in about 3,600 iterations.

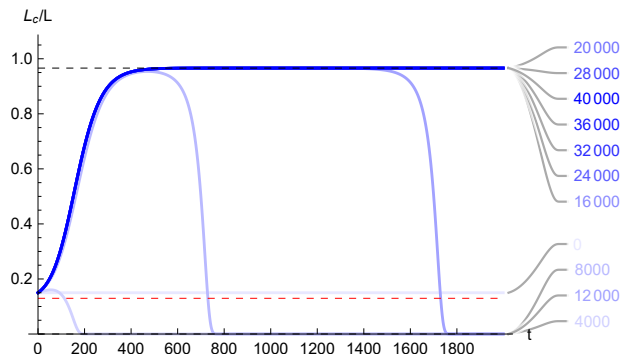
In unreported results, we have also experimented with other initial conditions farther away from either side of the unstable equilibrium, and other cities of varying sizes (like San Francisco, CA, Kansas City, MO-KS, Milwaukee, WI, Salt Lake City, UT, and Providence, RI), always reaching the same conclusion.

Figure A21: Tests for multiple equilibria

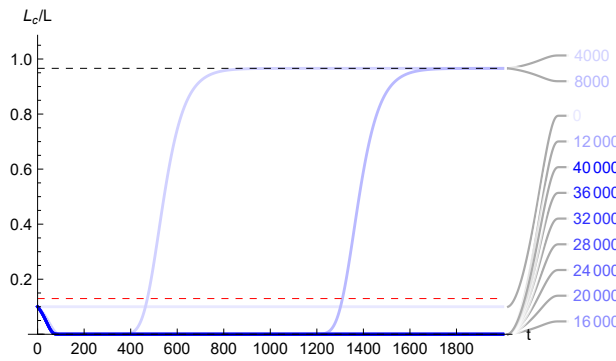
(a) $L_{c0}/L = 0.15$, shooting toward high-commuting equilibrium



(b) $L_{c0}/L = 0.15$, shooting toward low-commuting equilibrium



(c) $L_{c0}/L = 0.10$, shooting toward high-commuting equilibrium



(d) $L_{c0}/L = 0.10$, shooting toward low-commuting equilibrium

